

RU 567
4074
FE-AR 83

RTD Report No. 252

**POTENTIAL OILED ICE TRAJECTORIES IN
THE BEAUFORT SEA**

by

D. R. Thomas

January 1983



Flow Industries, Inc.
Research and Technology Division
21414-68th Avenue South
Kent, Washington 98032
(206) 872-8500
TWX: 910-447-2762

RTD Report No. 252

**POTENTIAL OILED ICE TRAJECTORIES IN
THE BEAU FORT SEA**

by

D. R. Thomas

January 1983



**Flow Industries, Inc.
Research and Technology Division
2141 4-68th Avenue South
Kent, Washington 98032
(206) 872-8500
TWX: 910-447-2762**

RTD Report No. 252

POTENTIAL OILED ICE TRAJECTORIES IN
THE BEAUFORT SEA

D. R. Thomas

January 1983

Flow Industries, Inc.
Research and Technology Division
21414 68th Avenue South
Kent, Washington 98032
(206) 872-8500
TWX : 910-447-2762

- i -

Foreword

This study was supported by the Bureau of Land Management through inter-agency agreement with the National Oceanic and Atmospheric Administration, under which a **multiyear** program responding to needs of petroleum development of the Alaskan Continental Shelf is managed by the Outer Continental Shelf Environmental Assessment (OCSEAP) Office.

Table of Contents

	Page
Foreword	i
1. Introduction	1
2. Technical Approach	3
2.2 General Approach	3
2.2.1 Quasi-Steady Ice Model	3
2.2.2 Free-Drift Ice Model	6
2.3 Driving Forces	7
2.3.1 Winds	7
2.3.2 Model Boundary Conditions	11
2.3.3 Ocean Currents	12
2.4 Ice Conditions	13
2.5 Procedure for Calculating Trajectories	15
3. Results	20
3.1 Seasonal Ice Trajectories	20
3.2 Variability in Modeled Trajectories	21
4. Comparisons with Observations	25
5. Discussion	26
References	28
Figures	31
Appendix A: A Model for Currents on the Alaskan Beaufort Shelf	A1
Appendix B: Observed Monthly Ice Motions	B1

-1-

1. Introduction

To perform oil spill risk analysis, it is necessary to describe the behavior and fate of the spilled oil from the time of the spill until it is no longer a threat to the environment. This description takes the form of a prediction of the most likely set of events that will follow an oil spill. This prediction may be partly based upon past experience, but more often than not it will have to be based upon an understanding of the processes that take place and a predictive model of those processes. This is especially true in the Beaufort Sea off the north coast of Alaska. There has been no practical experience with large oil spills in this region, especially during the winter when the sea surface is ice covered. Since a great deal of exploration activity takes place offshore during the ice season, it is necessary to predict the behavior and consequences of an accidental oil spill by means other than observations of actual spills.

There have been several experimental studies of oil spill behavior in ice-covered waters (NORCOR, 1975; Comfort and Purves, 1980; Buist et al., 1981), as well as laboratory studies of the interaction of oil and ice (Cox et al., 1980; Cox and Schultz, 1981; Martin, 1977). Several studies have looked at the available data in an attempt to synthesize oil spill scenarios for the nearshore Beaufort Sea (Lewis, 1976; NORCOR, 1977; Thomas, 1980). The conclusion has been that in the case of an oil spill during the ice growth season, from October through May, the spilled oil becomes trapped in, on top of or under the ice. It is partly or wholly protected from much of the weathering that normally takes place when oil is exposed to the atmosphere until springtime, when the oil, even that frozen into place beneath the ice cover, collects on the surface of the ice. As the weather warms later in the spring, accelerated melting takes place, which results in oil, somewhat weathered by now, floating on the sea surface surrounded by individual ice floes. At this time, the oil can have a particularly severe effect upon biological activity in and on the open water. It is also possible after breakup for oil slicks to be driven up onto beaches.

One important conclusion of the scenario outlined above is that an offshore oil spill during the ice season will probably not have significant effects on the environment until breakup the following spring. Since most of the Beaufort

-2-

Sea ice cover is in continual motion, the effective springtime spill site can be far removed from the site of the accidental spill. To predict the possible consequences of an oil spill occurring at any location, it is necessary then to be able to predict the motion of the ice cover between the time of the spill and spring breakup.

The purpose of this study has been to predict typical wintertime ice motions for ice passing over potential oil spill sites for the continental shelf region of the Beaufort Sea off the north coast of Alaska. A limited amount of ice motion data does exist for the Beaufort Sea, but these data are insufficient for computing meaningful statistics of ice motions. Our strategy has been to develop an ice trajectory model that accounts for the essential physical processes of the ice cover and that uses environmental data for the driving forces. Available ice motion data are used to tune the trajectory model, thus the results are at least consistent with the observed motions.

2. Technical Approach

2.1 General Approach

The most reliable method of predicting typical oiled ice trajectories and expected variations in trajectories would be to perform a statistical analysis on a large sample of observed ice motions. Unfortunately, the sample size of observed ice motions in the Beaufort Sea is nowhere near large enough to give reliable statistics. An alternative approach was decided upon whereby a model of large-scale sea ice behavior was used to predict ice motions from observed winds. This approach also has difficulties in that little real time data exist on ice conditions and ocean currents, which are also important in determining ice motions. These difficulties were resolved in the following manner.

Ice response (motion) **fields** were computed for a range of driving forces and ice conditions. Ice conditions were varied from free-drift conditions (zero strength) to very high strength conditions (zero motion). Ocean currents were assumed to be the long-term mean geostrophic velocity field derived from the dynamic topography of Newton (1973). From previous model studies, we were able to estimate the approximate error in daily velocities due to variations in the currents. Real wind data were used, but to reduce the number of model calculations to a manageable number, the daily wind fields were clustered into 16 groups with the winds within each group being similar in speed and direction in the region of interest near shore.

These ice response fields were then combined to form typical ice trajectories. The ice response fields due to winds were combined so that the statistics of the sequence of winds used matched those of the data. The ice conditions for each wind pattern were determined by choosing proportions of different ice strengths so that the resulting trajectories best matched the limited number of observed trajectories.

A complete description of the procedure outlined here is contained in the following sections.

2.2 Ice Model

2.2.1 Quasi-steady Ice Model

The mathematical model of ice dynamics used in this work incorporates a momentum equation which balances the forces due to air and water traction,

Coriolis effects, sea surface tilt, and internal ice stress divergence. The model also requires a constitutive law relating the internal ice stress to deformations. For this study, quasi-steady calculations were done in which ice strength is constant and no ice redistribution or thermal growth is allowed. The strength of the ice is varied as a parameter in different simulations. It has been shown that this quasi-steady form of the ice model will, when given accurate daily average winds and currents, **accurately model** daily average ice velocities and motions (Pritchard et al., 1977).

The ice model used in this study is basically the one developed and tested during AIDJEX (Arctic Ice Dynamics Joint Experiment), and it has been described in detail many times (Coon, 1980; Pritchard, 1981). The quasi-steady form of the model and results of quasi-steady calculations are given by Reimer et al. (1980) and Pritchard et al. (1977). A brief description of this form of the model follows.

In the plane of motion of the sea ice, the momentum balance is expressed as

$$m\dot{\mathbf{v}} = \tau_a + \tau_w - mfk \times \mathbf{v} - mg\nabla H + \nabla \cdot \sigma$$

where

- m is mass per unit area of ice,
- v is velocity in the horizontal plane,
- $\dot{\mathbf{v}}$ is horizontal acceleration,
- τ_a is traction exerted by the atmosphere on the upper ice surface,
- τ_w is traction exerted by the ocean on the lower ice surface,
- f is the **Coriolis** parameter,
- k is the unit vector in the vertical direction,
- g is gravitational acceleration,
- H is the height of the sea surface, and
- σ is the **Cauchy** stress resultant in excess of hydrostatic equilibrium (two-dimensional).

The air stress is determined from the geostrophic wind in the atmosphere as

$$\tau_a = \rho_a c_a |U_g| B_a U_g$$

where B_a is a rotational operator, turning the air stress an angle from the **geostrophic** wind, ρ_a is air density, and C_a is the drag coefficient. **Since**

-5-

wind speeds are generally orders of magnitude larger than ice speeds, the **geostrophic** wind, $U_{\sim g}$ is used rather than the wind velocity relative to the ice. Values of the parameters used in this study were:

$$\begin{aligned} \rho_a &= 0.00143 \text{ gm/cm}^3 \\ c &= 0.008 \\ f^a &= 2 \Omega \sin(\text{latitude}), \Omega = 7.29 \times 10^{-5} \end{aligned}$$

The water stress is modeled as a function of the relative velocity between the ice and the **geostrophic** ocean current, but the relationship is not quadratic. A three-layer ocean consisting of surface and bottom logarithmic layers and an interior Ekman layer is assumed. In shallow, well-mixed waters, the presence of the bottom modifies the turbulence and velocity structures in the boundary layer. In general, the bottom effects result in an increased ice speed relative to the bottom for the same surface stress. In deeper waters, the bottom effects are not important for typical winds and ice motions, and the surface stress/velocity relationship is approximately quadratic. McPhee (1982) has described this drag law in detail. A similar drag law development is described in Overland and Pease (1982).

The sea surface tilt defines the ocean geostrophic current, $v_{\sim g}$, in the form

$$mgVH = -mfk \times v_{\sim g} .$$

The last term in the momentum balance is the divergence of internal ice stress. The stress state is related to the deformation history by material constitutive laws. An elastic-plastic model is assumed which is made up of the following three elements: (1) a yield surface, (2) a flow rule, and (3) an elastic response. No plastic hardening occurs since a constant strength is assumed for each simulation.

The stress state, v , in a plastic model is constrained to lie within a function called the **yield** surface. For an isotropic model, this function depends only on the stress invariants and not on the principal direction. This constraint is

$$\phi \quad \sigma_I, \sigma_{II}, p^* \leq 0 \quad ,$$

where $\sigma_I = \frac{1}{2} \text{tr } \sigma$ (negative pressure), $\sigma_{II} = \frac{1}{2} \text{tr } \dot{\sigma}'\dot{\sigma}'^{1/2}$ (maximum shear), and $\dot{\sigma}' = \frac{\dot{\sigma}_I}{\sigma_I}$. The yield constraint may depend on other state parameters, in particular, the isotropic compressive strength, p^* . The yield surface **preferable** for sea ice (Pritchard, 1978) is shown in Figure 1. The stress invariants are constrained to be within the triangle for a given value of p^* . Along the straight-line portion of $\phi = 0$ passing through the origin, the stress state is that of **uniaxial** compression. The other straight line used to complete the yield surface is chosen for simplicity.

When the stress state in the ice lies inside the yield surface, then the stress, σ , is an isotropic function of the elastic strain, e :

$$\underline{\underline{\sigma}} = M_1 - M_2 \frac{1}{\underline{\underline{\sigma}}_I} \text{tr } \underline{\underline{e}} + 2 M_2 \underline{\underline{e}}$$

where M_1 and M_2 are elastic moduli set at 2.0×10^9 and 1.0×10^9 dyn/cm, respectively. The elastic strain satisfies the kinematic relation

$$\dot{\underline{\underline{e}}} = \underline{\underline{W}} \underline{\underline{e}} + \underline{\underline{e}} \underline{\underline{W}} = \underline{\underline{D}} - \underline{\underline{D}}_p$$

where the stretching $\underline{\underline{D}} = \frac{1}{2} (\underline{\underline{L}} + \underline{\underline{L}}^T)$, the spin $\underline{\underline{W}} = \frac{1}{2} (\underline{\underline{L}} - \underline{\underline{L}}^T)$, and the velocity gradient $\underline{\underline{L}} = \text{grad } v$.

When the stress state is on the yield surface $\phi = 0$, plastic stretching occurs. As plastic flow occurs, the stress is constrained to the loading surface by the occurrence of plastic stretching $\underline{\underline{D}}_p$. The associated flow rule $\underline{\underline{D}}_p = \lambda \frac{\partial \phi}{\partial \sigma}$, $\lambda > 0$ requires that plastic stretching be orthogonal to the loading function-at the instantaneous stress state.

The model equations are integrated using a finite difference scheme described by Pritchard and Colony (1976). The finite difference grid used in the calculations is shown in Figure 2.

2.2.2 Free-Drift Ice Model

During free-drift, motion of the ice cover may be determined by considering momentum balance locally. The forces acting on the ice cover are air stress,

τ_a ; water stress, τ_w ; Coriolis force, $-mfk \times v$; and sea surface tilt, $-mg\sqrt{H}$.
 Momentum changes then occur as

$$\dot{mv} = \tau_a + \tau_w - mfk \times v - mg\sqrt{H} .$$

The ice velocity may be determined at each point as a function of time whenever the barometric pressure field history is prescribed. The results sought have a time resolution of one day. For this case, inertia is negligible. Therefore, the analysis is performed for steady-state conditions.

A more complete description of the free-drift model and comparisons of model results with observations may be found in many sources. A partial list includes McPhee (1980), Thomas and Pritchard (1979), and Pritchard and Kollé (1981).

2.3 Driving Forces

2.3.1 Winds

One of the important forces that acts on floating sea ice is that exerted by the winds. The winds, due to their day-to-day and seasonal variability, are also the major source of variability in ice motion.

To drive the ice model, the average daily atmospheric pressure fields for the years 1979 and 1980 as reported by Thorndike and Colony (1980, 1981) were used. From the pressure fields, P the geostrophic and surface winds for the Beaufort Sea were computed:

$$u_g = \frac{-1}{\rho_a f} k \times \nabla P .$$

While only two years of data were used, these data were accurate, which may not be the case for other historical data for the Beaufort Sea. To assure ourselves that these two years of data were sufficient to derive reliable statistics, we compared the derived surface winds at 150° W, 71° N with the wind statistics for Lonely (in Brewer et al., 1977). The winds at Lonely were used for comparison instead of those at the closer station at Oliktok because the Lonely winds are affected less by the mountain barrier baroclinity effect (Kozo, 1980). The wind speed and direction histogram for Lonely is the average of the 12 monthly histograms from Brewer et al. (1977). The comparison of

-8-

derived surface winds with these annual statistics is shown in Figure 3. A comparison by season showed slightly more differences than is apparent in the annual statistics. While some of the differences are undoubtedly due to real differences in the samples, there are also differences due to geographical location and due to the difference between measured surface winds and winds calculated from daily average pressure fields. The 1979 and 1980 winds were thought to be sufficiently representative of recent historical winds, so no further effort was spent on improving the wind sample. It should be pointed out that since this study began, the 1981 sea level **pressure** data from the Arctic Ocean Buoy Program have become available (Thorndike et al., 1982) and more data are being collected during 1982. In addition, historical sea level pressure fields for the northern hemisphere are now available through the National Center for Atmospheric Research (Jenne, 1975). Though the data are available to improve the wind statistics we used, the improvement would be insignificant, and differences in the resulting ice trajectories would be masked by uncertainties in ice conditions. Further refinement of our wind statistics would, however, be useful for observing any long-term trends or cycles. The estimation of year-to-year variability in ice motions might also be improved if the more unusual periods were included, such as during the summer of 1975 and again the following winter when extreme ice conditions and motions were observed.

The ice model described above determines the response of sea ice to winds. This response is nonlinear, both in speed and direction. Therefore, it is desirable to retain as much variation as possible in the winds used to drive the model. On the other hand, an infinite variety of wind patterns and speeds occurs in the Beaufort Sea, making it impossible to model the ice response to every possible wind. We decided to form groups of similar wind patterns rather than to use an overall mean wind field or monthly mean wind fields. An attempt was first made to cluster the winds according to the pressure pattern over the Beaufort Sea, but the results indicated that either a very large number of groups must be used, or that each of a smaller number of groups must contain some within-group variability. The final clustering of winds was done according to the speed and direction of the surface winds near the north coast of Alaska at 71° N and 150° W. Wind direction was grouped into eight equal

-9-

direction categories, and wind speed was grouped into six intervals of 2 m/s: 0-2, 2-4, 4-6, 6-8, 8-10, and greater than 10 m/s. The resultant wind groups had reasonably small within-group variances in the region of interest near the Alaskan coast. Further away from shore, the within-group variability was relatively large but still acceptable, since the means were still consistent with the mean winds near shore and the more variable winds were far enough from the region of interest to have only minimal effects on computed ice motions.

Of the 48 possible wind groups (8 directions by 6 speeds), many groups contained none or only a fraction of a percent of the observations. It was decided to ignore these groups, since the effect of including them in the model would be insignificant in comparison with the uncertainties that would result from lack of data on other parameters. Furthermore, all the winds less than 2 m/s were combined into one group without regard to direction, since those winds would have little influence on ice motions. The final result was 16 groups of wind patterns as shown in Figure 4. After classifying each daily wind field into one of these 16 patterns (neglecting the small number of days which did not fit into these 16 patterns), the mean wind field for each group was computed. In Figure 5 we show the mean wind field and 50 percent **equi-**probability ellipses for the 16 groups. We note that near shore the variability is quite small, while in the northern Beaufort Sea the mean winds are relatively small and the variability is large.

There are several sources of error inherent in the wind grouping we have used. First, we chose to not use the total mean wind because of the nonlinear ice model. While each of the 16 groups selected to drive the model are considerably less variable than all winds are, the within-group variability does mean that a nonlinear model will not give the correct response. Thomas and Pritchard (1979) showed that free drift (which causes a majority of the ice motion) is nonlinear but that for larger wind speeds (greater than about 4 m/s), ice speed is nearly linearly related to wind speed, although the direction of ice motion during free drift continues to change with wind speed. Thorndike and Colony (1982) have estimated that over 70 percent of the variance in ice drift can be explained by a linear relationship between geostrophic winds and ice motion. Thus, the relatively small variability within each wind

-10-

group, combined with a nearly linear relationship (in speed), will result in insignificant errors in ice speed and only a few degrees of error in direction. In a later section of this report, we present the results of an analysis of the effect of the within-group variability in winds on ice motions for one of the wind groups.

Another possible source of error in the mean wind fields is that we neglected a few cases where the winds were very large in magnitude because of their low probability of occurrence. These large winds can cause a significant amount of ice motion. Part of this motion would be canceled because of the variability in direction of the larger winds, and the remainder, while significant as a daily motion, would only contribute an average of a few kilometers per month to the ice motions. **Over** an ice season, the motion caused by large winds would likely be noticeable in the ice trajectories, but the same effect on ice motions can be achieved with smaller wind magnitudes and lower ice strength. Since we can only approximate ice strength very coarsely, the effect of neglecting high wind speeds will not be observable in our results.

An important and real source of variation in sea ice motions caused by winds results from the temporal variation in the percentage of winds occurring from each group. The sequence of the wind patterns will also affect ice motions due to the spatial variation in the wind fields. These effects were accounted for in the computations of ice trajectories by using wind transition matrices. Four transition matrices were developed, one for each season. The division into seasons was done according to the similarity of the occurrence of winds during each month over the two years of our sample. These transition matrices show the probability of occurrence of each wind group following the occurrence the day before of every other wind group. That is, given that today the wind falls in group 1, the matrices give the probability of tomorrow's winds being in group 1, 2, 3, etc. Thus, it is possible to generate a sequence of random numbers with the same statistics as the observed sequence of wind patterns. To initiate the sequence of random numbers, another random number can be generated with the same probability of occurrence as the proportion of winds in each group during a season. Assuming that 1979 and 1980 were representative years as far as the winds in the Beaufort Sea are concerned, we were able to generate random sequences of wind patterns with the

-11-

same statistics as the real winds. The seasonal wind transition matrices are presented in Tables 1, 2, 3, and 4. Since we are sampling a uniformly distributed random number for the proportion of winds in each group, the sampled proportions **will** have some variation about the true proportion. For a sample of size 30 (one month's sequence of winds) the standard deviation of the sample proportions will be 0.09 [when $p=(1-p)=0.5$] or smaller. For trajectory calculations lasting several months, the standard deviation, computed as $SD = \sqrt{p(1-p)/n}$, will be smaller. This variation between samples (trajectories) of the proportions of winds from each group is acceptable since the proportion of actual winds will also vary from year to year.

2.3.2 Model Boundary Conditions

When the ice strength is zero, i.e., during free-drift conditions, ice motions are determined solely by a balance of forces acting locally on the ice. When ice conditions are such that the large-scale ice strength is significantly different from zero (greater than about $1.0 \times 10^7 \text{ dyn/cm}$), the far-field winds and resulting ice motions can have an increasing effect on ice motions in the region of interest. Ice conditions near shore **will** also affect ice motions away from shore when the motions have an onshore component. To account for these far-field and fixed-boundary effects, the ice model uses a prescribed boundary condition, the velocity of the boundary in the present case. These prescribed boundary motions were taken from the same data set as the winds used to drive the model, namely, the drifting buoys deployed during 1979 and 1980 as part of the Arctic Ocean Buoy Program (Thorndike and Colony, 1980, 1981). Average daily boundary velocities were interpolated from the average daily velocities of the same set of buoys that measured the sea level atmospheric pressure used to derive the wind fields. These daily boundary velocities were grouped and averaged in the same 16 groups as the winds were. The mean and 50 percent equiprobability ellipses of the boundary velocities for the 16 groups are shown in Figure 6. The boundary velocities interpolated from the buoy data were not as accurate as the winds used, but they have the important advantage of being consistent with the winds. The boundary motions also take into account to some degree the actual large-scale ice strengths **effective** from day to day. One of the major reasons for using only the 1979

-12-

and 1980 wind data instead of many more years of historical winds was the presence of these consistent ice motion data that could be used to drive the boundary of the ice model.

A zero-velocity boundary condition was used in the model for the Alaskan coast and along Banks and Prince Patrick Islands.

2.3.3 Ocean Currents

The ocean currents are also a source of variability in the computed ice trajectories. The currents used in the model calculations can be divided into two parts, a geostrophic velocity field in the Canada Basin, which was originally derived from the dynamic topography of Newton (1973), and a **shelf-break** current jet described by Aagaard (1983). McPhee (1982), included as Appendix A in this report, describes the inclusion of these ocean currents in the ice model. For the trajectory calculations, we included the effects of the geostrophic currents offshore as part of the long-term transport mechanism, but treated the shelf-break current jet as a source of variability in the computed trajectories.

We have considered the shelf-break current jet (called the Beaufort Current by Aagaard) as a source of error or variability in the computed trajectories rather than as a driving force. The direction of the Beaufort Current reverses frequently, having a **bimodal** distribution. Approximately half the time the current flows eastward with a mean speed of 15 to **25** cm/s, and the rest of the time it flows westward at a mean speed of 10 to 15 cm/s. Much of the time, during changes in direction, this current is very slow. Overall, a long-term mean of about 7 cm/s eastward results. This jet is relatively narrow, though, and does not affect ice motions away from the shelf break to any significant extent. During periods of free-drift ice motion, the current does have a pronounced effect on local ice motions. Using extreme values of the current of 40 cm/s eastward and 30 cm/s westward, a potential difference in ice velocities of 70 cm/s can exist, or about **60 km/day** in ice motion. This does not mean that there is an uncertainty in long-term ice motions of **60 km/day**. Obviously, since the current frequently reverses, the long-term uncertainty in ice motion will be dependent upon the variability of the current itself. The long-term mean current of about **7 cm/s** to the east can affect ice motions,

-13-

mostly during periods of free drift, but the effect is probably not apparent in long-term ice motions. The currents will cause ice motions under some ice conditions, but the ice motions, especially localized motions, will tend to change the ice conditions, making the compacted ice cover better able to resist further motions. That is, during the winter ice season, the ice cover **itself** tends to reduce the effect of any local perturbation in driving forces on the ice.

While we used a free-drift model to compute ice velocity fields to use in the trajectory calculations, it should be noted that these free-drift velocities were only an approximation to the velocities resulting from a large range of ice strengths. Ice strengths ranging from zero to about 1.0×10^7 dyn/cm result in approximately the same velocity fields. In the real world and in full time-dependent model calculations, however, this range of ice strengths results in different long-term ice motions. The higher strength ice cover will, under conditions where the ice cover converges, quickly become stronger with a resulting reduction in ice motion.

The Beaufort Current will play a more important role in the motion of oil slicks during the summer when open water and/or a loose, unconsolidated ice cover is present.

2.4 Ice Conditions

The response of an ice cover to the winds depends upon some ice strength parameter (p^*) that is a function of the thickness distribution of the ice cover. The ice strength is particularly sensitive to the amount of thin ice and open water present. It is generally assumed that sea ice has no **large-scale** tensile strength.

During periods when a great deal of thin ice and open water is present, the large-scale ice strength is small, the ice cover will not support stresses, and the ice responds to the winds and currents freely. This condition only occurs during the summer when the ice concentration **is** low (floes do not touch) and open water exists in the leads. During the ice season, when open water quickly freezes into thin ice, periods of zero ice strength occur only rarely, but model runs with ice strengths of up to about 1.0×10^7 **dyn/cm** show that the ice response (velocities) differs insignificantly from the response at a strength of zero. For a wide range of ice conditions, then, the effects of

-14-

ice conditions on ice motion are minimal. Data seem to support this observation. Thorndike and Colony (1982) found that for the central Arctic Ocean, over 70 percent of the variance of ice velocities is explained by the **geostrophic** winds through a linear relationship, which is an approximation to free drift for larger wind speeds. It is assumed that part of the remaining variance is due to stress gradients within the ice cover.

There have also been times when the ice cover was observed to remain motionless even though strong winds were blowing over a large fetch. Pritchard (1978) estimated that the ice strength during one such event must have been at least 1.0×10^8 **dyn/cm**. Although larger winds than those observed during that period (about 10 m/s) may have caused additional ice motion, those larger winds are relatively rare. For the range of wind speeds used in the present study, we assumed that an ice strength of greater than 1.0×10^8 dyn/cm would result in no ice motion.

We therefore have essentially three ranges of ice conditions which result in different responses to applied wind loads. The first set of ice conditions result in large-scale ice strengths of from zero to 1.0×10^7 **dyn/cm**, and the ice response is essentially free drift. For strengths above about 1.0×10^8 dyn/cm, the ice is assumed to be able to almost completely resist wind forces, with little motion resulting. It is in the strength range from 1.0×10^7 to 1.0×10^8 **dyn/cm** that ice response is most affected by changes in ice conditions. Since there have been very few measurements made of actual ice thickness distributions over the Beaufort Sea, it is difficult to predict the spatial and temporal variations in ice conditions in sufficient detail to describe the distribution of ice strengths in the critical range.

Our strategy has been to assume an ice strength of 5.0×10^7 **dyn/cm** as representative of the range from 1.0×10^7 to 1.0×10^8 **dyn/cm**, and to let the differences in ice response at low, medium, and high ice strengths be the residual uncertainty in ice response due to variations in strength. This uncertainty is actually a range of possible ice responses, though, and probably represents only extreme events. The winter of 1975-76 appears to be such an extreme event where, for several months, ice motions were much smaller than for other years. This is unfortunately the time of the AIDJEX experiment, when most of the available data on ice motion was collected concurrent with -accurate wind **fields** and ice thickness information.

2.5 Procedure for Calculating Trajectories

The procedure used for calculating ice trajectories was to first calculate a set of ice responses for each of a set of combinations of ice conditions and wind fields. For each trajectory to be computed, a sequence of randomly chosen numbers corresponding to the different wind fields was chosen in such a way that the sequence had the same statistics as the sequence of winds during 1979-80. Different statistics were used for each season. This set of numbers determined the sequence of wind fields and thus partly determined the ice response. To choose between different ice conditions that might exist for each wind field, and thus complete the determination of ice response, a separate sequence of random numbers was chosen representing different ice conditions. This sequence was not chosen to satisfy some a priori condition or statistic, but was the result of a trial and error process. For each season, a set of ice conditions was chosen so that the statistics of computed monthly displacements best fit the observed monthly displacements. This "best fit" was done in a subjective manner, since few data were available in the area of interest near the coast and we knew that our calculated trajectories were more unreliable further from shore. Finally, some of the ice response fields were modified to better account for the effects of the coast and the developing fast ice zone. These modifications were seen to also improve the comparison between computed and observed displacements.

The following ice response fields were used to compute anticipated ice trajectories:

- 1) Quasi-steady velocity fields, one for each of the 16 wind patterns for ice with thickness of 300 cm and a strength of 5.0×10^7 dyn/cm. These 16 velocity fields are shown in Figure 7.
- 2) Free-drift velocity fields, one for each combination of the 16 wind patterns and ice thicknesses of 50, 150, and 300 cm. The 16 velocity fields for an ice thickness of 300 cm are shown in Figure 8. The velocity fields for other thicknesses are similar to these.
- 3) Velocity field of zero velocity representing ice conditions where strength is so high (greater than about 1.0×10^8) that the ice is essentially motionless.

-16-

To account for a varying average ice strength through the ice season, we combined various proportions of the low-strength (free-drift), medium-strength (5.0×10^7 dyn/cm) and high-strength (zero motion) ice velocity fields so that the resulting statistics of ice motion best agreed with the limited amount of observed ice motions. For the fall period (October and November) 80-percent free drift and 20-percent medium strength were found to give the best fit. For the winter (December through March), 70-percent free drift and 30-percent medium strength were used. In the spring, (April and May), 20-percent free drift and 80-percent medium strength were used. In the summer (June through September) 100-percent free drift was used. The inclusion of high-strength ice responses was a modification made to some of the ice response fields to account for an increasing ice strength when the winds blow toward shore.

To simulate the effect of increasing ice strength near the coast when winds blow onshore, we arbitrarily increased the ice strength one category whenever ice motions were toward shore. That is, in place of free-drift motion, a motion corresponding to a strength of 5.0×10^7 dyn/cm was used, and when the medium-strength (5.0×10^7 dyn/cm) motion was called for, the high-strength motion (zero motion) was used. This procedure tended to reduce the ice motion, but the majority of the reduction was in the shoreward component. Not only did the results conform more closely to our notions of how the ice behaves near shore, the agreement with observed ice motions improved considerably. During the months of October and November, this increase in ice strength is probably not justified, since the thin ice during this period is less able to resist shoreward motion. We did not treat these months differently, however, since the occurrence of onshore winds was low during the fall.

Ice thickness was not varied for ice strengths greater than zero (free drift) since it was determined that doing so would result in insignificant changes in ice motion. For free-drift velocities, ice mass has a small effect on the angle between the ice motion and the wind, so thickness was allowed to vary seasonally. During October and November, a thickness of 50 cm was used, representing mostly thin ice with some **multiyear** ice and ridges present. A value of 150 cm was used during December through March, representing the increasing thickness through thermal growth and deformation. In the spring, a

-17-

value of 300 cm was used for the same reason. One can reasonably argue that these values are wrong, especially since no spatial variation was allowed; however, they are approximately correct for the southern Beaufort Sea, assuming growth rates of 1 cm/day and that about 5 percent of the area is always open water or very thin ice and about 5 percent of the area is ridges. More importantly, the effect of small changes in ice mass on ice velocity fields is small and, while seasonal changes may be important, monthly changes or errors of a few tens of centimeters are accounted for in the overall error of the ice model.

On the fixed boundary along the north coast of Alaska, ice velocities were assumed to be zero, except in one case. During the fall, when the ice cover near the coast is generally thin, it may be moved about by the winds. To account for this, we computed free-drift velocities for the region nearshore for the months of October and November and assumed that the nearshore ice could drift as freely as the ice further offshore.

After November, though, all ice velocities were assumed to be zero at the shoreline. At the first row of computational nodes, about 50 km offshore, the computed ice velocities were assumed to hold. Between the shore and this first row of computed velocities, we linearly interpolated velocities. One result of this is that, after the fall season, the ice near shore moves slower than ice further from shore. Observations of nearshore ice indicate that generally the ice remains in contact with the shore through most of the ice season, and that a great deal of shearing takes place seaward of the shorefast ice. Ice motions measured by the few buoys deployed on the ice in this region indicate that motions near the Alaskan coast tend to be small during most of the year. So, in general, we feel the method we used to treat motions near shore approximates reality. Some improvement could be made by using a finer scale grid near shore and by using a more detailed division of ice strengths, but on the basis of several test runs using a finer grid or different ice strengths, the improvement was hardly noticeable.

The method of accounting for shorefast ice in the trajectory model was also somewhat arbitrary, but was based upon what is presently known about the development of the fast ice zone. The following scenario is typical of the formation and growth of the fast ice zone.

-18-

Early in the fall, the area near shore is usually nearly ice free, with **the** ice edge (area with more than 50 percent ice cover) lying from 100 to 200 km offshore (Webster, 1982). During the first two weeks of October, temperatures drop enough to cause ice to begin to form on the surface. This early ice cover is thin and subject to movement and deformation by moderate winds. Some of the ridges that are formed near shore become grounded in the shallow water. These grounded ridges tend to anchor the surrounding ice and to protect the inshore ice from forces exerted by the moving pack ice. The thickening ice sheet near the shore also becomes strong enough so that eventually it is not moved by the winds acting over a fetch limited by the shore, by barrier islands, and by grounded ridges. **By** early December, there is usually a region of fast ice near shore that does not move until breakup (Barry, 1979). As the winter progresses, more ridges are built in the region where the moving pack ice interacts with the motionless fast ice. Some of these new ridges also become grounded, extending the fast ice region seaward. Studies using satellite images show that this system of large grounded ridges extends out to about the 20-m **isobath** (Stringer, 1978, 1982). Studies of the scour marks on the sea floor (Reimnitz et al. , 1978) also indicate that the 20-m **isobath** is approximately the limit of the bottom-anchored fast ice zone.

The development of the fast ice zone is more or less a sporadic process that continues throughout the winter. It is not continuous since individual storms that cause ice motion and deformation are responsible for a large part of the fast ice extension. There is also a great deal of geographical variation in the extent of the fast ice zone , as well as variations from year to year.

For the trajectory model, we included the extension of the fast ice zone in the following manner. During October and November, there is assumed to be no fast ice. Ice near **shore is** allowed to move, but the motions are generally small for reasons mentioned above. On 1 December, **we** assume that all ice shoreward of the 10-m **isobath** becomes fast due to ridges becoming grounded out to water depths of 10 m. Ice inside the 10-m **isobath** does not move, and ice outside cannot move into water less than 10-m deep. On 1 March, the fast ice zone is assumed to move all the way out to the 20-m isobath as new ridges are built and become grounded. Allowing for the actual variation in the extent of

-19-

fast ice from year to year and from area to area, our method, while only a coarse approximation, is a reasonable one. The approximate locations of the 10- and 20-m isobaths used are shown **in** Figure 2.

3. Results

3.1 Seasonal Ice Trajectories

The final results of this study consist of a set of 2250 ice trajectories. These trajectories are divided among 30 different launch sites and three different ice seasons. The 30 launch sites are shown in Figure 9. Beginning on 15 October, 30 trajectories were computed originating from each launch site. These 900 trajectories were continued until 1 August if possible. Trajectories that left the computational grid at the western boundary before 1 August were ended at that date and location. A tracked ice particle that lay within the 10-m **isobath** by 1 December or the 20-m isobath by 1 March was considered to have become incorporated into the shorefast ice, and the trajectory was terminated at that point.

On 1 December, another 30 trajectories were begun at each of the 26 launch sites that lay outside the 10-m **isobath**. Ice located at the remaining four sites in shallow water was assumed to be within the fast ice zone, remaining motionless until spring breakup. The 780 trajectories beginning in winter were also continued until 1 August, except for those that left the computational grid before then or lay inside the 20-m isobath by 1 March.

At the start of the spring season on 1 April, the fast ice zone includes all ice inside the 20-m **isobath**; at this time, 11 of the launch sites lay within this zone. Another 30 trajectories were begun at each of the remaining 19 launch sites and were continued until 1 August, except, again, for those trajectories that left the computational grid. None of these 570 trajectories were incorporated into the fast ice since the model assumed that the fast ice had reached its outermost extent by 1 March.

The distribution of trajectory end points for each of the three starting seasons, fall, winter, and spring, is shown in Figures 10, 11, and 12, respectively. The locations of each ice particle at 1-day intervals along the trajectories were also computed, but are not displayed.

Several general observations can be made regarding the distribution of trajectory end points and the typical trajectory path. The general trend of ice motions in the southern Beaufort Sea is westward, following the direction of the Beaufort Gyre and the modal winds. The long-term ice displacements seem to have an onshore component along the Alaskan coast except near

-21-

Point Barrow where a northward, offshore component is evident. These modeled motions agree with observed ice motions. A full range of ice motions is displayed by the modeled trajectories, from no motion or even a slight net eastward motion during a month to about 300 km of westward motion. This is also about the range of observed monthly displacements.

3.2 Variability in Modeled Trajectories

If one were to place a buoy on the sea ice every year at the same geographical location and at the same time, the buoy would in general describe a different trajectory each year. By doing this enough times at enough different locations, one could calculate the mean and variability of the ice motion field for the Beaufort Sea. The confidence limits of these statistics would depend upon the number of repetitions of the experiment, assuming that the errors in locating the buoy's position is small. While a great deal of buoy data has been collected in the Beaufort Sea, the total number of buoys passing through each small region of the Beaufort Sea during each small time segment of the year is too small to provide accurate statistics of ice motion.

Another method of getting ice trajectories from which statistics of ice motion can be estimated is to use an ice model and real environmental data to hindcast historical ice motions. Unfortunately, no perfect model of sea ice exists and, more importantly, a complete environmental data set for driving an ice model does not exist. The only realistic approach, then, is to use the data that exist to drive the best model available, and then to estimate the total error due to variations in the driving forces and incorrectly modeled processes.

The best model available is the one developed during AIDJEX, which is described in Section 2. Typical errors in ice motion using this model have been shown to have a standard deviation of about 3 km/day with a mean daily error of about 1 km/day for daily motions (Pritchard and Kollé, 1981). Over a period of N days, the mean error accumulates as N times the mean and the standard deviation according to N times the standard deviation. Over a period of six months, substantial errors can occur. The mean difference in modeled versus actual trajectory end points would be 180 km, with a standard deviation of about 40 km. Of course, accumulating the mean in this manner

-22-

assumes that the error in direction is constant each day. It is probable that, while the magnitude of the daily velocity error averages 1 km/day, the **direction** may vary so that over long periods of time, the total error in displacement will be much smaller than N days times 1 km/day. Insofar as possible with the limited number of observed ice trajectories available, we adjusted our trajectory model so that for periods of one month, the mean of computed monthly trajectories **nearly** matched the mean of observed motions. While we do not claim to be 100 percent successful in this, we do feel that the standard deviation does more nearly represent the actual variation between computed and actual ice motions due to inaccuracies in the model. It might be noted that some of this variability will be due to inaccuracies in the data used to drive the model, so a standard deviation of 3 km/day is probably a maximum error due to the sum of errors in the model, the errors **in** the daily winds, and errors in the mean ocean current field.

Another source of variation that we are able to account for in the trajectory model is that due to the use of mean winds rather than daily winds to calculate the daily ice motions. Due to ice strength, and the ability of ice to transmit stresses when strength is high, the ice cover may at times be determined more by the boundary motions than by the local winds. We also used mean boundary motions in the model, so, while we discuss the error due to the use of mean wind fields, the errors are partly due to using the corresponding mean boundary motions.

For one wind group, that with the largest magnitudes, we examined the variability in ice motions due to within-group wind variability and the nonlinear ice model. Both the quasi-steady and free-drift models were run using each of the daily wind fields that made up the group, as well as the group mean wind field. In Figure 13, we show the mean and 50 percent **equi-**probability ellipses of the daily ice motions for a strength of 5.0×10^7 **dyn/cm** and, in Figure 14, the ice motion field computed from the mean wind field is shown. Daily and mean boundary motions were used along with the daily and mean winds. In Figure 15 we show the mean and 50 percent **equi-**probability ellipses of the daily ice motions for a strength of zero (free drift) and, for comparison, the ice motion field computed using the mean wind field is shown in Figure 16. Again, the appropriate daily or mean boundary

-23-

motions were used. The model results shown in Figures 13 through 16 contain a constant angular error, which caused these results to not conform to any of the other modeled motions; however, this error does not affect the comparison illustrated in Figures 13 through 16. The within-group standard deviation of daily displacement for this wind group is approximately 3 km/day for both ice strengths. A small difference between the mean of 20 daily displacements and the displacement calculated using the mean wind is evident, but the difference is relatively small and can be assumed to be partly canceled when all 16 wind groups are considered. The within-group variation for the other 15 groups was not calculated, but would in general be smaller than that for this group since the ice motions are generally smaller. We therefore considered 3 km/day to be the standard deviation of daily ice motions resulting from the use of group mean winds instead of daily winds. The standard deviation of errors resulting from the model itself and inaccuracies in daily driving forces was also shown to be about 3 km/day. Combining the two standard deviations, each equal to 3 km/day, we get a standard deviation of $3\sqrt{2}$ or about 4.25 km/day. Over a six-month period, this will accumulate to about 57 km. The uncertainty will likely be greater than this in the east-west direction and smaller in the north-south direction, but resolutions of these kinds of differences do not seem appropriate.

There are other uncertainties in the calculated trajectories that we are not able to estimate reliably. The two major ones arise from variations in the ocean currents and from unknown statistics of ice strength. Theoretically, there may be "extreme event" situations where the extreme range of these conditions is felt. During periods of low ice concentration, the range of velocities that the Beaufort Current jet experiences can cause differences in daily ice motions of as much as 60 km. These differences are not to be expected, however, during the ice season. The occasional reversing of the Beaufort Current itself will tend to cancel part of the ice motion it may cause. The presence of a solid ice cover, which will be able to resist forces exerted over the relatively small area of the current jet, will tend to reduce the effect of the current. Although we are not able to accurately estimate the variation in ice motion due to the Beaufort Current, we see no reason to expect that variation to be comparable with the variation caused by the winds or by ice conditions.

-24-

It is possible to estimate the range of ice motions resulting from the range of possible ice conditions. These are just free-drift motion when ice strength is low, and no motion at all when ice strength is very high. Thomas and Pritchard (1979) have calculated this range of motion for the Beaufort Sea using historical wind data. Those historical free-drift motions compare reasonably well with the trajectories computed in this present study. The historical free-drift motions were also alongshore toward the west, they were generally larger than the motions computed in this study (which were not entirely free drift), and the year-to-year variability in historical free drift is comparable to the variability found in this work. One major difference can be seen, though: the historical free-drift motions tended to be to the right of the motions found in this study. Two obvious explanations are possible. First, the historical winds were computed from sea level pressure analysis that likely to be in error for the arctic regions due to lack of input data. The pressure data available from the Arctic Ocean Buoy Program which were used in this work, were much more accurate. It is a different data set though, so some of the differences may be due to sampling. Another reason for the differences in historical free drift and the modeled trajectories reported herein, is that the ice motions in this study were not entirely free drift. Part of the motions were due to the effects of boundary motions and ice strength. The boundary motions are the result of far-field winds when ice strength is significant. This effect is minor though, when trajectories were computed using 100 percent free-drift, the motions were still to the left of those reported for historical winds.

4. Comparisons With Observations

The lack of observed ice motion data, especially in the southern Beaufort Sea, makes comparisons between observations and model results difficult. The proper statistical comparison would require many observed, long-term (month or longer) ice trajectories in one relatively small area. These are not available. The observed trajectories are spread over the entire Beaufort Sea, with the fewest observations in the area near shore where the model is most applicable. In addition, a large proportion of the nearshore observations was taken during the 1975-76 AIDJEX project. Comparison of observed motions during that ice season with observations from other years strongly suggests that anomalous winds and/or ice conditions prevailed during that ice season. It is well-known that the summer of 1975 was a bad year for shipping along the Beaufort Sea coast due to heavy ice near shore.

One method of making comparisons is to model the motion of individual buoys using an ice model and real data. This has been done in previous studies (see Pritchard and Kollé, 1981, for instance) using the same ice model used in this study, and is not repeated here.

The complete trajectory model used in this study made use of that ice model to produce ice response fields, which were then combined in a stochastic model to produce a distribution of ice trajectories. This stochastic trajectory model was "tuned" by comparing resultant ice trajectories with a subset of the observed ice motions. The comparison was done in the following manner. From the observed monthly ice motions, a sample of observations was chosen and plotted. These observations were selected to be as near the region of interest as possible, and only a limited number of observations were selected from any one ice season to avoid biasing the observations toward possibly anomalous years when, by chance, more data were available. For instance, only one observation from any month would be chosen and a random sample of spatially distributed computed trajectories would also be plotted for comparison. Seasonal comparisons could then be made. As an example, we have plotted monthly trajectories originating at each launch point used in this study. The monthly trajectories for winter, spring, summer, and fall are shown in Figures 17 through 20, respectively. The trajectories may be compared with the observed monthly trajectories plotted by season as shown in Appendix B of this report. For any one year, it will be possible to find some computed trajectories which agree with the sense of the observed motions.

5. Discussion

The results of this work are useful as an aid in predicting the ultimate fate of oil spilled during the ice season in the Beaufort Sea. Inside the fast ice zone the best prediction is that spilled oil becomes incorporated into the ice cover soon after the spill occurs, and that the oiled ice will remain in the ice with no significant ice motion occurring until spring breakup. As temperatures rise in the spring, oil is released from the ice, first onto the ice surface and then, as breakup continues and the ice melts, into the ocean. In general, wintertime oil spills in the fast ice zone become open-water spills at breakup in the same vicinity as the original spill. The primary differences are that the oil will have weathered some-what before being released into the water and that the ice cover will be broken up.

Early in the ice season, while the fast ice zone is covered with thin, newly formed ice, significant ice motions are possible. Accounts exist of the newly formed ice cover being blown out to sea. No ice motion data have been taken for the newly formed ice in the fast ice zone early in the ice season. The modeled trajectories, however, show that there is a tendency for the ice to be held against the shore by the prevailing winds. Seaward ice motions do occur in response to specific storm events, but longer term wind patterns tend to move the ice back toward shore. Ice deformation will take place during these back and forth motions, with some possibility of oiled ice being built into ridges.

Outside the fast ice zone, the same processes of incorporation into and release from the ice take place in the event of an oil spill, but significant motion of the oiled ice will usually have occurred. . Again, very **little** ice motion data exist for the area between the fast ice zone and the polar pack ice zone. This area, the seasonal pack ice zone, lies within the 100 to 200 km region offshore that is mostly ice free during the late summer but is covered by a solid ice cover the rest of the year. This is the area where much of the oil exploration and development may take place, where, in the event of an oil spill, significant ice motions will occur, and where data on ice motions are most sparse. The ice trajectory model developed during this study was designed to predict typical ice motions in this region.

-27-

The computed trajectories reported here show that the ice has a long-term motion toward the west, with occasional eastward motions for short periods of time. The average westward motion is about 3.7 km/day during the fall, 1.3 km/day during the winter, 2.1 km/day during the spring, and about 3.6 km/day during the early summer. These motions are for the launch points outside the 20-m **isobath** and east of Point Barrow. There is a great deal of variation in the motions, amounting to a standard deviation of daily motions of about 5 to 10 km.

The motions near shore are smaller than those further offshore, but this is mostly a result of the model design.

Along with the westward motion, the ice tends to be forced shoreward along most of the north Alaskan coast, with more northward motion occurring west of Point Barrow. This shoreward motion, combined with the westward shearing motion, will produce ice deformations, namely, ridges parallel to the shore. Observations of the ice morphology outside the fast ice zone bear this out. An active shear zone is evident throughout much of the winter, and a great many ridges, many of them grounded in shallow waters near shore, are usually evident along the Beaufort Sea coast. The present trajectory model does not allow an estimate to be made of the amount of ice that might be built into ridges. The ice strength, along with the shoreward component of the driving forces, will determine the amount of deformed ice. Ice strength was one of the parameters varied in this study and, while the general sense of the resulting motions are reasonable, errors of only a few kilometers in the amount of shoreward motion can make large differences in the amount of deformed ice. Thomas (1980) examined the motion of a buoy that was only about 30 km offshore from Cross Island during the winter of 1975-76. The net onshore motion of this buoy was about 6 km during an 80-day period, with some back-and-forth motion also probable (the positioning error of the buoy was about 2 km). Therefore, it is possible that approximately 20 percent of the ice outside the barrier islands may become built into ridges. The computed ice trajectories for this study show that shoreward trend, with a variability of computed motions large enough to allow almost any amount of deformation. To better determine the amount of ice deformed into ridges, more data on ice motions near shore are needed. The use of a full time-dependent ice model would also aid in this determination.

-28-

REFERENCES

- Aagaard, Knut (1981) "The Beaufort Current," to appear in The Alaskan Beaufort Sea (P. Barnes, E. Reimnitz, and D. Schell, editors), The Academic Press, N.Y.
- Barry, R. G. (1979) "Study of Climatic Effects on Fast Ice Extent and Its Seasonal Decay Along the Beaufort-Chukchi Coasts," Environmental Assessment of the Alaskan Continental Shelf, Vol. 2 Physical Science Studies, Final Reports, NOAA/OCSEAP, Boulder, Colorado, pp. 272-375.
- Brewer, W. A., H. F. Diaz, A. S. **Prechtel**, H. W. Searby, and J. L. Wise (1977) Climatic Atlas of the Outer Continental Shelf Waters and Coastal Regions of Alaska, Vol. III, Chukchi-Beaufort Sea. Arctic Environmental Information and Data Center, University of Alaska, Anchorage.
- Buist, I. A., W. M. Pistruzak, and D. F. **Dickins** (1981) "Dome Petroleum's Oil and Gas Undersea Ice Study," Proceedings of the Fourth Arctic Marine Oilspill Program Technical Seminar, Edmonton, Alberta, pp. 647-686.
- Comfort, G., and W. Purves (1980) "An Investigation of the Behaviour of Crude Oil Spilled under Multi-year Ice at Griper Bay, NWT," Proceedings of the Third Annual Marine Oilspill Program Technical Seminar, Edmonton, Alberta, pp. 62-86.
- Coon, M. D. (1980) "A Review of AIDJEX Modeling," Sea Ice Processes and Models, (R. S. Pritchard, ed.), University of Washington Press, Seattle, pp. 28-33.
- Cox, J. C., L. A. Schultz, R. P. Johnson, and R. A. **Shelsby** (1980) "The Transport and Behavior of Oil Spilled In and Under Sea Ice," Final Report of Research Unit #568 to OCSEAP Arctic Project Office, September.
- Cox, J. C., and L. A. Schultz (1981) "The Mechanics of Oil Containment Beneath Rough Ice," Proceedings of the Fourth Arctic Marine Oilspill Program Technical Seminar, Edmonton, Alberta, pp. 3-44.
- Jenne, R. L. (1975) "Data Sets for Meteorological Research," National Center for Atmospheric Research Technical Note NCAR-TN/IA-III, Boulder, Colorado.
- Kozo**, Thomas L. (1980) "Mountain Barrier **Baroclinity** Effects on Surface Winds Along the Alaskan Coast," Geophysical Research Letters, Vol. 7, No. 5, pp. 377-380.
- Lewis, E. L. (1976) "Oil in Sea Ice," Pacific Marine Science Report 76-12, Institute of Ocean Sciences, Victoria, B.C.
- Martin, S. (1977) "The Interaction of Oil with Sea Ice," OCSEAP Annual Report, Outer Continental Shelf Environmental Assessment Program, NOAA/Arctic Project Office (University of Alaska), Fairbanks.

-29-

- McPhee, M. G. (1980) "An Analysis of pack Ice Drift in **Winter," Sea Ice processes and Models**, (R. S. Pritchard, cd.), University of Washington Press, Seattle, pp. 62-75.
- McPhee, M. G. (1982) "The Turbulent Boundary Layer in Shallow Water," **OCSEAP Annual Report for RU#567**, Appendix C.
- Newton, J. L. (1973) "The Canada Basin: Mean Circulation and Intermediate Scale Flow Features," Ph.D. Thesis, University of Washington, **Seattle**.
- NORCOR Engineering and Research, Ltd. (1975) "The Interaction of Crude Oil with Arctic Sea Ice," Beaufort Sea Technical Report #27, Beaufort Sea Project, Dept. of the Environment, Victoria, B.C.
- NORCOR Engineering and Research, Ltd. (1977) "Probable Behaviour and Fate of a Winter Oil Spill in the Beaufort Sea," Technical Development Report **EPS-4-EC-77-5**, Environmental Protection Service, Edmonton, Alberta, p. 111.
- Overland, J. E., and C. H. Pease (1982) "Wind-Driven Ice Dynamics in a Shallow Sea," Submitted to Journal of Geophysical Research.
- Pritchard, R. S. (1978) "The Effect of Strength on Simulations of Sea Ice Dynamics," POAC 77, Vol. I. (D. B. Muggerridge, cd.), Memorial University of Newfoundland, St. John's, pp. 494-505.
- Pritchard, R. S., and R. Colony (1976) "A Difference Scheme for the **AIDJEX Sea Ice Model**," Numerical Methods in Geomechanics, Vol. 11 (C. S. Desai, cd.), American Society of Civil Engineers, New York, pp. 1194-1209.
- Pritchard, R. S., M. D. Coon, M. G. McPhee, and E. Leavitt (1977) "Winter Ice Dynamics in the Nearshore Beaufort Sea," AIDJEX Bulletin No. 37, University of Washington, Seattle, pp. 37-94.
- Pritchard, R. S., and J. J. Kollé (1981) "Modeling Sea Ice Trajectories for Oil Spill Tracking," Final report to U.S. Department of Transportation, United States Coast Guard, Office of Research and Development, Washington, **D.C.** Also, Flow Research Report No. 187, Flow Industries, Kent, Washington.
- Pritchard, R. S. (1981) "Mechanical Behavior of Pack Ice," Mechanics of Structured Media (A. P. S. Selvaduri, cd.), **Elsevier** Scientific Publishing Company, Amsterdam, Part A, pp. 371-405.
- Reimer, R. W., J. C. Schedvin, and R. S. Pritchard (1980) "Ice Motion in the **Chukchi Sea**," Flow Research Report No. 168, Flow Industries, Kent, Washington, p. 44.
- Reimnitz, E., L. J. Tomil, and P. W. Barnes (1978) "Arctic Continental Shelf Morphology Related to Sea-ice Zonation, Beaufort Sea, Alaska," Marine Geology, Vol. 18, pp. 179-210.

-30-

- Stringer, W. J. (1978) Morphology of Beaufort, Chukchi and Bering Seas Nearshore Ice Conditions by means of Satellite and Aerial Remote Sensing, Vol.I, Geophysical Institute, University of Alaska, Fairbanks.
- Stringer, W. J. (1982) "Ice Concentration in the Eastern Beaufort Sea," Draft report.
- Thomas, D. R. (1980) "Behavior of Oil Spills Under Sea Ice-Prudhoe Bay. Flow Research Report No. 175, Flow Industries, Kent, Washington.
- Thomas, D. R., and R. S. Pritchard (1979) "**Beaufort and Chukchi** Sea Ice Motion, Part 1, Pack Ice Trajectories," Flow Research Report No. **133**, Flow Industries, Kent, Washington.
- Thorndike, A. S., and R. Colony (1980) "Arctic Ocean Buoy Program Data Report, 19 January 1979 to 31 December 1979," Polar Science Center, University of Washington, Seattle, pp. 131.
- Thorndike, A. S., and R. Colony (1981) "Arctic Ocean Buoy Program Data Report, 1 January 1980 to 31 December 1980," Polar Science Center, University of Washington, Seattle, pp. 127.
- Thorndike, A. S., and R. Colony (1981) "Sea Ice Motion in Response to **Geostrophic Winds**," Journal of Geophysical Research, Vol. 87, No. C8, July 20, 1982.
- Thorndike, A. S., R. Colony, and E. A. Munoz (1982) "Arctic Ocean Buoy Program Data Report, 1 January 1981 to 31 December 1981," Polar Science Center, University of Washington, Seattle, pp. 137.
- Webster, B. D. (1982) "Empirical Probabilities of the Ice Limit and Fifty Percent Ice Concentration Boundary in the **Chukchi** and Beaufort Seas," NOAA Technical Memorandum NWS AR-34, National Weather Service, Regional Headquarters, Anchorage, Alaska.

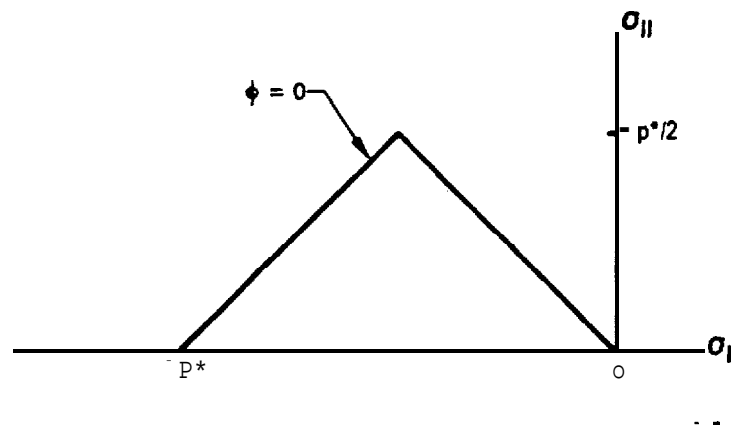


Figure 1. Diamond Yield Surface for Large-Scale Sea Ice Model

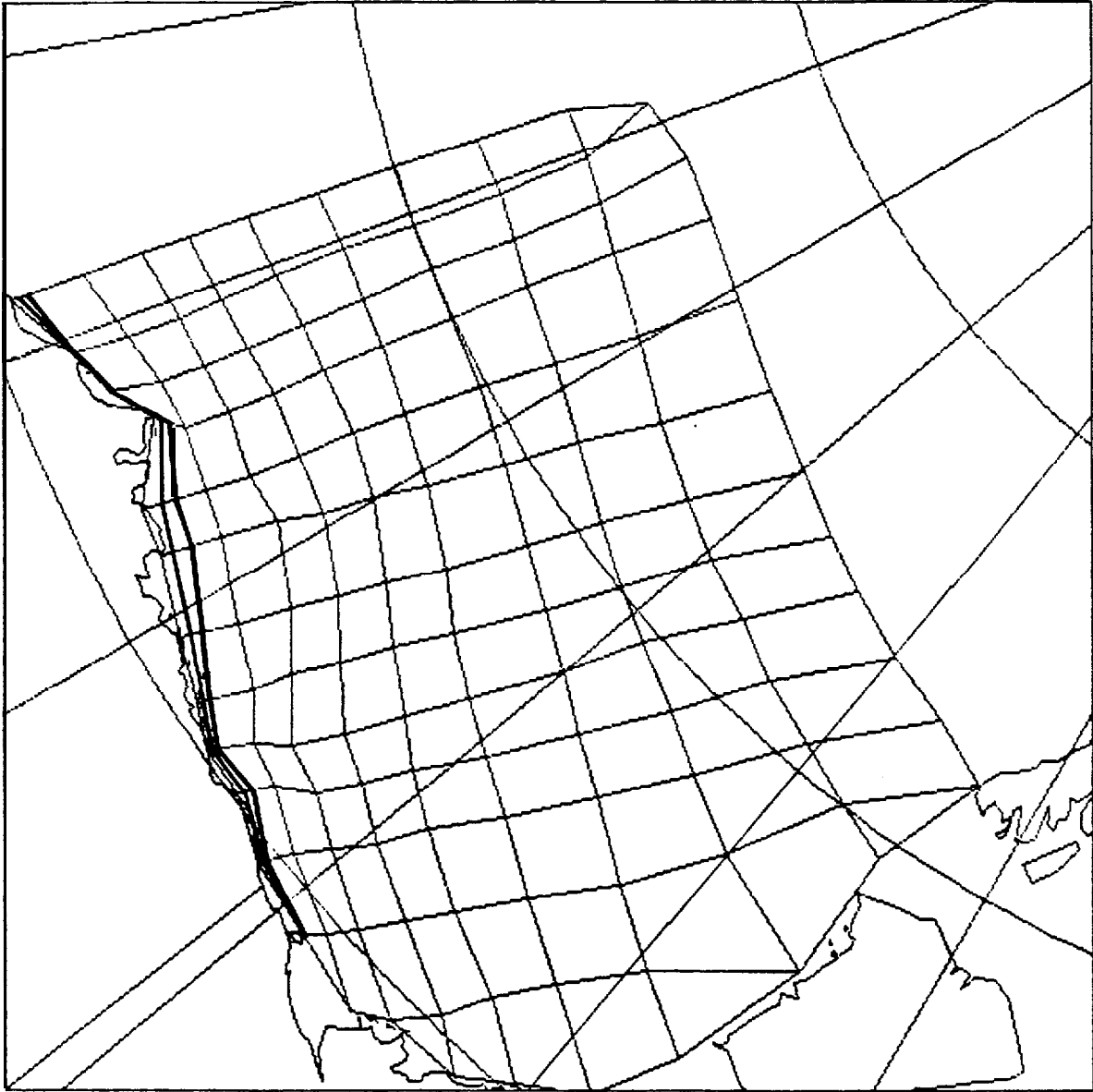


Figure 2. Computational Grids Used in the Calculations. The Approximate Locations of the 10-m and 20-m Isobaths are Also Indicated. These Contours were Used to Approximate the Seaward Extent of Fast Ice on 1 December and 1 March, Respectively.

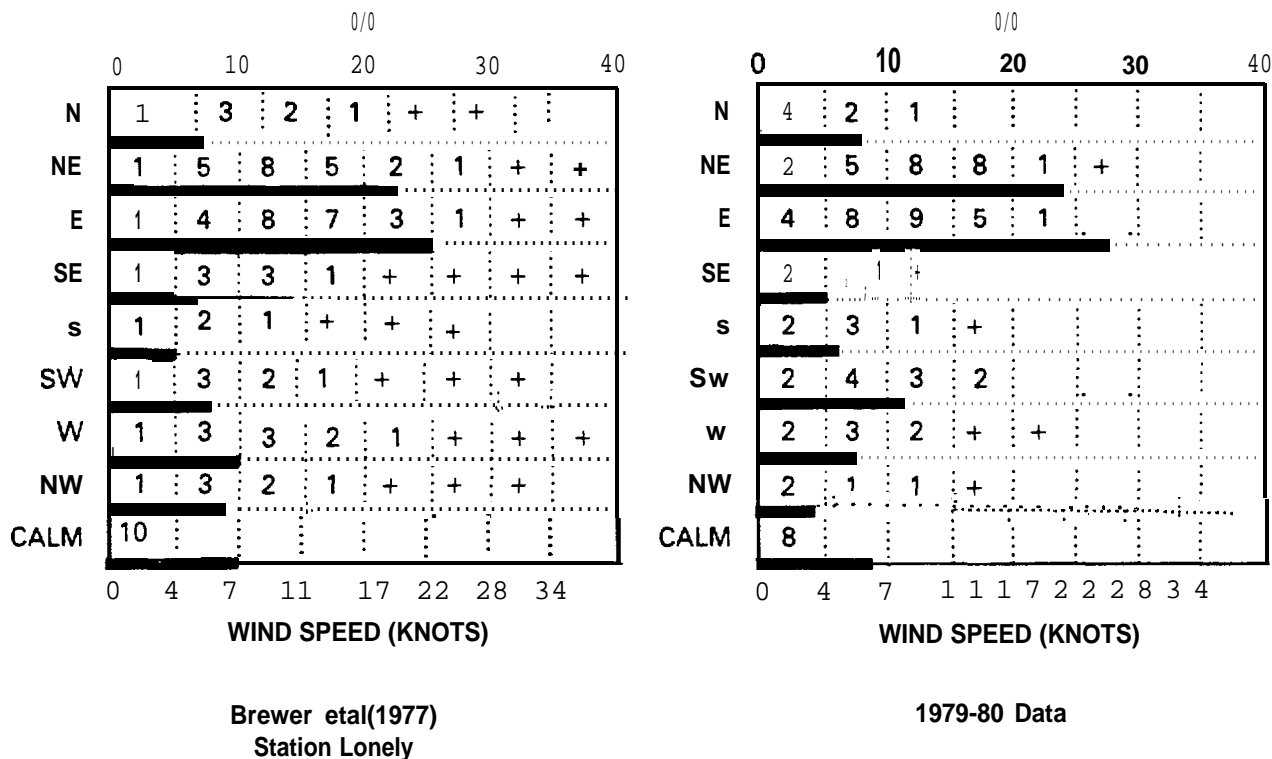


Figure 3. Annual Wind Speed and Direction Summaries for the North Alaskan Coast, The Information for Lonely was Taken from Brewer et al. (1977). The Offshore Winds Were Computed from the 1979-80 Artic Buoy Program Pressure Data as Used in the Trajectory Calculations.

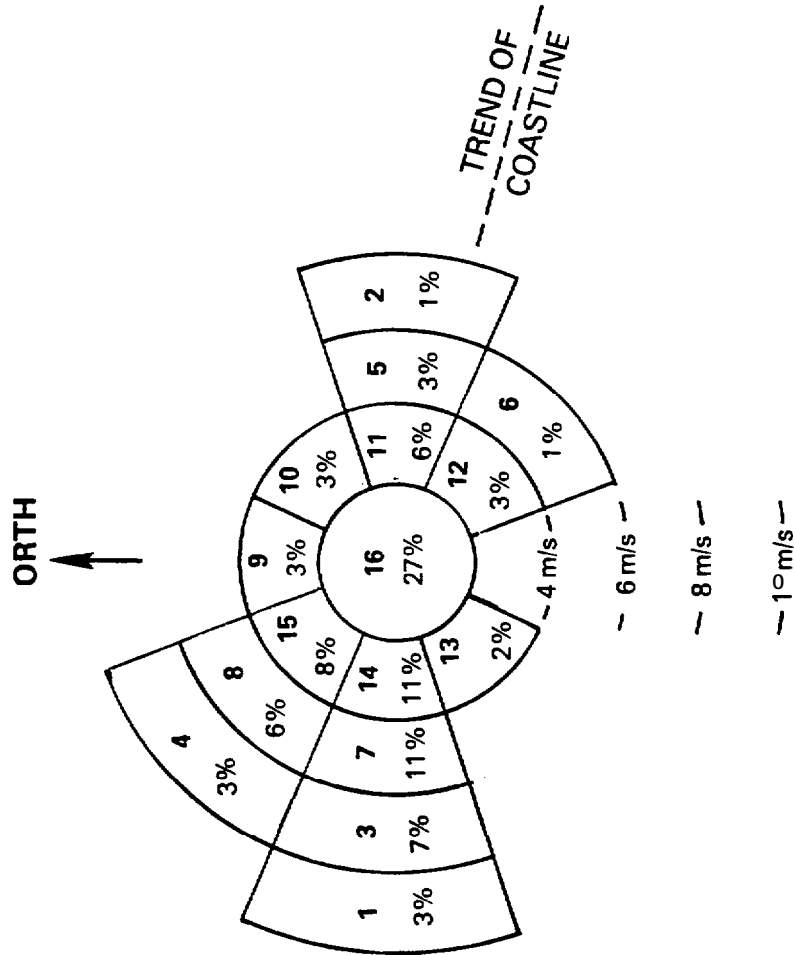


Figure 4. Wind Rose Showing the Distribution of all Winds for 1979-80 for the Nearshore North-Central Alaskan Coast. The 16 Wind Categories are Those Used in the Trajectory Calculations.

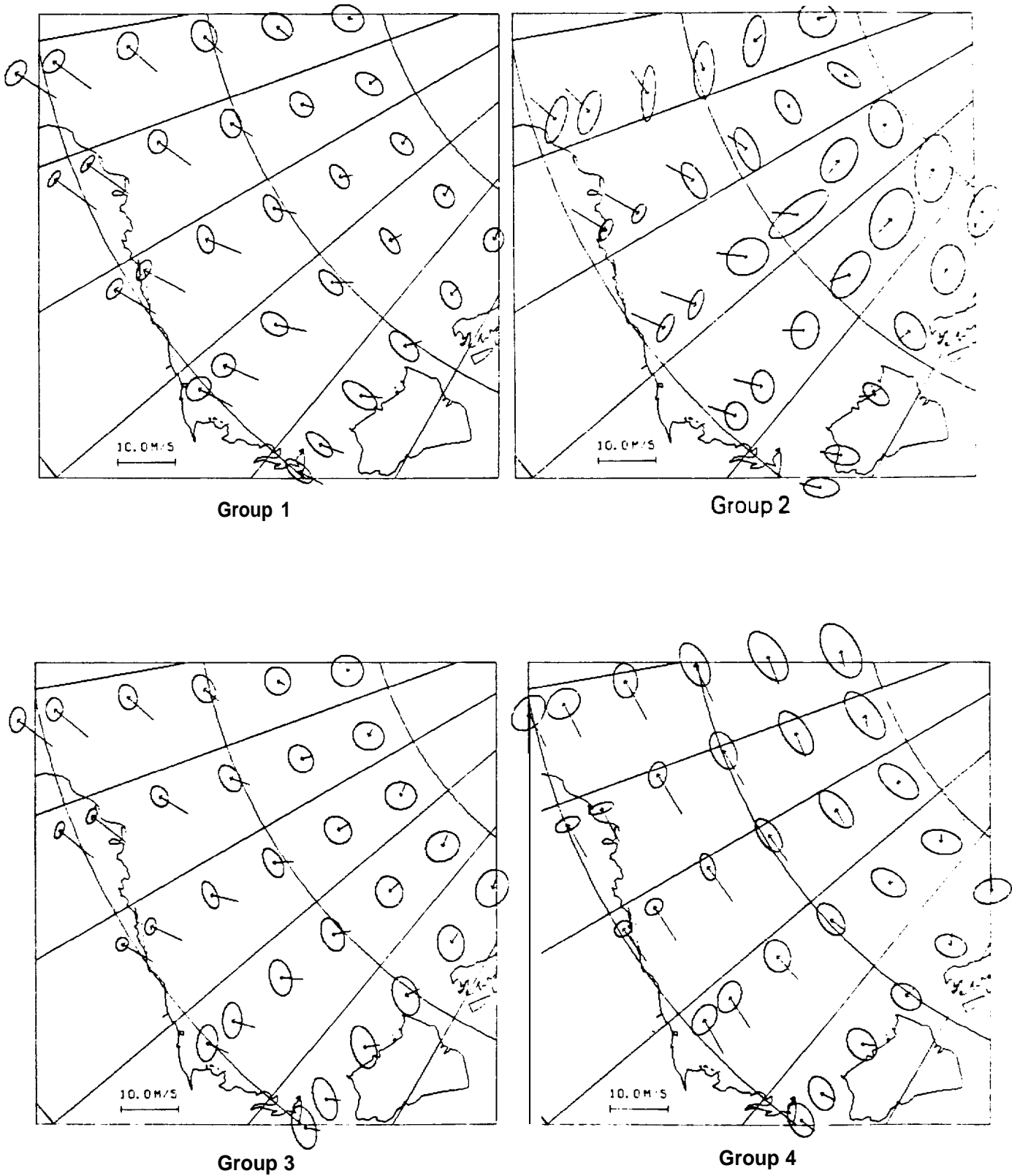
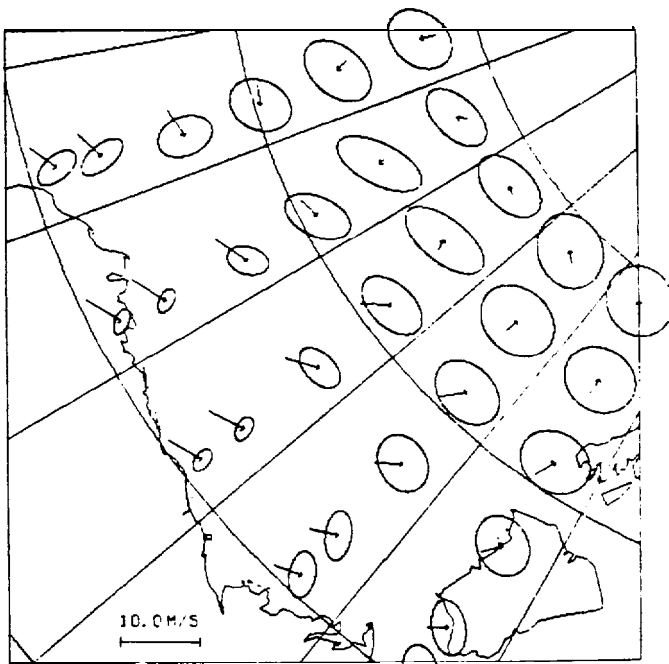
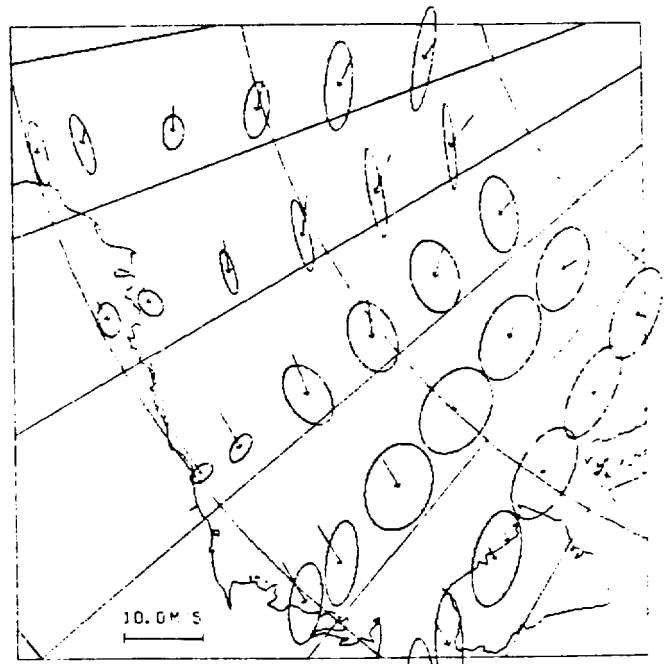


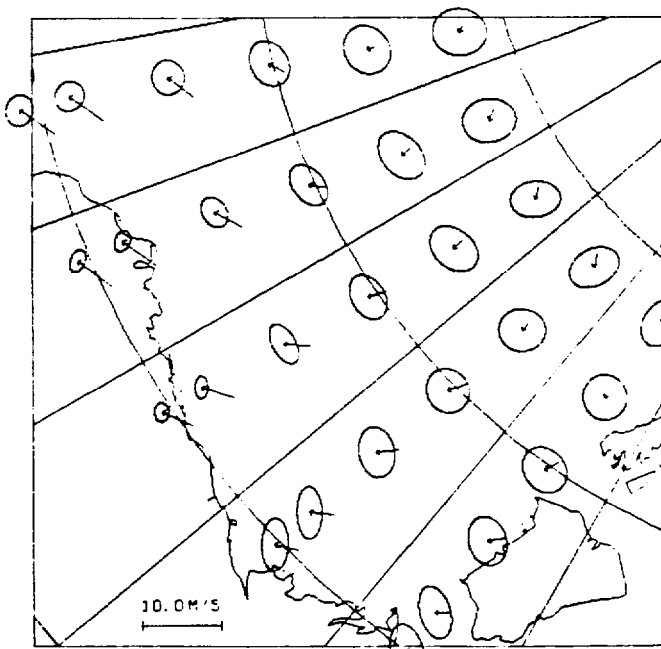
Figure 5. Mean Wind Fields and 50% Equiprobability Ellipses for the 16 Wind Groups Shown in Figure 4.



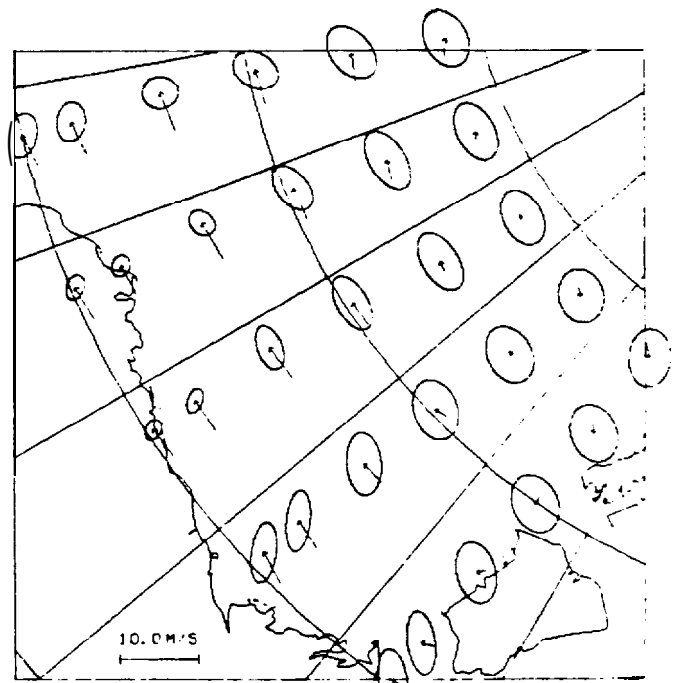
Group 5



Group 6



Group 7



Group 8

Figure 5. Mean Wind Fields and 50% Equiprobability Ellipses for the 16 Wind Groups Shown in Figure 4 (Continued).

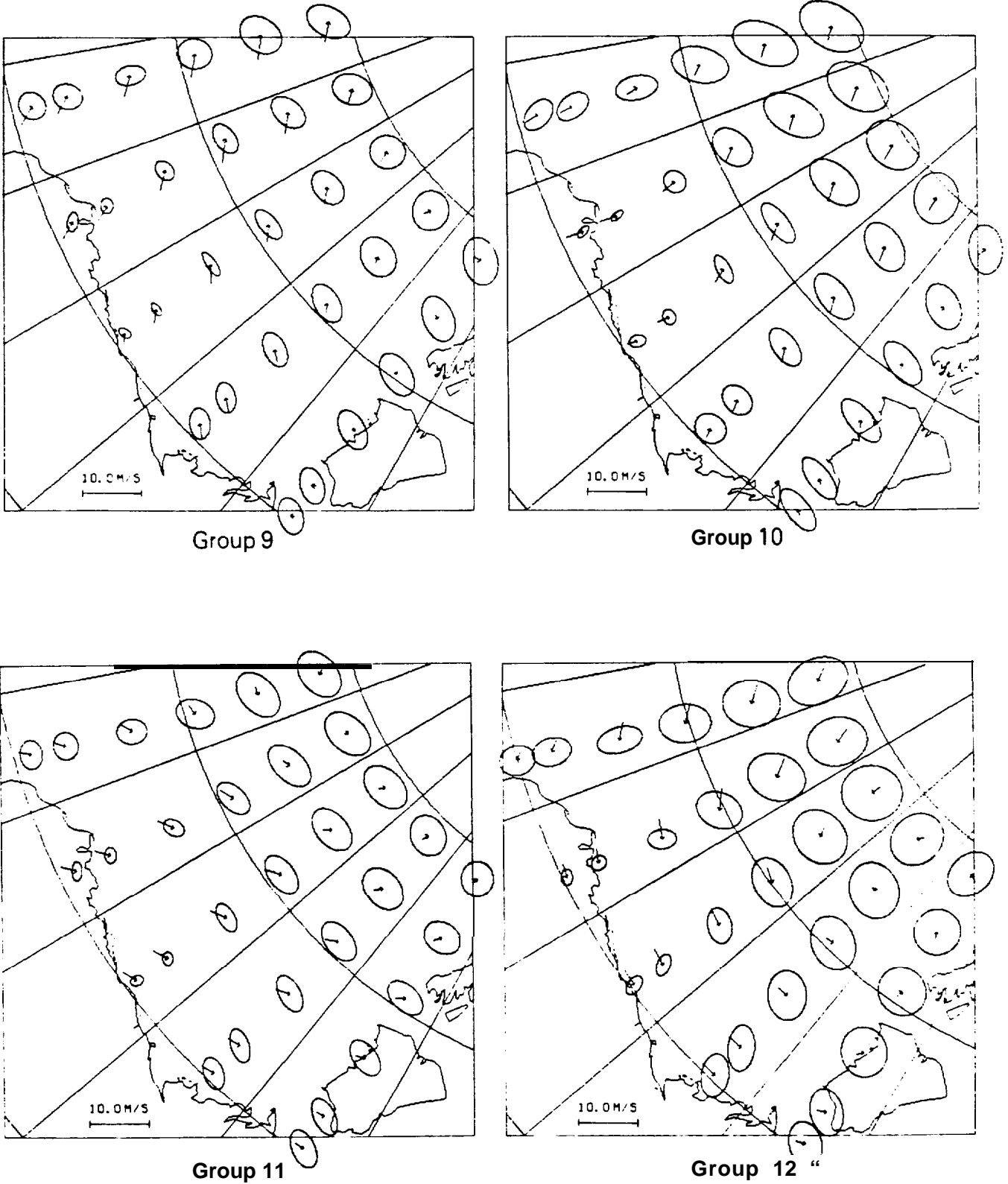


Figure 5. Mean Wind Fields and 50% Equiprobability Ellipses for the 16 Wind Groups Shown in Figure 4 (Continued).

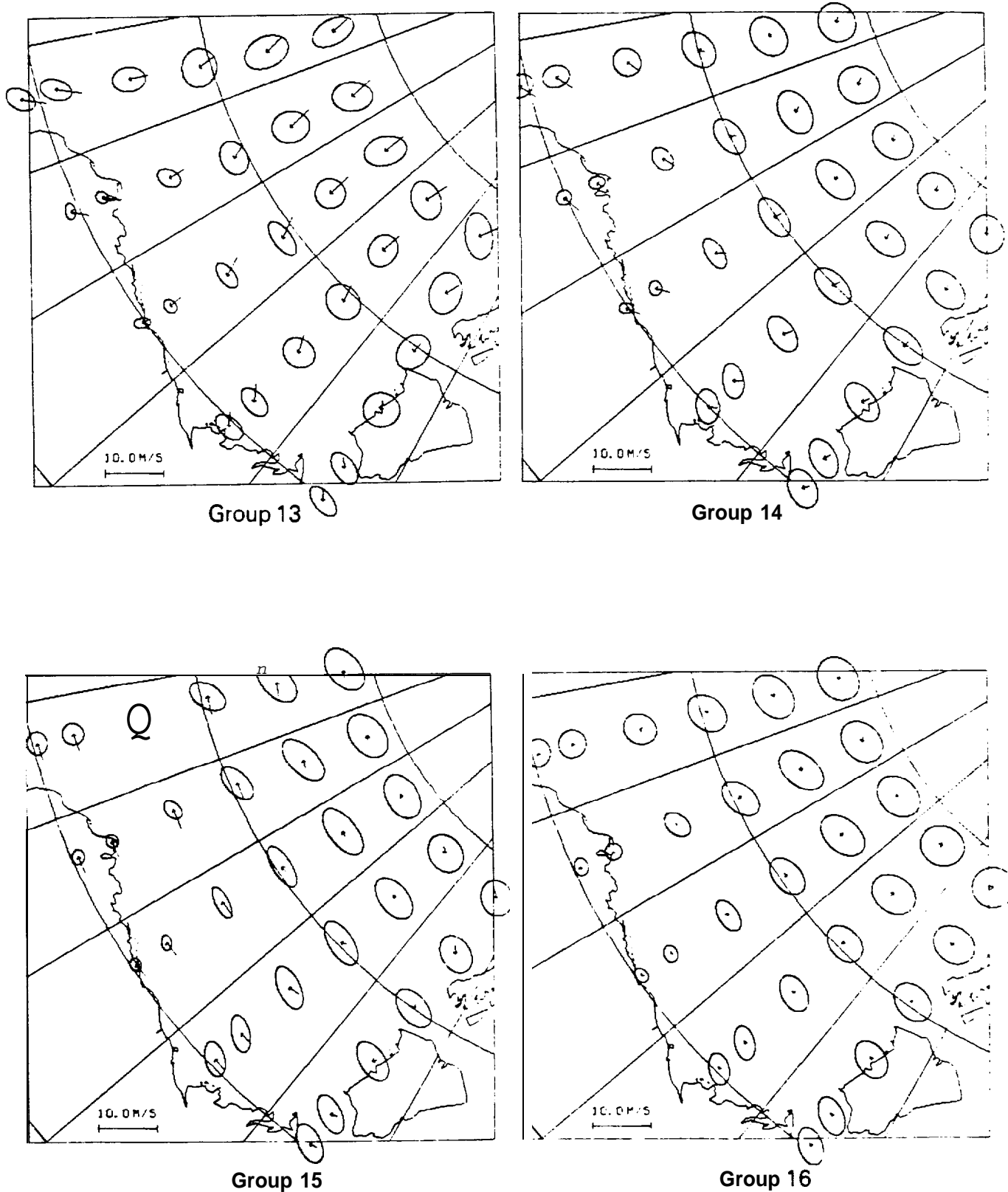
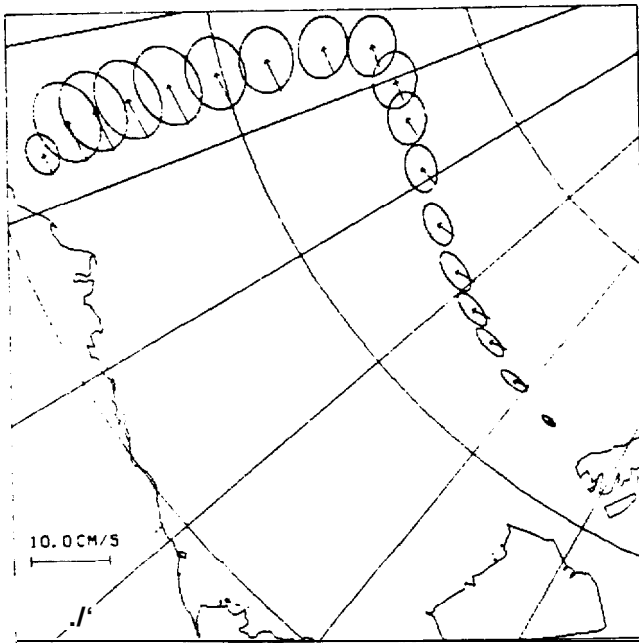
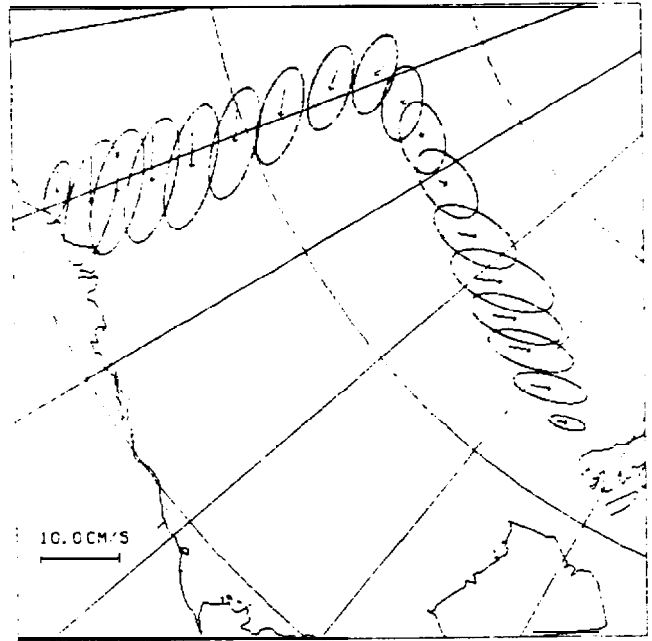


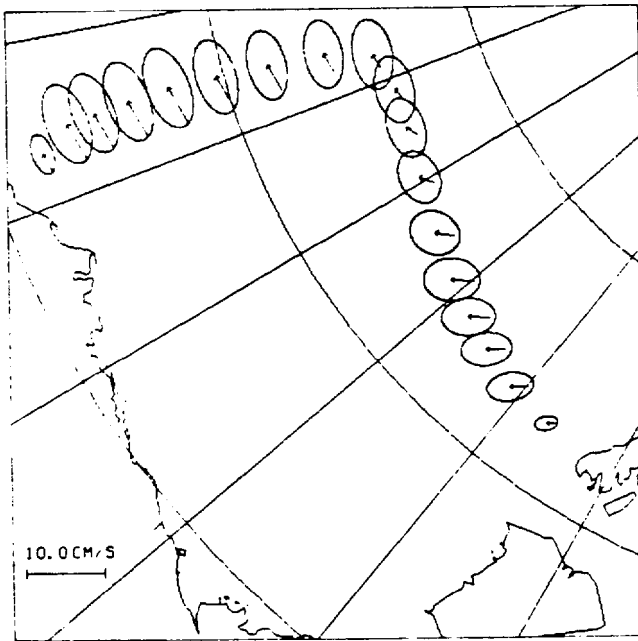
Figure 5. Mean Wind Fields and 5096 Equiprobability Ellipses for the 16 Wind Groups Shown in Figure 4 (Concluded).



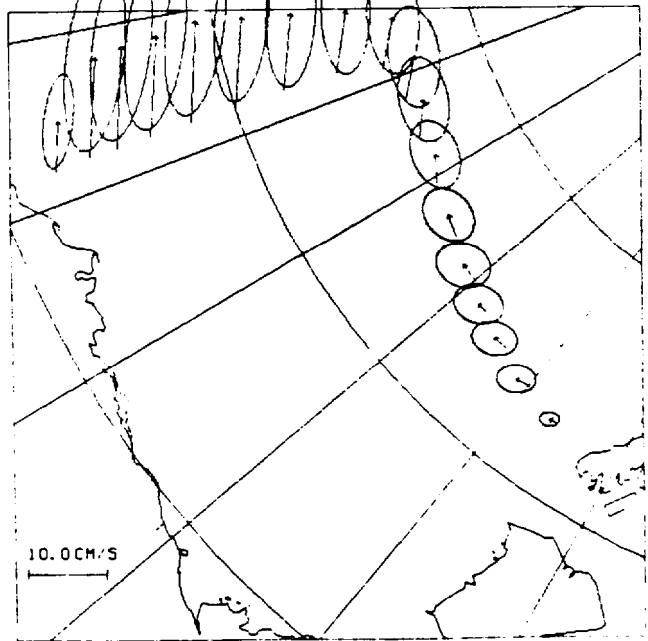
Group 1



Group 2

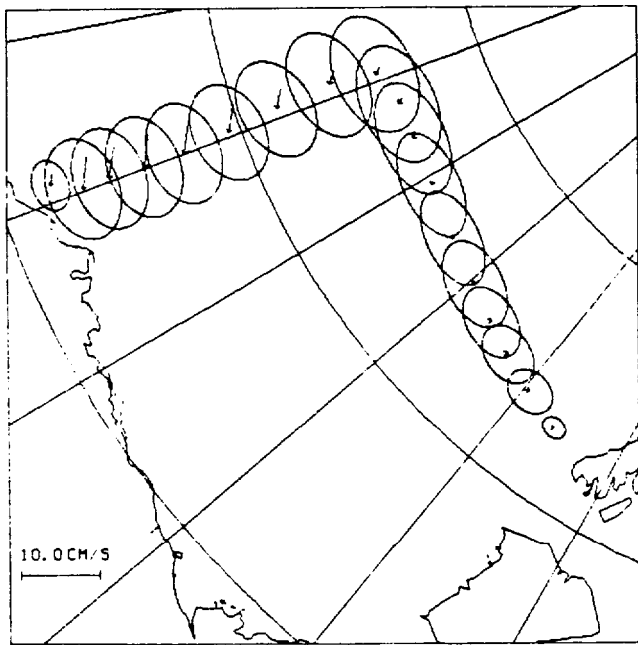


Group 3

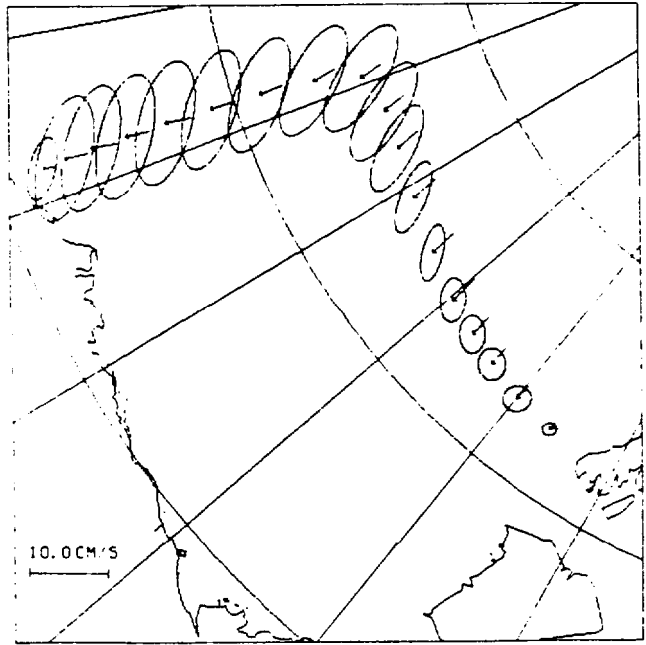


Group 4

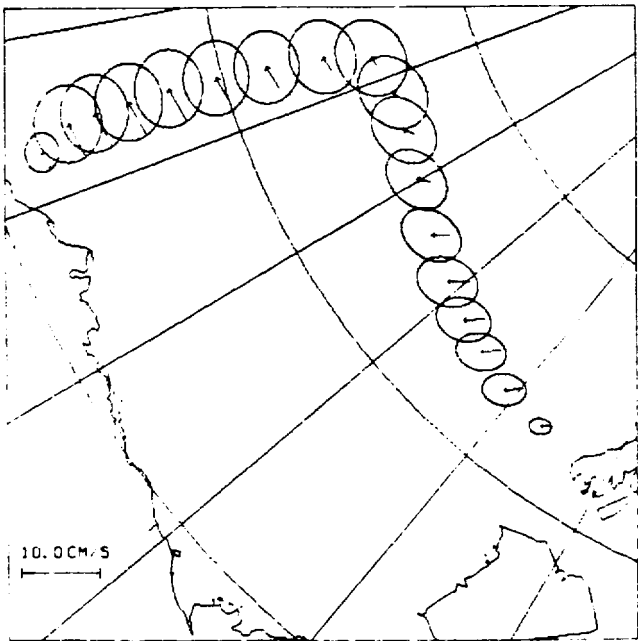
Figure 6, Mean Boundary Velocities and 50% Equiprobability Ellipses for the Same 16 Groups Shown in Figure 4.



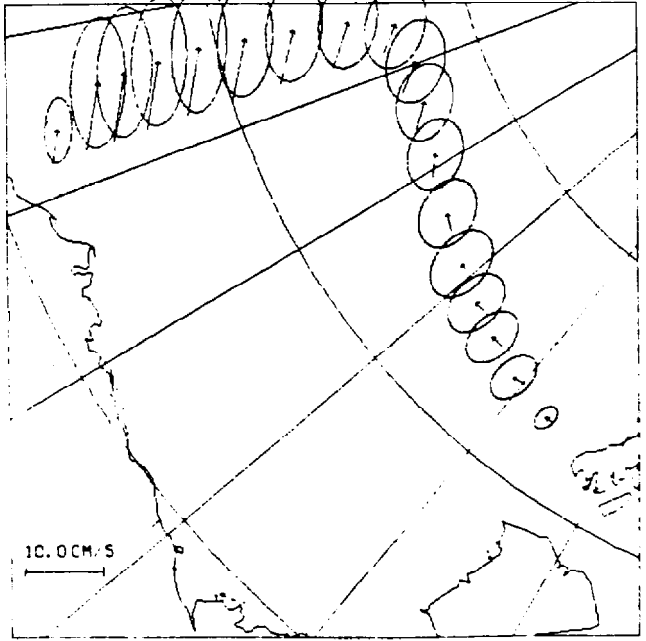
Group 5



Group 6

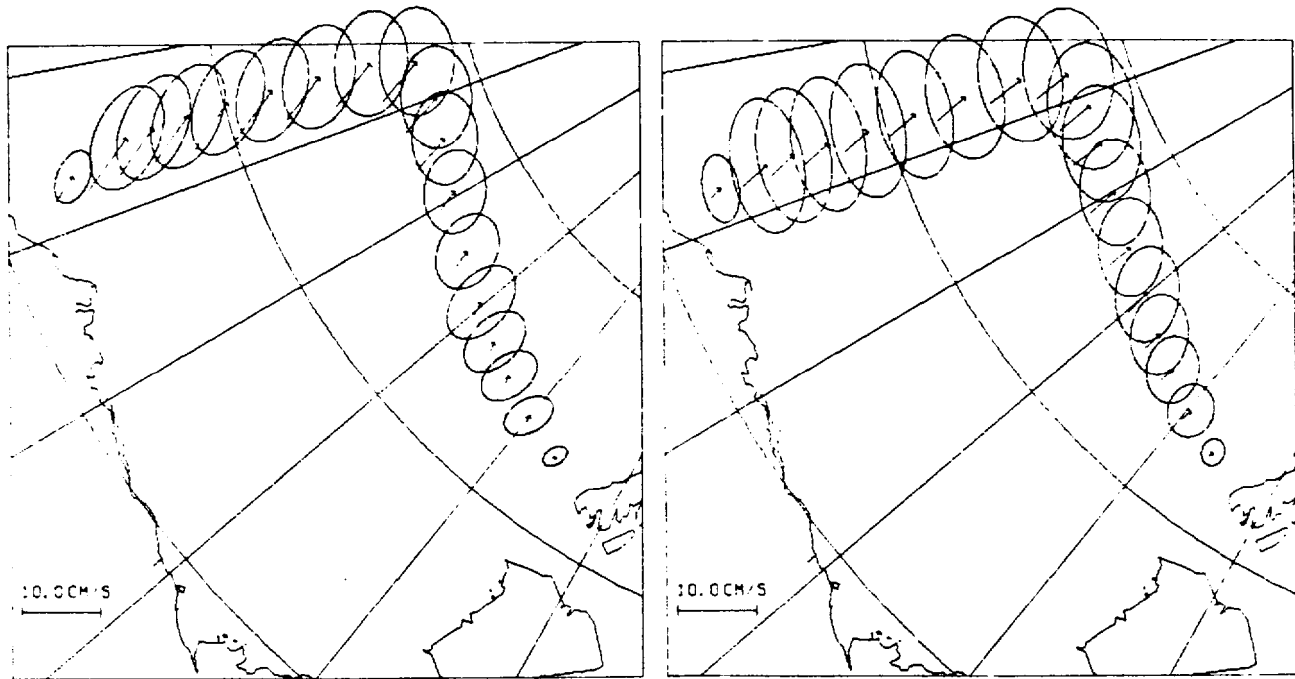


Group 7



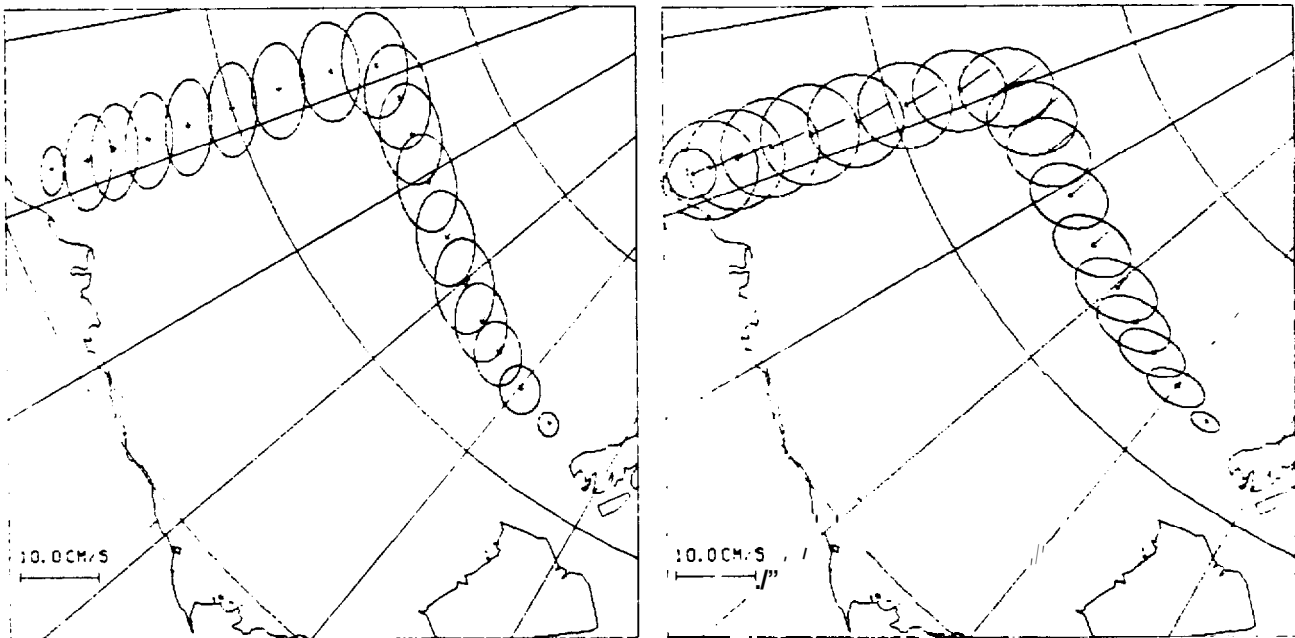
Group 8

Figure 6. Mean Boundary Velocities and 50% Equiprobability Ellipses for the Same 16 Groups Shown in Figure 4 (Continued).



Group 9

Group 10



Group 11

Group 12

Figure 6. Mean Boundary Velocities and 50% Equiprobability Ellipses for the Same 16 Groups Shown in Figure 4 (Continued). (Concluded)

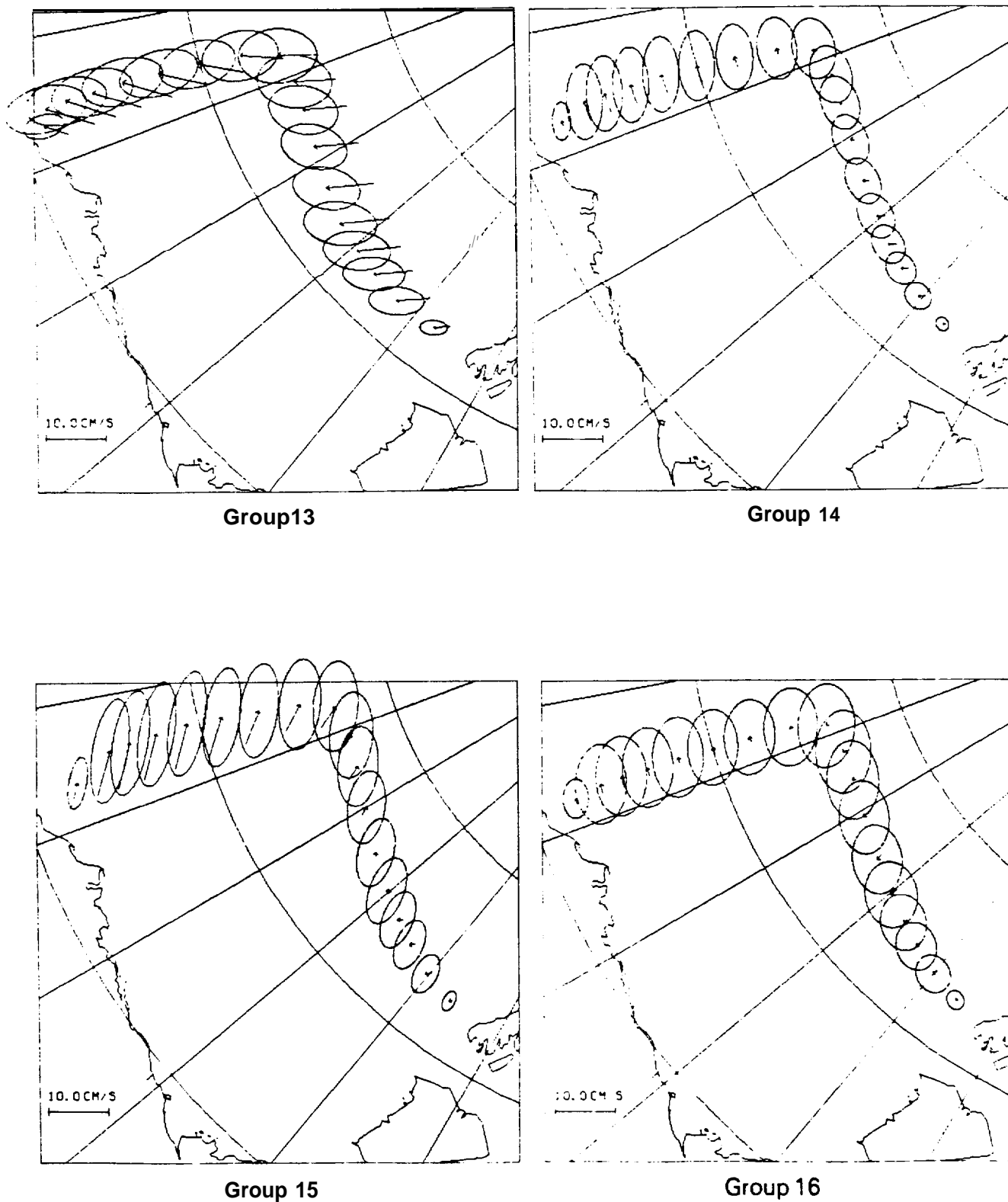


Figure 6. Mean Boundary Velocities and 50% Equiprobability Ellipses for the Same 16 Groups Shown in Figure 4 (Concluded).

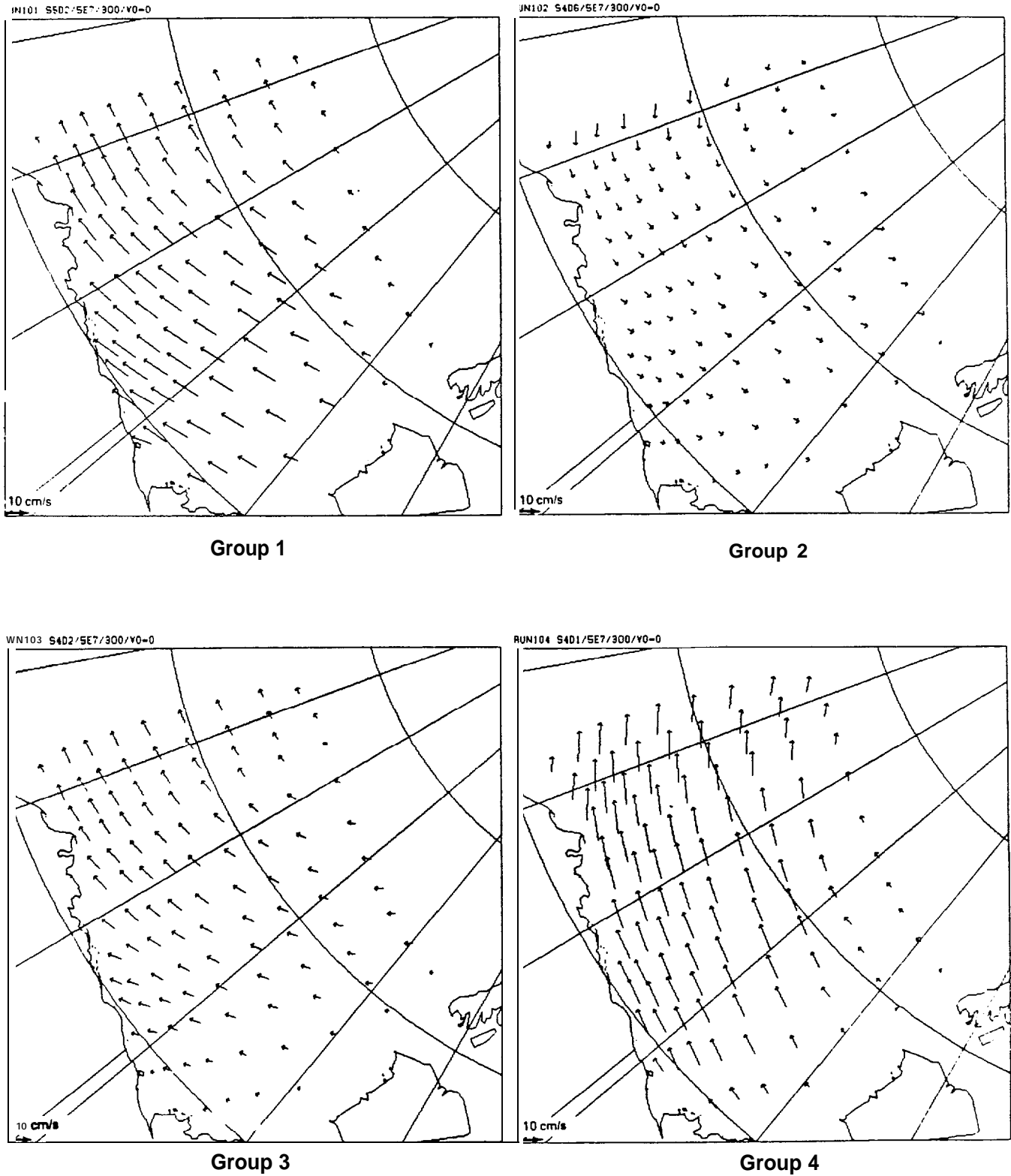


Figure 7. Ice Velocity Fields Resulting from Model Calculations Using the 16 Mean Wind Fields and Boundary Velocities. An Ice Strength of $5E7$ dyn/cm and Average Ice Thickness of 300 cm were used in the Model. Geostrophic Currents were Used Beyond the Shelf Break, and the Beaufort Current Jet was Set to Zero.

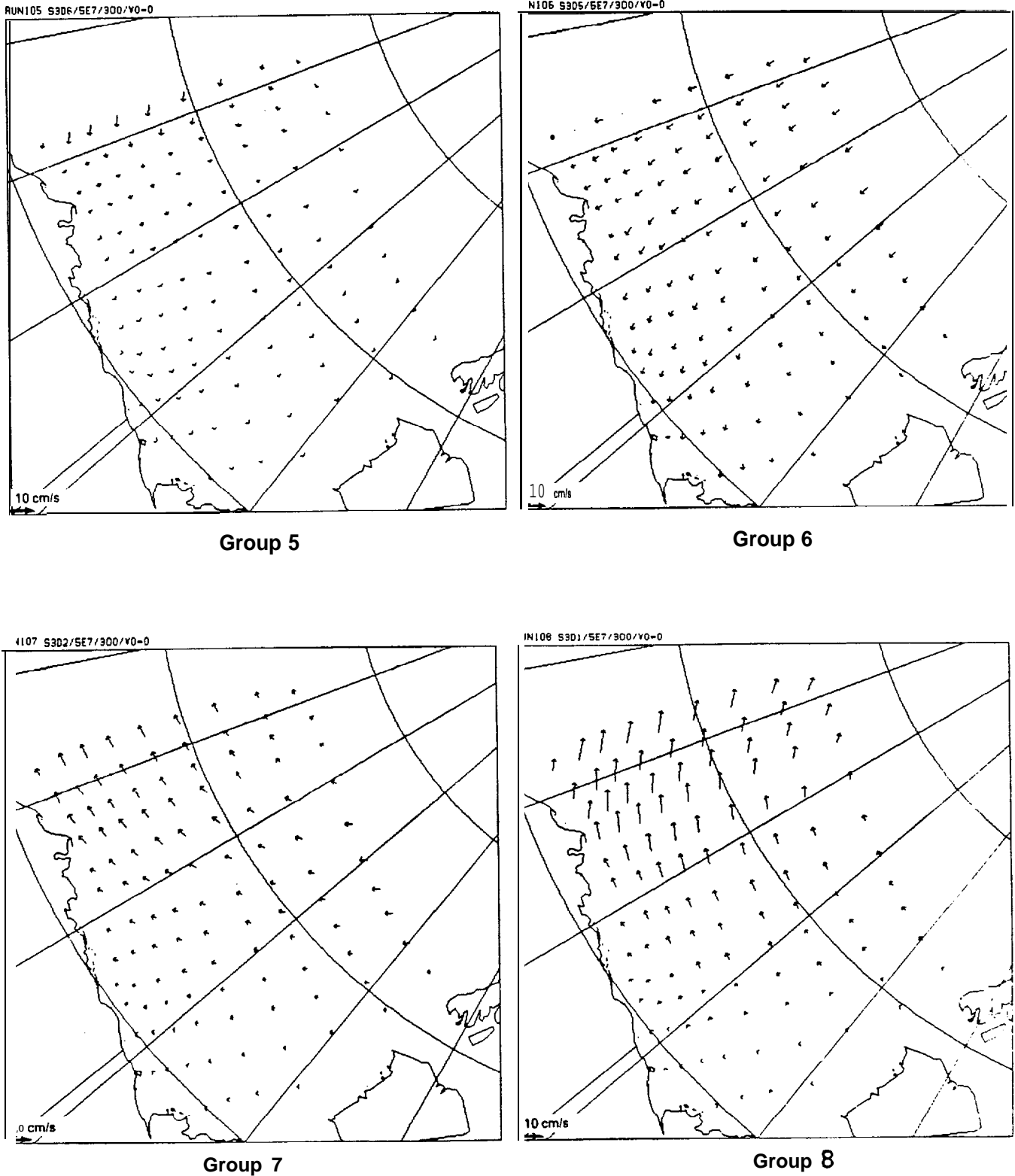


Figure 7. Ice Velocity Fields Resulting from Model Calculations Using the 16 Mean Wind Fields and Boundary Velocities. An Ice Strength of $5E7$ dyn/cm and Average Ice Thickness of 300 cm were used in the Model. Geostrophic Currents were Used Beyond the Shelf Break, and the Beaufort Current Jet was Set to Zero (Continued).

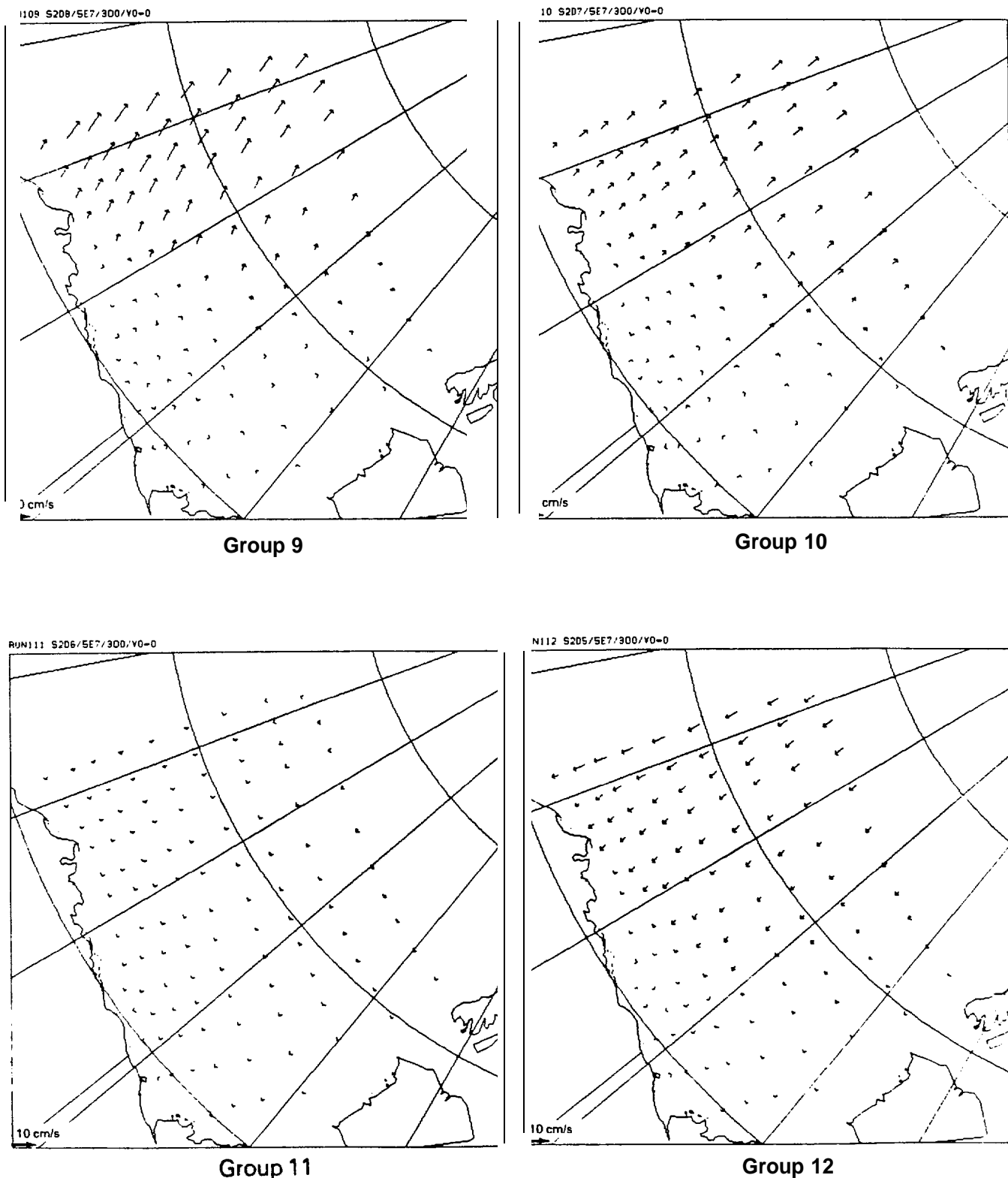


Figure 7. Ice Velocity Fields Resulting from Model Calculations Using the 16 Mean Wind Fields and Boundary Velocities. An Ice Strength of 5E7 dyn/cm and Average Ice Thickness of 300 cm were used in the Model. Geostrophic Currents were Used Beyond the Shelf Break, and the Beaufort Current Jet was Set to Zero (Continued).

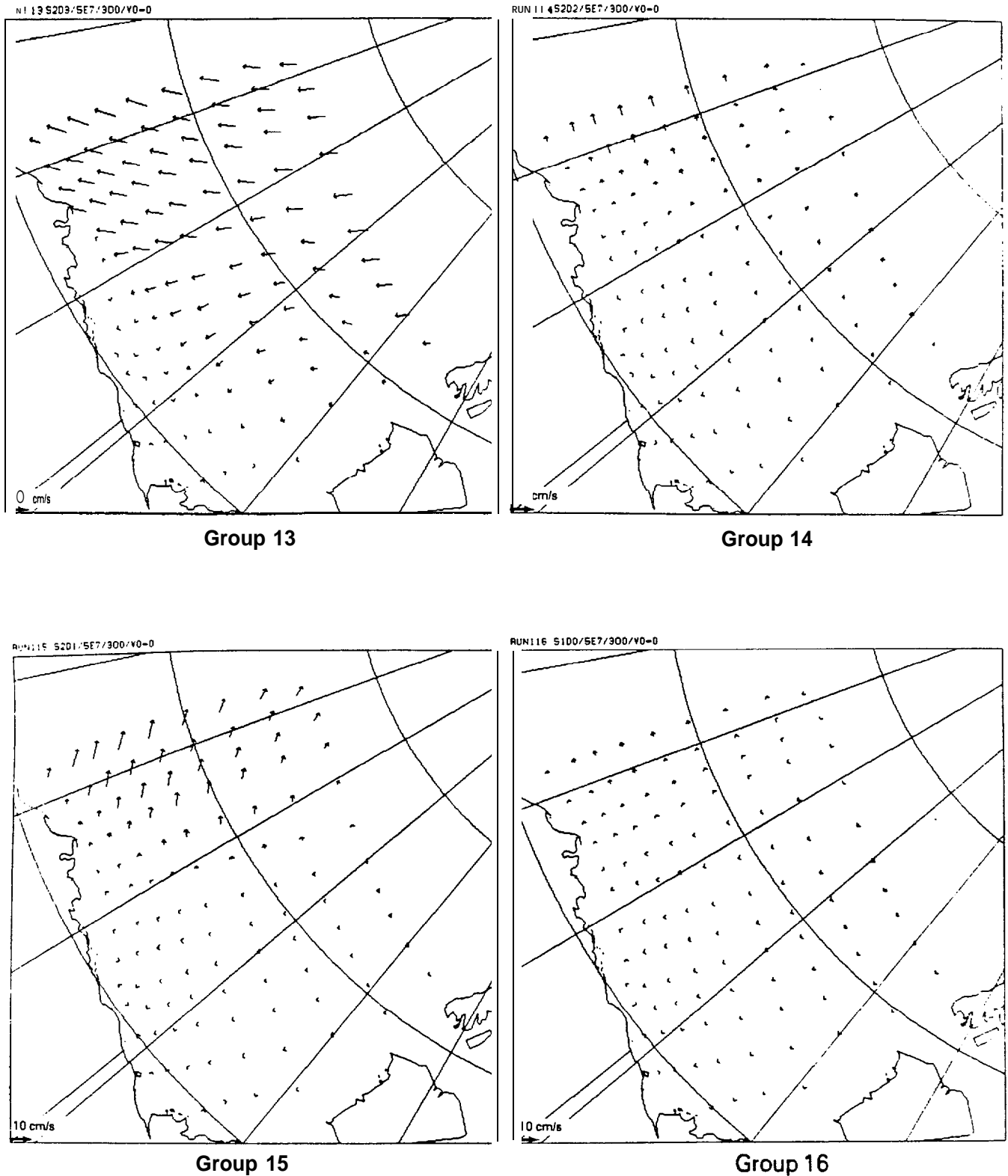


Figure 7. Ice Velocity Fields Resulting from Model Calculations Using the 16 Mean Wind Fields and Boundary Velocities. An Ice Strength of $5E7$ dyn/cm and Average Ice Thickness of 300 cm were used in the Model. Geostrophic Currents were Used Beyond the Shelf Break, and the Beaufort Current Jet was Set to Zero (Concluded).

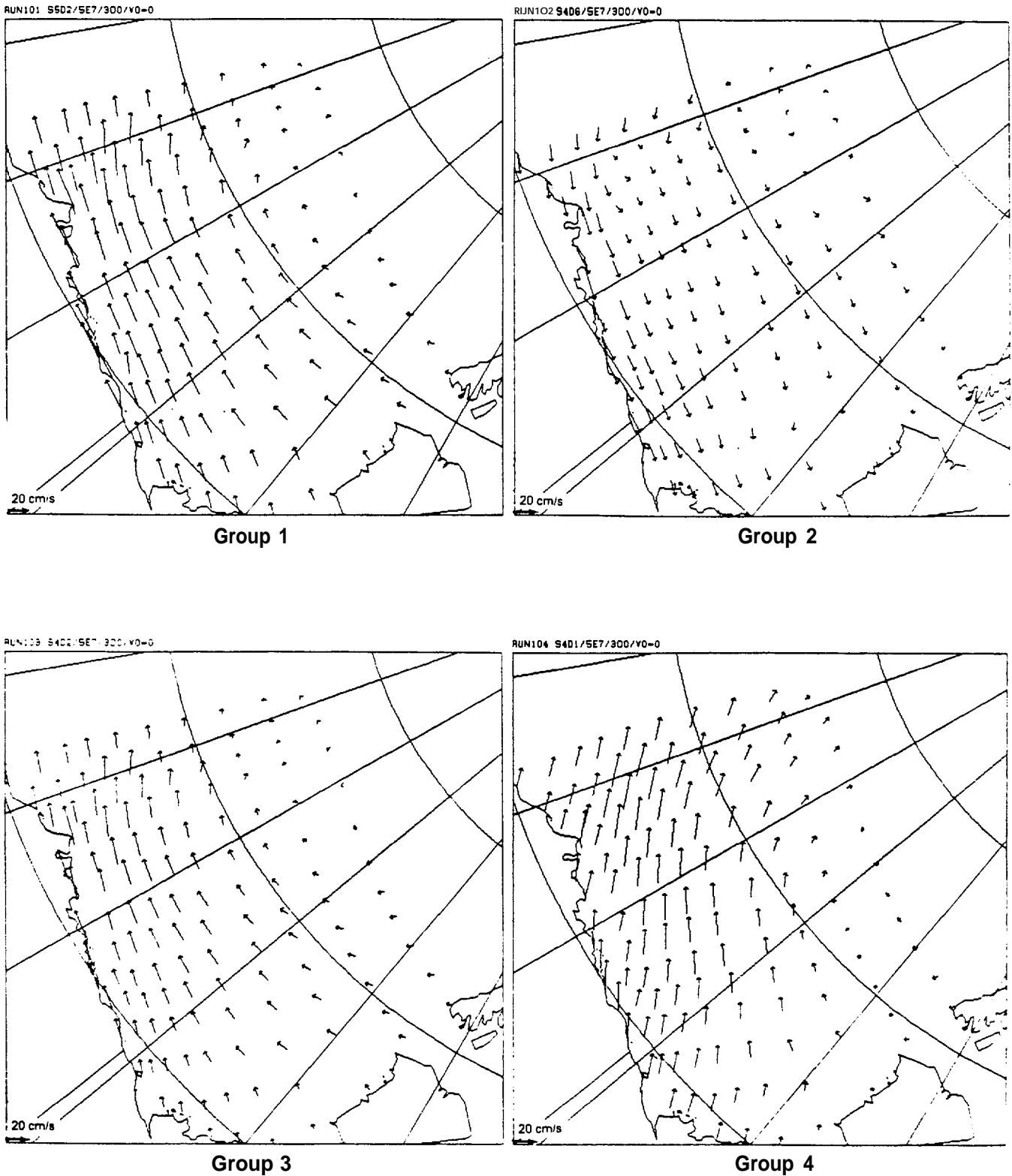


Figure 8. Free-Drift Velocity Fields Resulting from Model Calculations Using the 16 Wind and Boundary Velocity Fields. An Ice Strength of Zero and Average Ice Thickness of 300 cm were Assumed. Geostrophic Currents were Used Beyond the Shelf Break, and the Beaufort Current Jet was Set to Zero.

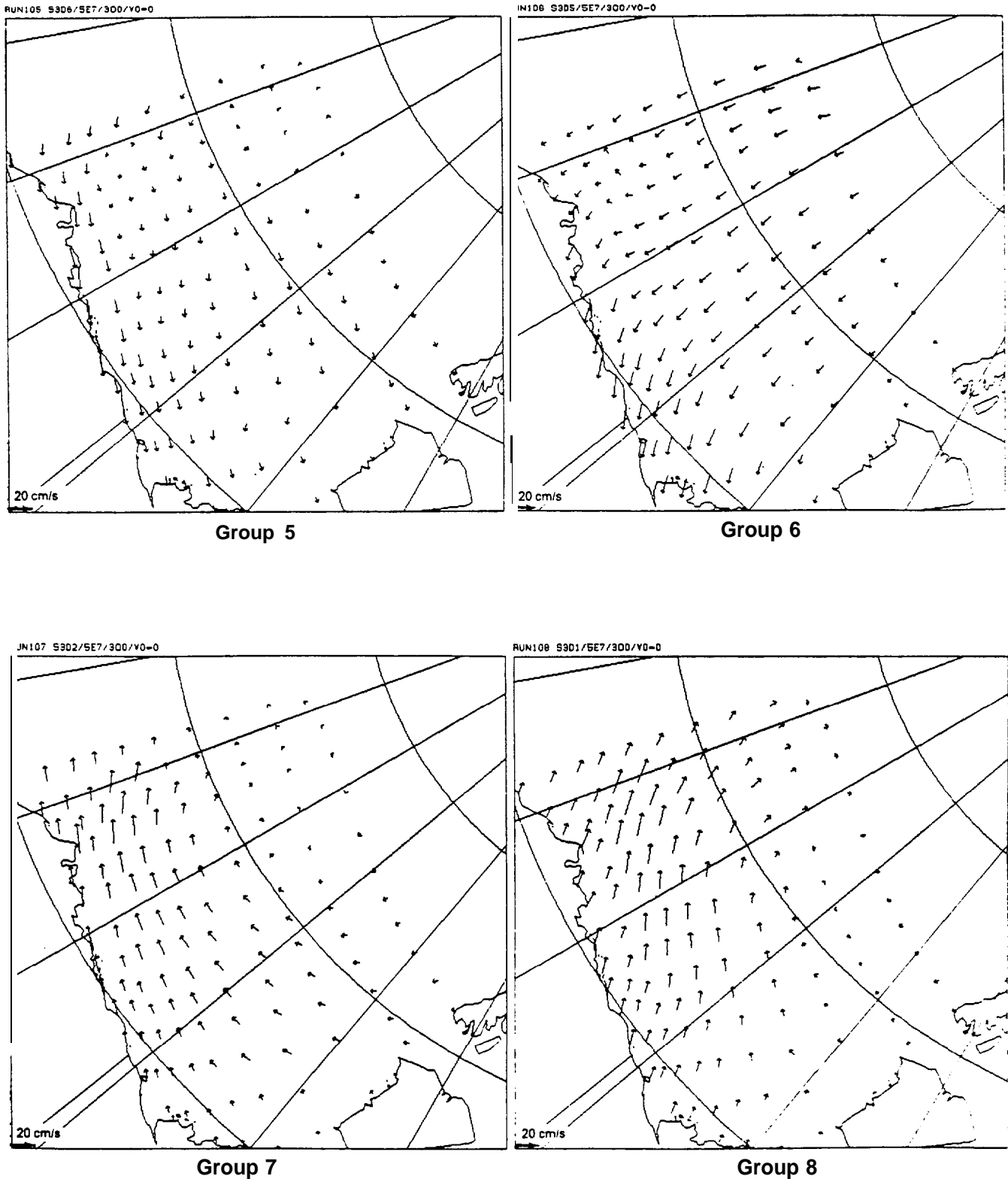


Figure 8. Free-Drift Velocity Fields Resulting from Model Calculations Using the 16 Wind and Boundary Velocity Fields. An Ice Strength of Zero and Average Ice Thickness of 300 cm were Assumed. Geostrophic Currents were Used Beyond the Shelf Break, and the Beaufort Current Jet was Set to Zero (Continued).

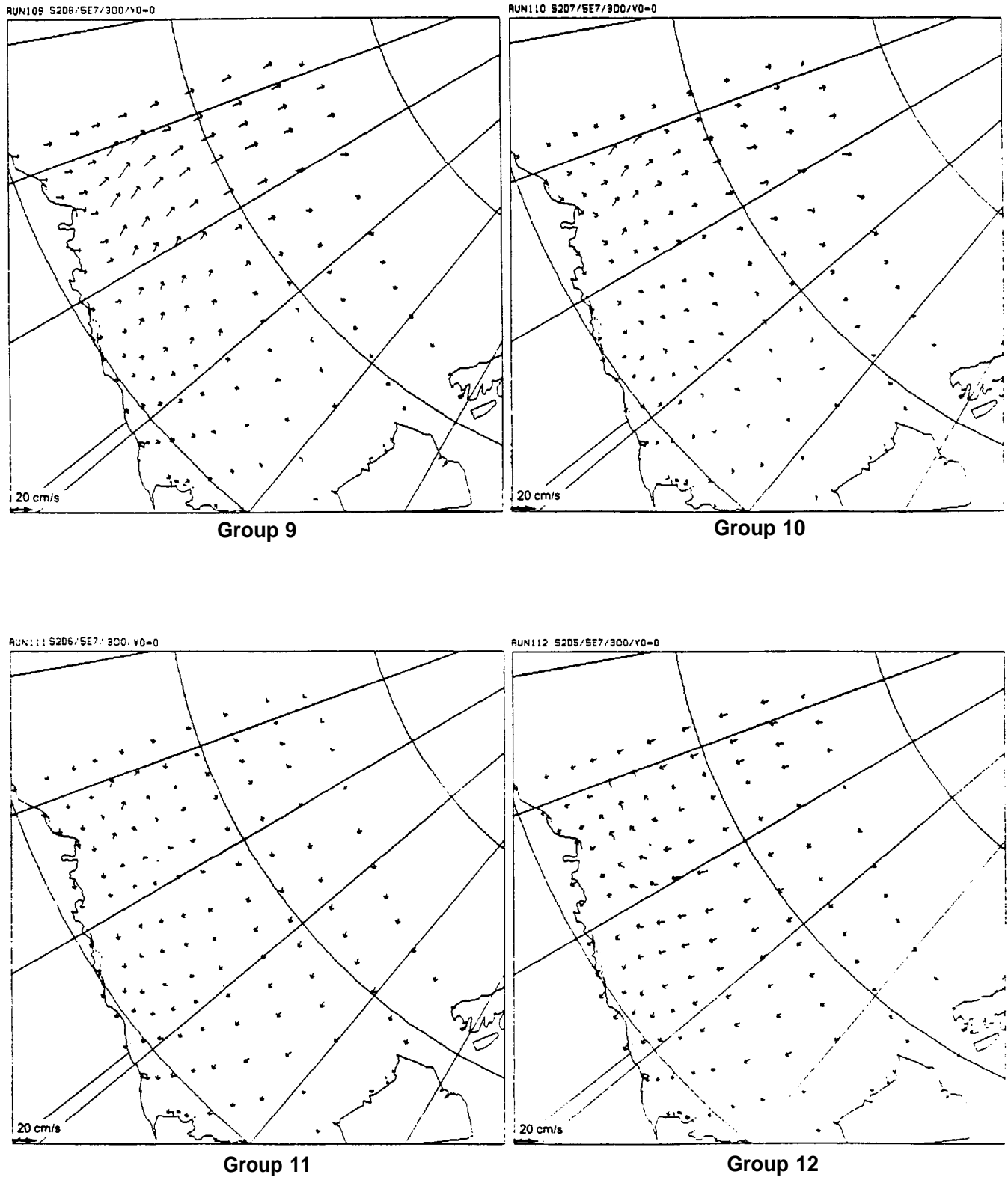


Figure 8. Free- Drift Velocity Fields Resulting from Model Calculations Using the 16 Wind and Boundary Velocity Fields. An Ice Strength of Zero and Average Ice Thickness of 300 cm were Assumed. Geostrophic Currents were Used Beyond the Shelf Break, and the Beaufort Current Jet was Set to Zero (Continued).

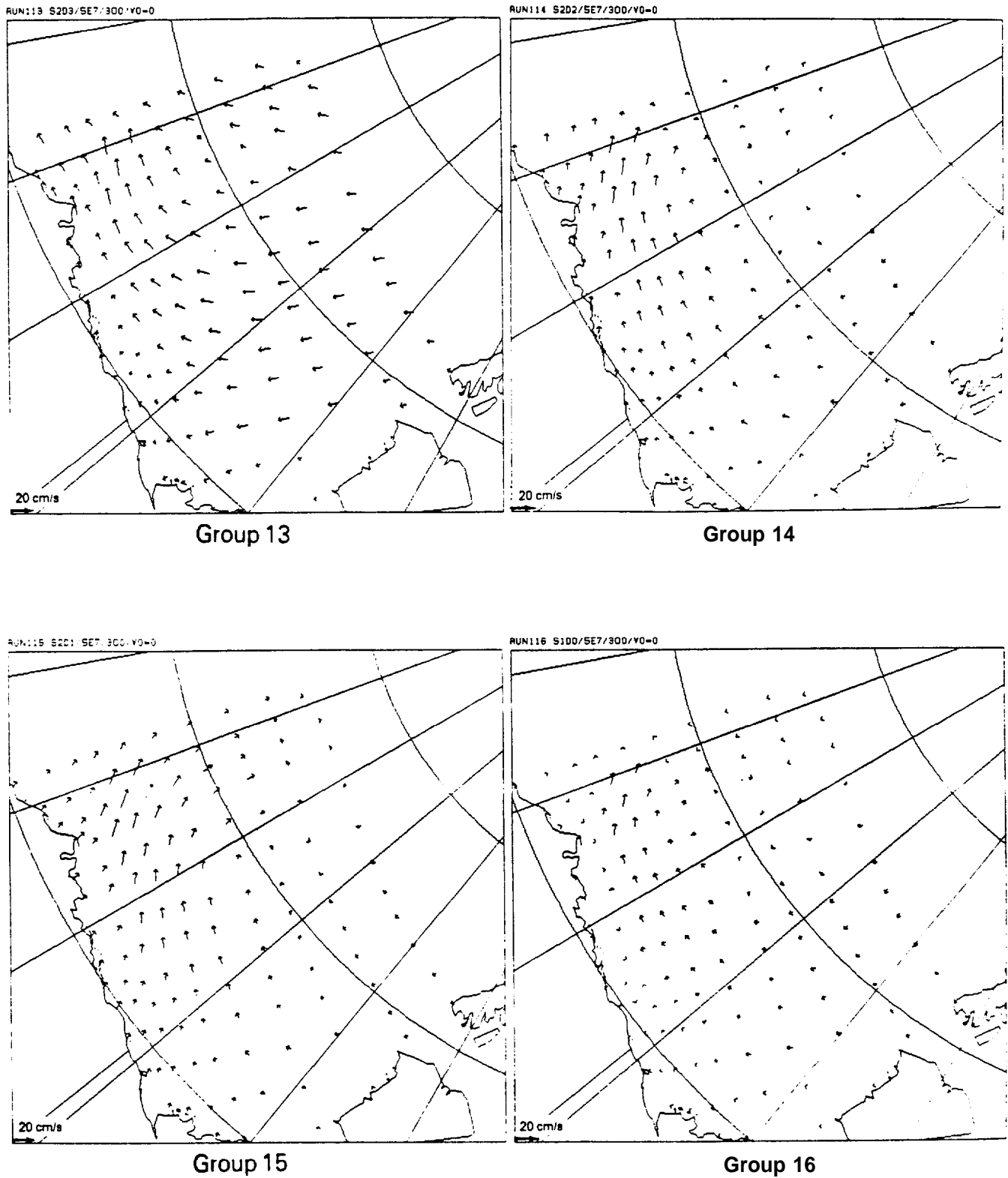


Figure 8. Free-Drift Velocity Fields Resulting from Model Calculations Using the 16 Wind and Boundary Velocity Fields. An Ice Strength of Zero and Average Ice Thickness of 300 cm were Assumed. Geostrophic Currents were Used Beyond the Shelf Break, and the Beaufort Current Jet was Set to Zero (Concluded).

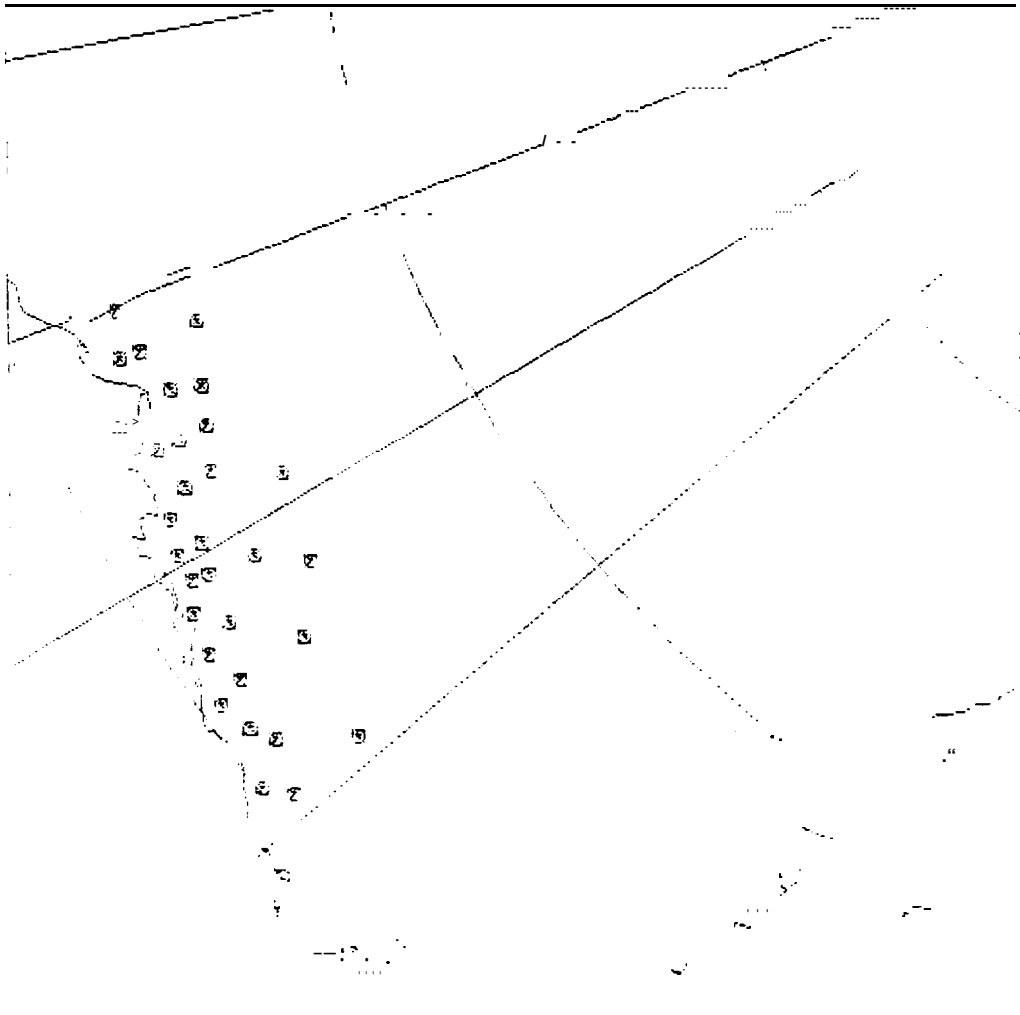
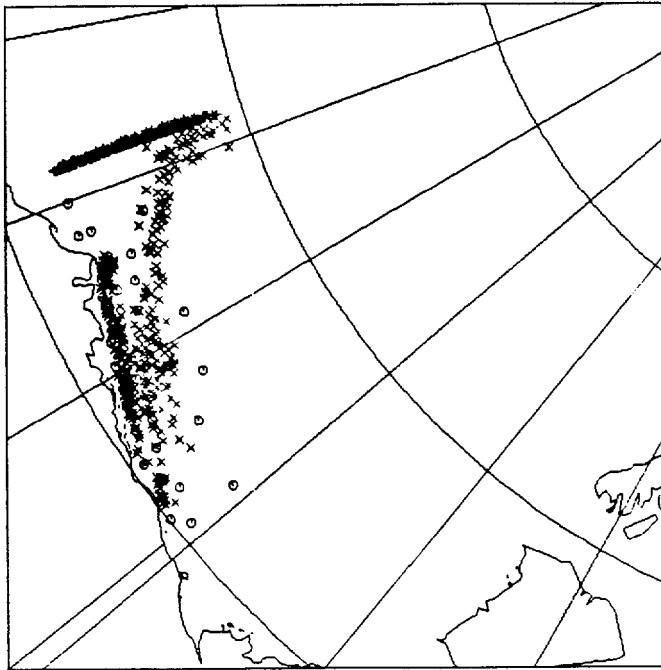


Figure 9. Locations of the 30 Launch Sites Where Seasonal Ice Trajectories were Assumed to Begin.

591 TRAJ LEFT GRID

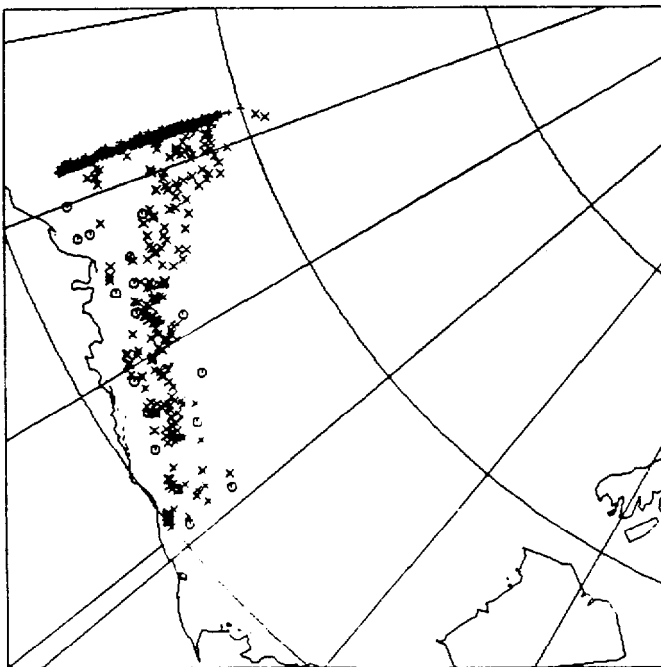
-52-



SEASON 1

Figure 10,
Distribution of End Points on
1 August for 30 Trajectories
Originating from Each of the
30 Launch Sites on 15 October.
The Cluster of Points to the
West is Where individual
Trajectories Crossed the
Computational Grid Boundary
Before 1 August.

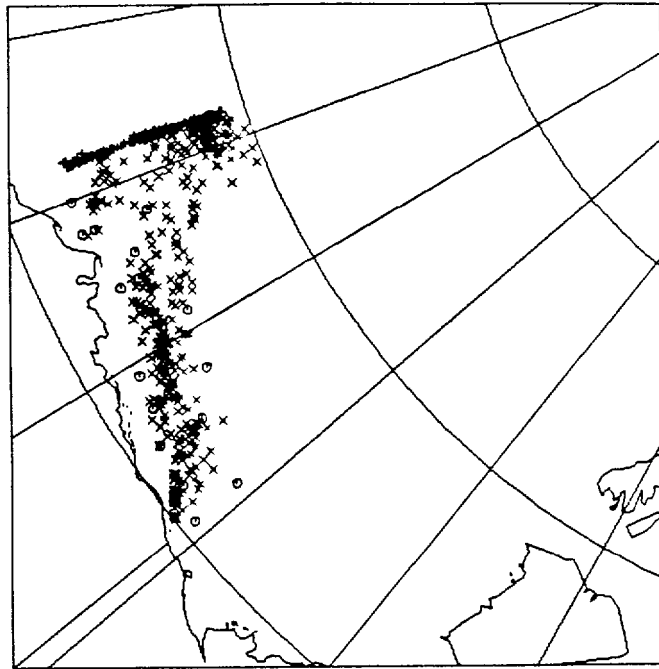
341 TRAJ LEFT GRID



SEASON 2

Figure II.
Distribution of End Pointson
1 August for 30 Trajectories
Originatingfrom Each of the
30 Launch Sites on 1 January.
The ClusterofPoints totheWest
isWhereIndividual Trajectories
Crossed the Computational
Grid Boundary Before 1August.

225 TRAJ LEFT GR10



SEASON 3 -

Figure 12. Distribution of End Points on 1 August for 30 Trajectories Originating from Each of the 30 Launch Sites on 1 April. The Cluster of Points to the West is where Individual Trajectories Crossed the Computational Grid Boundary Before 1 August.

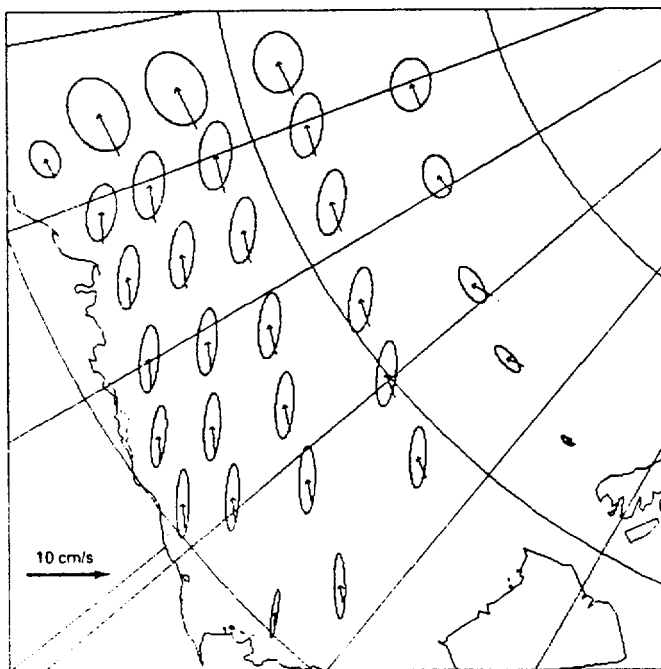


Figure 13.
Mean and 50% Equiprobability Ellipses of Modeled Ice Velocities for the 20 Days Classified as Group 1. Daily Wind Fields and Boundary Velocities were Used. An Ice Strength of $5E7$ dyn/cm and Average Ice Thickness of 300 cm were Used. The Winds Used in These Calculations were Inadvertently Rotated.

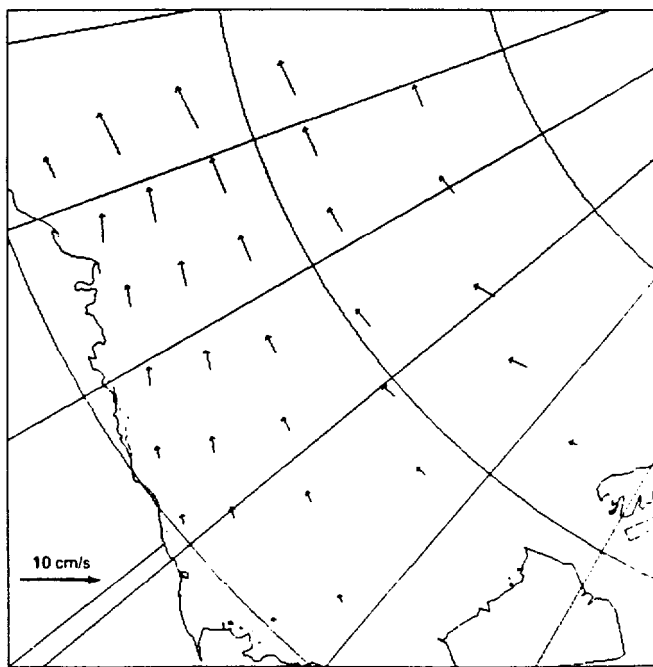


Figure 14.
Modeled Ice Velocity Field Using the Mean Winds and Boundary Velocities for Group 1, An Ice Strength of $5E7$ dyn/cm and Average Ice Thickness of 300 cm were Used. The Winds Used in this Calculation were Inadvertently Rotated.

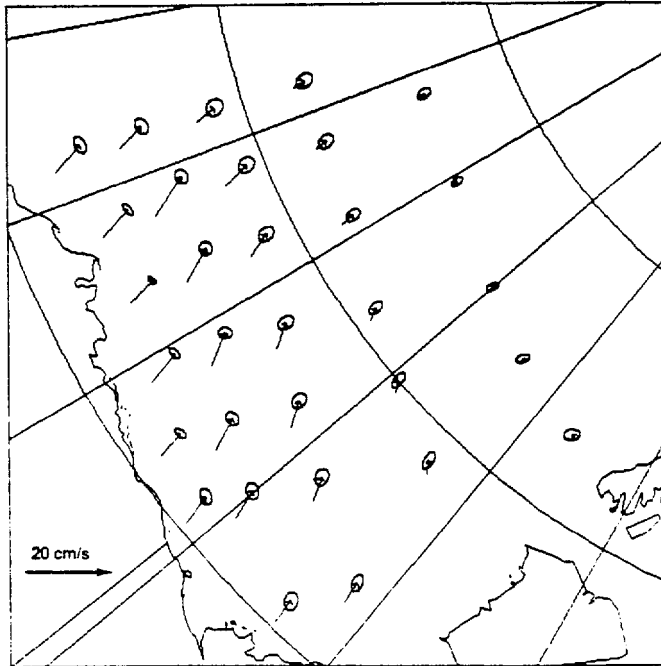


Figure 15.
Mean and 50% Equiprobability
Ellipses of Free-Drift Ice Velocities
for the 20 Days Classified as
Group 1. Daily Wind Fields and
Boundary Velocities were Used.
The Winds Used in These Calculations
were Inadvertently Rotated.

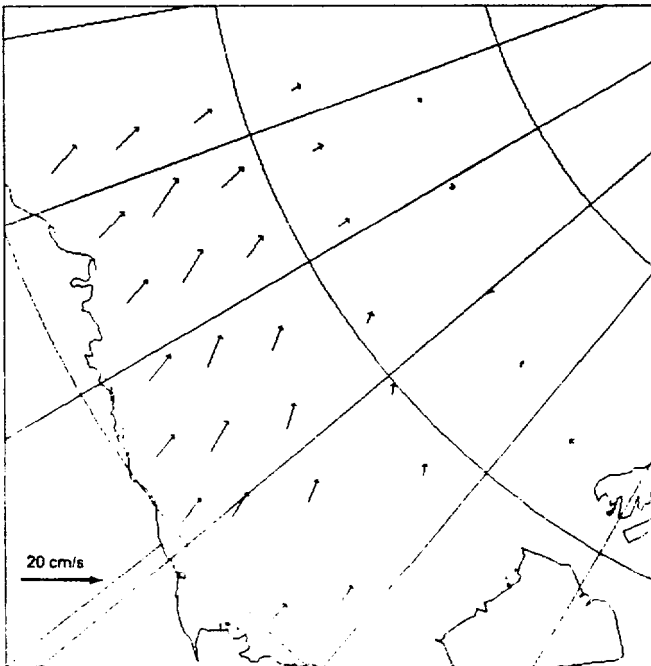
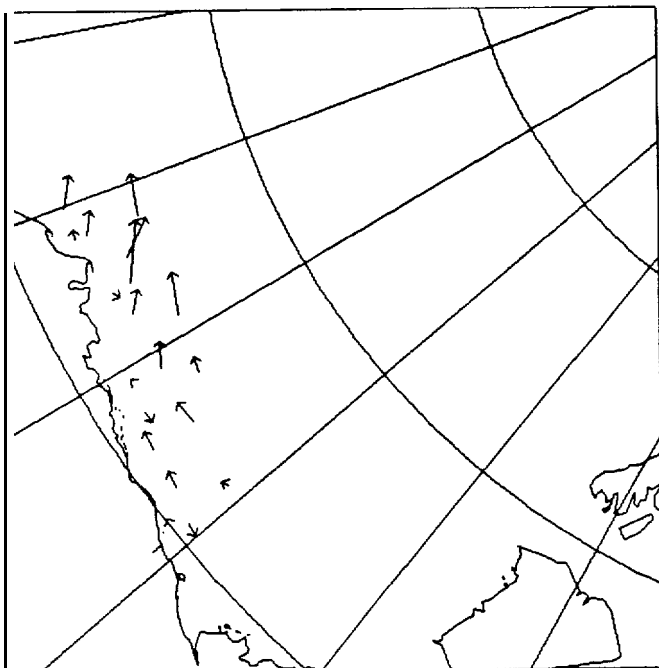
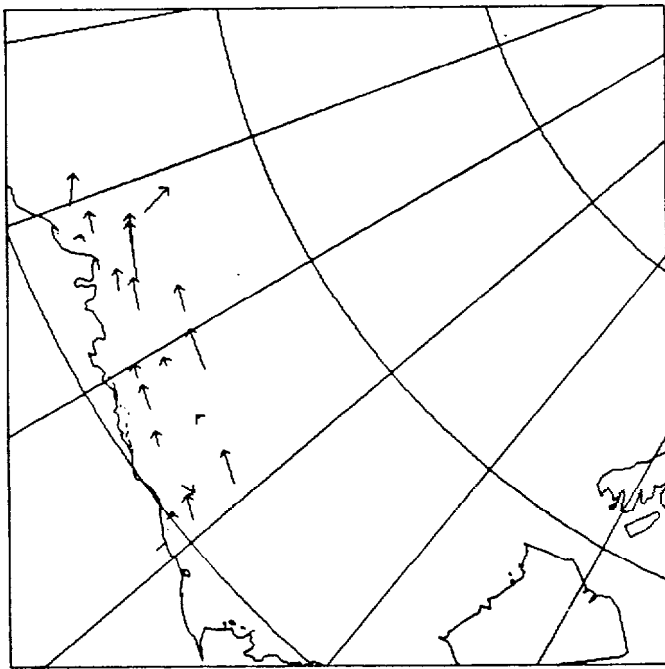


Figure 16.
Free-Drift Ice Velocity Field
Using the Mean Winds and
Boundary Velocities for Group 1.
An Ice Strength of Zero and
Average Ice Thickness of 300 cm
were Used. The Winds Used in
This Calculation were Inadvertently Rotated.



SEASON 2

Figure 17.
Modeled Monthly Ice Motions
for the Winter Season (January,
February, and March). Modeled
Trajectories Originate at the
Launch Points Used in this Study.



SEASON 3

Figure 18.
Modeled Monthly Ice Motions
for the Spring Season (April,
May, and June). Modeled Tra-
jectories Originate at the Launch
Points Used in this Study.

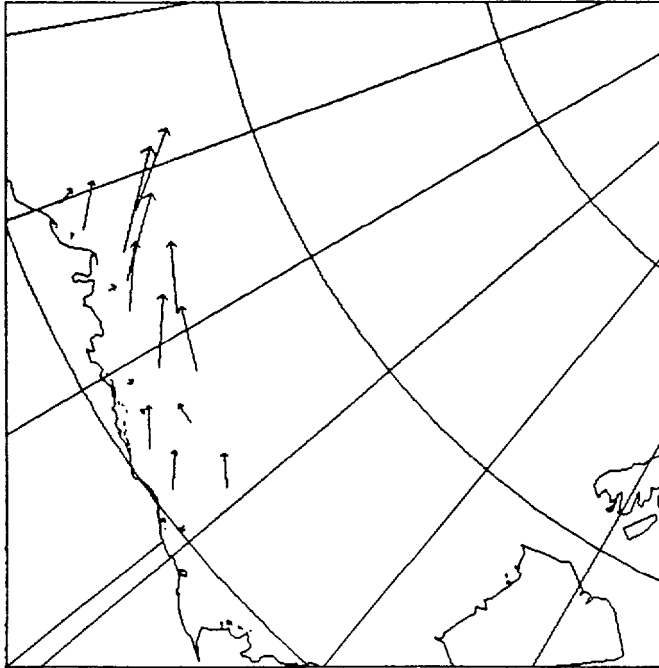


Figure 19.
Modeled Monthly Ice Motions
for the Summer Season (July,
August, and September). Modeled
Trajectories Originate at the
Launch Points Used in this Study.

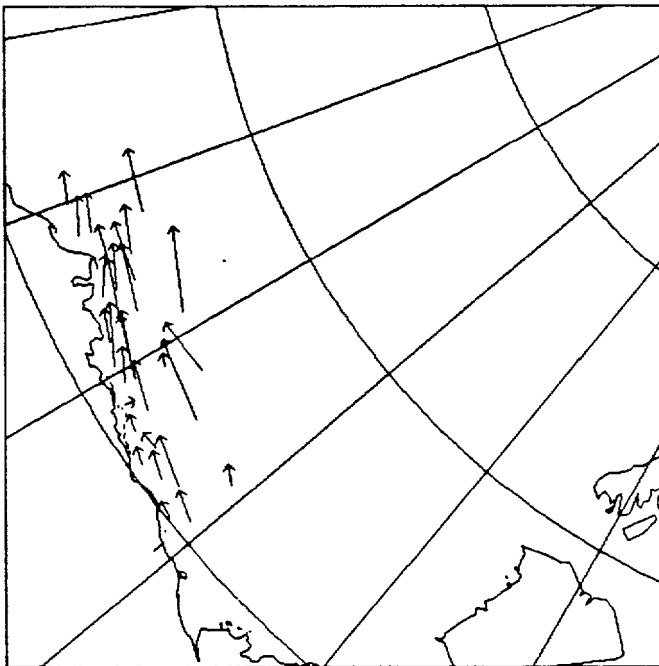


Figure 20.
Modeled Monthly Ice Motions for
the Fall Season (October,
November, and December). Modeled
Trajectories Originate at the
Launch Points Used in this
Study.

SEASON 1

Table 1. Fall Wind Group Transition Matrix

A	1	2	3	4	5	6	7	B	9	10	11	12	13	14	15	16
Probability of group A winds occurring.																
P(A)	.17	.09	.12	.05	.01	.03	.03	.08	.15	.01	.03	.05	.12	.00	.04	
Probability of group A winds occurring given that group B last occurred.																
B	P(A B)															
1	.37	.00	.21	.05	.00	.05	.00	.00	.11	.16	.00	.00	.05	.00	.00	.00
2	.10	.10	.10	.00	.10	.00	.00	.10	.10	.10	.00	.20	.00	.00	.00	.00
3	.15	.15	.00	.00	.00	.00	.00	.00	.08	.23	.00	.08	.08	.15	.00	.00
4	.00	.00	.17	.33	.17	.00	.00	.00	.00	.17	.00	.00	.00	.17	.00	.00
5	.00	.00	.00	.10	.00	.00	.00	.00	.00	.00	.00	.00	.00	.00	.00	.00
6	.33	.00	.00	.00	.00	.00	.33	.00	.00	.00	.00	.33	.00	.00	.00	.00
7	.00	.00	.00	.33	.00	.00	.00	.00	.00	.00	.00	.00	.33	.33	.00	.00
8	.33	.00	.00	.00	.00	.00	.33	.33	.00	.00	.00	.00	.00	.00	.00	.00
9	.22	.33	.22	.00	.00	.00	.00	.11	.11	.00	.00	.00	.00	.00	.00	.00
10	.19	.06	.19	.00	.00	.00	.00	.00	.25	.00	.00	.00	.00	.25	.00	.06
11	.00	.00	.00	.00	.00	.00	.00	.00	.00	.00	.00	.00	.00	.00	.00	.00
12	.00	.00	.00	.00	.00	.00	.00	.33	.33	.00	.00	.33	.00	.00	.00	.00
13	.00	.00	.00	.00	.00	.17	.17	.00	.33	.00	.00	.00	.17	.00	.00	.17
14	.15	.15	.00	.00	.00	.00	.00	.00	.08	.31	.00	.00	.00	.15	.00	.15
15	.00	.00	.00	.00	.00	.00	.00	.00	.00	.00	.00	.00	.00	.00	.00	.00
16	.00	.00	.00	.00	.00	.00	.00	.00	.00	.00	.00	.00	.00	.00	.00	.00

Table 2. Winter Wind Group Transition Matrix

A	1	2	3	4	5	6	7	B	9	10	11	12	13	14	15	16
Probability of group A winds occurring.																
P(A)	.26	.03	.11	.03	.07	.09	.05	.03	.05	.07	.03	.05	.03	.05	.01	.02
Probability of group A winds occurring given that group B last occurred.																
B	P(A B)															
1	.35	.08	.10	.00	.10	.04	.04	.02	.04	.10	.04	.08	.00	.02	.02	.00
2	.43	.00	.14	.00	.00	.00	.14	.00	.00	.00	.00	.00	.29	.00	.00	.00
3	.48	.00	.22	.04	.04	.00	.00	.04	.00	.13	.00	.00	.00	.00	.00	.04
4	.17	.00	.33	.00	.00	.17	.00	.00	.00	.00	.00	.00	.00	.17	.00	.17
5	.29	.00	.07	.00	.14	.07	.14	.00	.07	.00	.14	.00	.00	.00	.07	.00
6	.16	.00	.00	.11	.11	.16	.11	.11	.00	.05	.05	.11	.00	.00	.05	.00
7	.30	.00	.00	.00	.10	.30	.10	.10	.10	.00	.00	.00	.00	.00	.00	.00
8	.57	.00	.00	.00	.00	.00	.29	.00	.14	.00	.00	.00	.00	.00	.00	.00
9	.10	.00	.00	.00	.00	.10	.00	.00	.30	.20	.00	.00	.20	.10	.00	.00
10	.14	.00	.21	.21	.00	.07	.00	.00	.07	.07	.00	.00	.00	.14	.00	.07
11	.00	.00	.00	.00	.17	.33	.00	.17	.17	.00	.17	.00	.00	.00	.00	.00
12	.10	.00	.00	.00	.10	.40	.00	.10	.00	.10	.00	.20	.00	.00	.00	.00
13	.33	.17	.17	.00	.00	.00	.00	.00	.00	.00	.00	.00	.17	.00	.00	.17
14	.00	.00	.36	.00	.09	.00	.00	.00	.00	.09	.00	.00	.09	.18	.00	.09
15	.00	.00	.00	.00	.00	.33	.00	.00	.00	.00	.00	.67	.00	.00	.00	.00
16	.00	.00	.20	.20	.00	.00	.00	.00	.00	.00	.00	.00	.00	.60	.00	.00

-A1-

APPENDIX A

A MODEL FOR CURRENTS ON THE ALASKAN BEAUFORT SHELF

Miles G. McPhee

3 June 1982

1. Introduction

The intent of this report is to describe a method for estimating oceanic currents on the Beaufort shelf north of Alaska to be used as one of the input driving force fields for a model of nearshore sea ice drift. The report presents an outline of a definitive summary of work done in the past decade on the Beaufort shelf, prepared by Aagaard (1981), and then extrapolates the results from that work to surface geostrophic currents. Not a great deal is known about currents in this **region**, especially near the surface where sea **ice interacts with** the **geostrophic** current, so **it** should be stressed that the proposed current **regime is** speculative.

There are two **principles** to be kept **in mind** in what follows. **First**, results of **OCSEAP** current meter **studies** on the Beaufort shelf show that there **is** often a strong current **flowing** along the **isobaths** near the shelf **break** (**i.e.**, where the offshore **gradient in depth** suddenly increases), and that **this** current reverses from east-setting to west-setting frequently. Most of the measurements have been made at mid-depth or lower in the water column, so there is no clear picture of what the surface manifestation of the current is, nor how it interacts with the ice. There is evidence, however, that the current is confined to a rather narrow band, following the bathymetry of the shelf break. We thus have a "river" embedded within the oceanic flow that coincides roughly with the pack ice shear zone.

The second principle is that our proposed treatment of currents in the shallow part of the shelf (as a rough guide, inshore from the 40-m **isobath**) **is** predicated on using ice-water drag as modified by the shallow boundary layer effects described by McPhee (1982). It would thus be mistaken to assume that the absence of geostrophic current in the nearshore region means that a drag

-A2-

law appropriate for deep water ice drift can be used with no modification by ocean currents. Instead, currents exist in the water column that are driven by stress between ice and water, but that are different from currents which would be observed at corresponding levels under ice far offshore because the bottom has a pronounced effect on turbulence, provided the water column is well mixed.

-A3 -

2. Background

This section summarizes a review prepared by **Aagaard** (1981), especially as it pertains to current/ice interactions on the Beaufort shelf north of Alaska.

Aagaard describes the Beaufort shelf as relatively narrow with numerous embayments and several lagoon/barrier island systems. There is comparatively little fresh runoff--the discharge of the **Colville**, the largest of the rivers west of the Canadian **Beaufort**, is estimated to be about 5 percent of the discharge from the Yukon. Astronomical tides are small, with mean ranges of from 10 to 30 cm. Storm surges occur when wind systems move the shelf waters around, and have been observed to be an order of magnitude larger than astronomical tides. Except where topographic constrictions occur near shore, it is thus probable that tidal currents are relatively small over most of the shelf, which is borne out in most of the measurements. Surface winds, as measured at shore locations, are predominantly ENE in the western portion of the Beaufort and are bimodal ENE and WSW in the eastern part.

The measurements from which Aagaard's report was derived consist of hydrographic surveys totaling 110 CTD stations from October 1975 through March 1977, and a total of 2335 days of current meter records, mostly from bottom-moored instruments. This represents by far the most extensive data set for Beaufort shelf processes, and is particularly notable in that the hydrography spans the winter season--previous studies have been heavily weighted to summer (melt season) measurements.

As it pertains to ice drift analysis, perhaps the most important result of the hydrography is the seasonal change in water column structure. By the end of the melt season, a low-salinity mixed layer roughly 20 m thick has developed, which is separated from the deeper water by a sharp vertical density gradient. Sections from November 1975 showed that mixed-layer salinity increased in the offshore direction from 27 to 29 ppt. A survey three months later showed a decrease in the offshore direction from 30.7 to 29.9 ppt. The winter profile was still stratified vertically, but with much less total density difference. Because the salinity of the water column increased dramatically at all depths, and the entire column was near its freezing point in the winter (February) section, **Aagaard** argues that the winter structure results more from horizontal advection of water that has been exposed to

-A4-

freezing at various salinities than to direct, one-dimensional mixing processes. With this in mind, it seems likely that during the intense freezeup period before the sea ice has become fast, the water column is often well mixed from top to bottom; consequently, the turbulent structure will be quite different from the highly stratified summer situation.

Another important aspect of the hydrography traces the influx of Alaska coastal and Bering Sea waters flowing eastward along the shelf seaward of the 40- to 50-m **isobaths**. During summer this shows up as a **distinct** subsurface tongue of warm water **hugging** the shelf break. **Combined with** the current meter records **described** later, the temperature structure delineates a current jet **flowing mainly** eastward. Unfortunately, near the surface, the Alaska coastal water **mixes rapidly with** the **ambient** shelf water and loses **its utility** as a tracer.

Very few data **exist** on currents over the inner shelf, **which is** the **region** landward of the 40- to 50-m depth zone. **Summertime** measurements **imply** that the **circulation is** more or less **directly wind driven, with** the net motion westward **in keeping with** the **prevailing** easterly **winds**. Two current meters, suspended at 10 m in water of 30-m and 40-m depths, also implied a wind-driven current regime in winter, although the energy levels were much reduced from summer levels. In each case, there was negligible mean current in the **three-** week records. What forces wind-associated currents under fast ice is not immediately obvious: Aagaard mentions horizontal entrainment, but pressure gradients associated with water transport under mobile ice just outside the fast ice zone might also be a factor. Regardless of the mechanism, **Aagaard's** work suggests that no organized **alongshelf** motion exists on the inner shelf in the absence of wind forcing, so any currents affecting the ice motion would be caused mainly by the recent wind history.

On the outer shelf, which is essentially the shelf-break zone, the situation **is** quite different. Most of the current records were obtained from fixed moorings positioned along the shelf break between the 100-m and 200-m **isobaths**. Exceptions were the **OL-1** and **FLAX-1** sites, which were in 60-m-deep water. At **OL-1** the bottom slope is so steep that the distance to the 200-m **isobath** is only a few kilometers. Heavy ice conditions precluded mooring current meters above the 40-m depth in the water column. This is well down

-A5 -

into the pycnocline, and is not necessarily indicative of near-surface conditions, a fact which should be kept in mind in the following discussion.

The main features of the current jet along the shelf break are shown in Figure 3 of Aagaard's report. The current is clearly steered by the topography, with by far the most frequent current directions being generally eastward or westward along the local isobaths. In the mean, the current appears to be eastward at about 7 cm/s, but the mean apparently represents an infrequent realization since it is a vector sum of generally larger eastward and westward flows. The mean eastward flow varies among the various sites somewhere in the range of 15 to 25 cm/s, with the secondary mode (westward) being perhaps two-thirds of the primary.

One item of note is that the geostrophic shear between the surface and 40 dbar indicates a mean westward shear of about 7 cm/s. Based on this, Aagaard reasons that the mean surface flow may be close to zero or slightly westward.

Aagaard speculates that the overall driving force behind the mean eastward motion is the climatological factors, which cause the sea level in the Pacific to be about 1 m higher than in the Atlantic, and that the current jet persists eastward into the Canadian Beaufort, then north along Banks Island, through M'Clure Strait and into the Canadian Archipelago.

What causes the frequent flow reversals from east-setting to west-setting is not well understood. Statistical treatment in Aagaard's report tends to give somewhat contradictory indicators. There is a moderate coherence between current and both geostrophic and surface winds measured at Barter Island, yet there are also cases in which a reversal occurs with no obvious connection with the wind over the shelf. Visual comparison of currents at two moorings separated by 65 km in the alongshore direction indicates that most of the major current events are similar with little time lag, but coherence statistics for the same current meters indicated rather low average coherence.

To confuse matters further, an example is shown where two major flow reversals observed in the Chukchi, some 650 km "upstream", show up about 106 days later in a current meter record from the Beaufort shelf. If the features are related, the implication is that momentum associated with the disturbance is advected downstream at about the long-term mean velocity. On the other hand,

-A6-

certain reversals coincide almost exactly with reversals in the wind, and persist pretty much in phase along the entire shelf, so if the mechanism described above operates, it is probably not a dominant factor.

Aagaard's conclusion regarding the importance of wind forcing is that "the **longshore** (sic) wind plays an important, but not all-prevailing, role in the low-frequency variability of the subsurface longshore flow." He goes on to state that when winds along the shelf are easterly at 8 to 10 m/s, currents will normally reverse and set westerly.

There is little predictable seasonal variation in the current meter records. The presence of ice apparently has little impact on the strength of the current signal; analysis of current records from two different years showed the strongest east and west three-week-mean currents to be in the January-February period. Random fluctuations on a **one-** to two-month time scale appear to dominate the low-frequency variability.

From the **bathymetry** it appears that the current jet follows closely the 200-m isobath, which marks the shelf break along the Beaufort coast, since the offshore slope is consistently large there. The width of the jet is not well known; however, there are indications that it is confined to a rather narrow zone. The tongue of warmer water observed during the summer appears to extend across about half a degree of latitude (see **Aagaard's** Figures 5 and 6). Current meters at the FLAX-1 site, which was moored in 59 m of water, show decreased **bimodality** and generally lesser current speeds. **Aagaard** suggests that FLAX-1 is **in a transition** zone between the outer and inner shelf **regions**. The jet has not been observed **inside** the 40-m isobath, which is on the average about 30 km inshore from the 200-m **isobath**. The only evidence for the **off-shelf** limits of the feature that I am aware of comes from comparing **AIDJEX** met-ocean buoy records with concurrent **OCSEAP "OL"** mooring records. The moored current meter at 100 m showed sizable eastward motion near the 150-m **isobath**, but a current meter about 50 km farther offshore, suspended at 30 m below the met-ocean buoy, indicated very small currents. The met-ocean buoys were originally deployed over the 1000-m **isobath**, and most of the resolvable currents they measured were westward following the main sense of the **Beaufort Gyre**.

-A7 -

3. Current Model

The intent here is to include the shelf current features discussed in the previous section and in McPhee (1982) in a way that can be easily included in a numeric model for sea-ice drift.

The interaction between the sea ice and the ocean is divided into three zones: the shelf-current jet, as described in the previous section, in which the **geostrophic** current is a function of position relative to the core of the jet, which is assigned a particular velocity; an outer zone seaward of the current jet, which uses the same geostrophic velocity field as the AIDJEX model, derived originally from the dynamic topography of Newton (1973); and a shallow zone in which the **geostrophic** current is zero, but the drag relation between sea ice and water is modified by the effect of bottom turbulence. The **geostrophic** velocity field, interpolated at the nodes of the large computational grid, is shown in Figure A1.

The approach is keyed to the **large-** and small-scale grids of the Flow **Near-**shore Model. The main tasks for each grid point are (1) determine the water depth at the grid location from a bathymetric chart; (2) determine the position relative to the 200-m **isobath**, which is taken to be the core axis of the **alongshelf** jet; and (3) determine the geostrophic velocity according to which zone the grid point belongs.

The depth of each grid point is estimated by interpolating between known positions of depth contours obtained from an **OCSEAP** bathymetric chart of the Beaufort Sea. The interpolation grid was set up by determining the latitude of the 20-, **40-, 80-, 120-, 200-**, and 2000-m **isobaths** along meridians for each half degree in longitude from 142°W to 155°W. The "shore" contour skirts the barrier islands in keeping with the grid, and for the sake of interpolation between it and the 20-m **isobath**, is assigned a depth of 3 m. The depth of a particular grid point is found from the latitude and longitude of the grid location by interpolating between contour latitudes on adjacent meridians.

The current jet is modeled under the following assumptions:

- (1) The center of the jet follows the 200-m **isobath** and is characterized by one core velocity, V_0 , which is positive if eastward and negative if westward.

-A8 -

- (2) The width of the jet is taken to be 60 km, and velocities within the jet fall off to zero at the inshore boundary. Velocity is also zero for all points shoreward of the inner jet boundary (again, with the caveat that the shallow boundary layer drag law is used). Offshore, the jet blends into the long-term geostrophic flow of the AIDJEX model at a distance of 30 km from the core.
- (3) The strength of the jet varies sinusoidally from the maximum at the center (200-m **isobath**) to zero at the inner boundary and to the **geostrophic** velocity at the outer boundary.

The algorithm for computing the velocity at a given grid point is set up so that the core strength, V_0 , of the jet can be varied without having to recalculate its position relative to the jet each time. The velocity is given by the complex equation

This is accomplished by preparing an array with the following variables for each grid point:

Depth, $V_i(x)$, $V_i(y)$, ,

Figure A2 shows examples for a segment of the shelf current from about 153°W to 149°W . Current vectors are plotted along each half-degree meridian at 10-km spacings. In the upper plot, V_0 is 20 **cm/s** to the east (positive), while in the lower plot it is 20 cm/s to the west or -20 cm/s. In the upper plot, the construction lines along the 150°W meridian show how the cosine fairing smoothes the jet from the core to the boundaries. When the current is in its predominant east-setting mode, there is an intense zone of current shear near the 72nd parallel.

Figures A3, A4 and A5 show examples of the shelf current plotted for each grid point of the small-scale grid for values of V_0 of 0, +20 cm/s (eastward flow), and -14 cm/s (westward flow), respectively.

The bathymetry near the mouth of the Barrow Submarine Canyon leads to rapid changes in the current direction, which may not be realistic. Farther east, the current settles into a fairly well-behaved pattern. One thing that shows up from these plots is that the spatial coverage of the small-scale array is not very dense in the vicinity of the jet, which may distort its effect somewhat.

-A9 -

References

- Aagaard, K. (1981) "The Beaufort Current," to appear in the The Alaskan Beaufort Sea (P. Barnes, E. Reimnitz, and D. Schell, editors), the Academic Press, N.Y.
- McPhee, M. G. (1982) "The Turbulent Boundary Layer in Shallow Water," Appendix C of Annual Report to OCSEAP, RU#567, March.
- Newton, J. L. (1973) "The Canada Basin: Mean Circulation and Intermediate Scale Flow Features," Ph.D. Thesis, University of Washington, Seattle.

-A10-

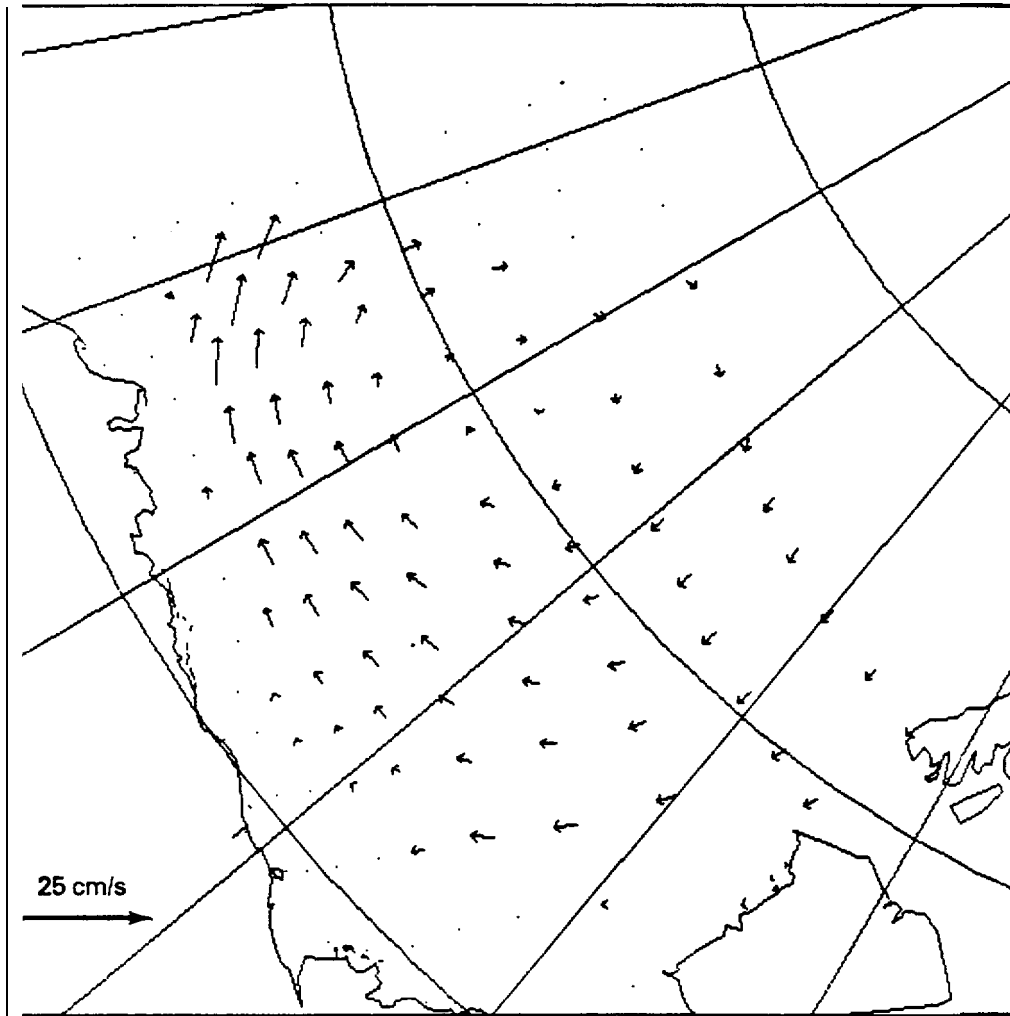


Figure A1. Geostrophic Velocity Field

-A1 1-

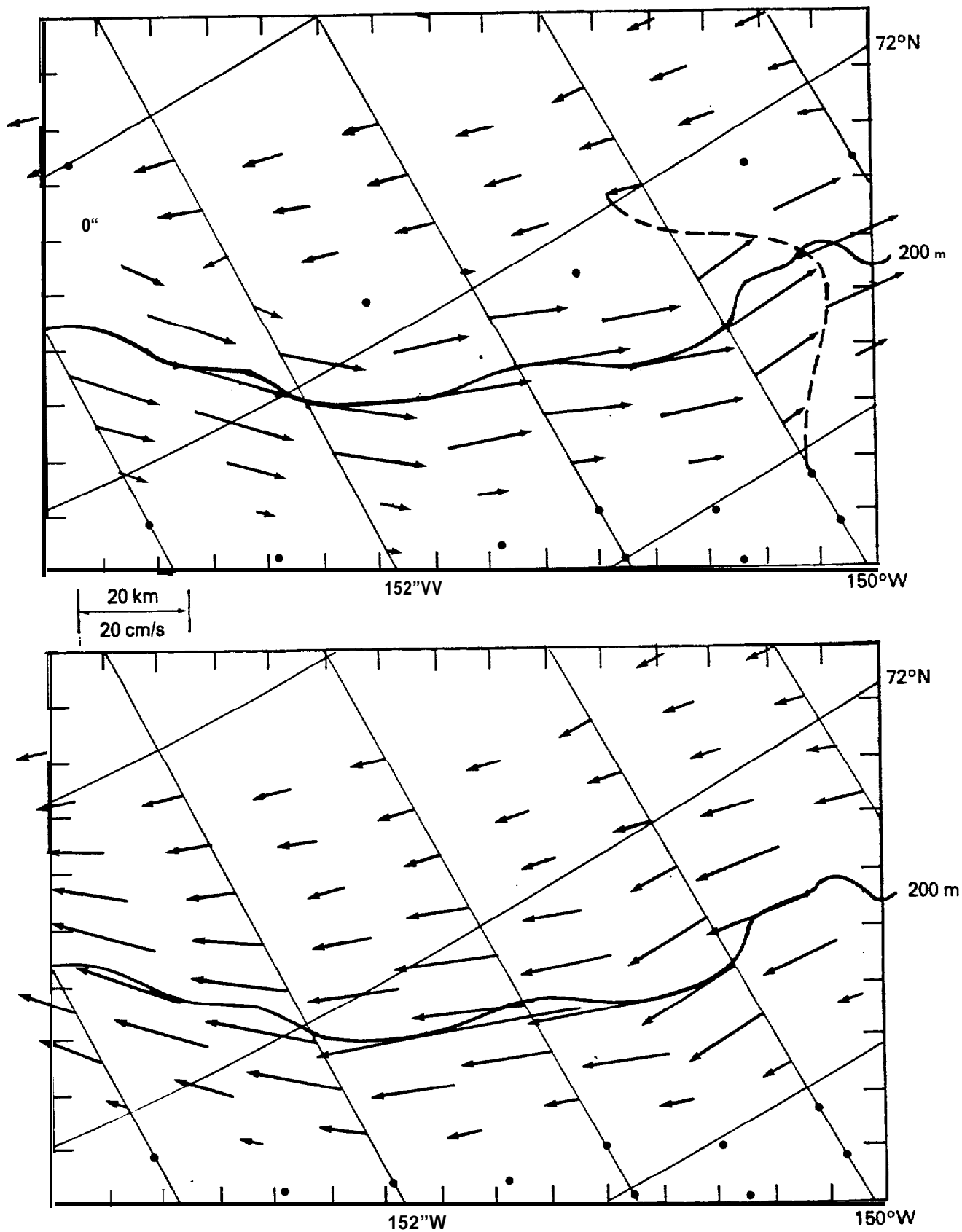


Figure A2. Segment of Modeled Beaufort Current Velocity Field for 20 cm/s Current Jet Flowing East (Above) and West (Below).

-A12-

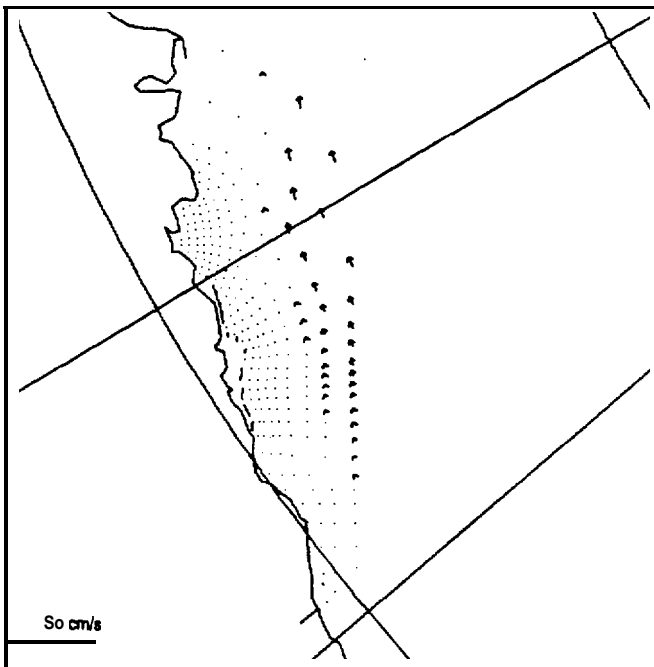


Figure A3. Modeled Beaufort Current Velocity Field for Jet with Zero Velocity.

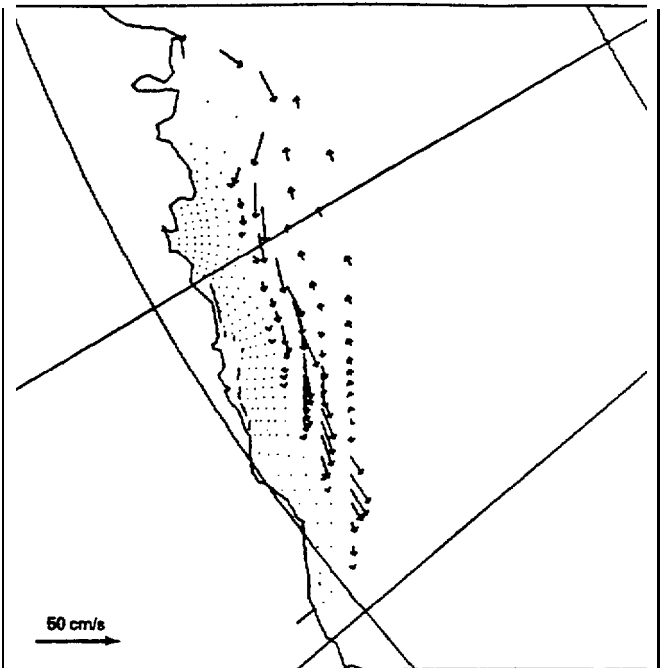


Figure A4. Modeled Beaufort Current Velocity Field for Jet with 20 cm/s Eastward Velocity,

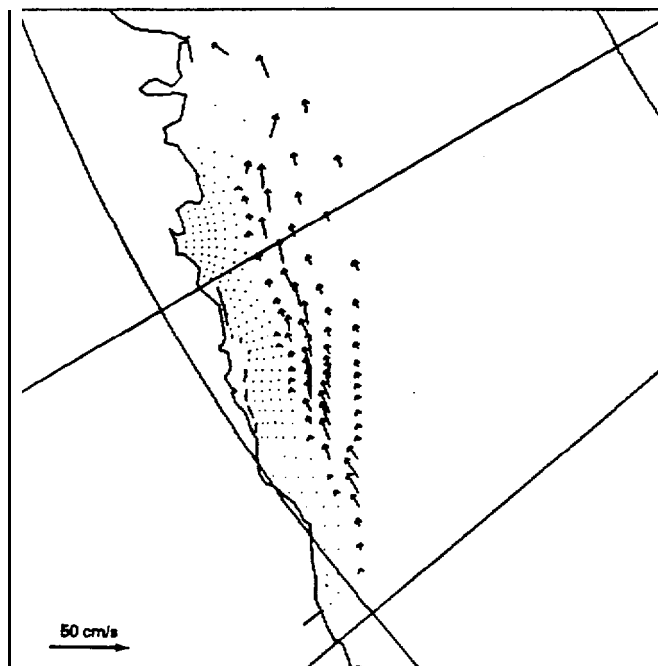


Figure A5 Modeled Beaufort Current Velocity Field for Jet with 14 cm/s Westward Velocity.

-B 1-

APPENDIX B

OBSERVED MONTHLY ICE MOTIONS

The drift of Arctic sea ice has long been of interest to Arctic explorers and researchers. They have all recognized that the ice moves in response to winds and underlying ocean currents, and that knowledge of ice motions gives knowledge of the circulation of Arctic air and water masses. Early information on long-term ice motion came from ships that were either accidentally or intentionally caught in the ice pack. Later, manned camps, using celestial navigation, tracked the ice motion. Although enormous efforts were involved in those studies, the amount of motion data collected remained small. In recent times, though, the use of automated data buoys dropped or placed upon the ice and located by satellites has greatly increased the amount of ice motion data throughout the Arctic.

The primary use of most of the recent ice motion data has been to aid in understanding how the ice cover moves and deforms in response to winds and ocean currents. In addition, we now have a general understanding of the circulation of the atmosphere and the ocean in Arctic regions. Not enough data exist, however, to adequately describe the spatial and temporal variability of ice motions throughout the Arctic.

The Beaufort Sea is of particular interest to the U.S. and has more ice motion data available than most of the Arctic. While the amount of data is small in a statistical sense, it can give a suggestion of the interannual variability of large-scale ice motions, as well as suggest the need for further data collection. We have collected the readily available ice motion data and present here monthly ice motions based on those data.

Due to resource limitations, we restricted the area of study to the Beaufort Sea, between 125° W and 165° W longitude, and south of about 80°N. The actual criterion was that the monthly displacement vector must fall within the area plotted. Only monthly locations and motions are presented here, although location data exist for most stations and buoys for much shorter intervals (several times a day). All the data presented here came from only a few sources, those taken during **AIDJEX** (Arctic Ice Dynamics Joint Experiment)

-B2-

from 1971 through 1976, earlier historical data collected by the AIDJEX data bank, data from OCSEAP (Outer Continental shelf Environmental Assessment Program) buoy programs, and the Arctic Ocean Buoy Program data taken by the Polar Science Center at the University of Washington. Although this data set may not be complete, only a few buoy month's worth, at the most, are missing.

The data are presented in the form of maps showing monthly ice motions as vectors at the same scale as the map. Each map shows all the monthly ice motions for a three-month period, beginning with January, February, and March 1959, and continuing through October, November, and December, 1981. Many maps show no ice motions, and where a full 12 months occur without data, the maps were left out to conserve space. The vectors are labeled with an ID number which is internal to this report and which must be cross-referenced to the actual ID in the accompanying tables to identify the data source. The ID number for a buoy will be different each ice season. The ice season is considered to begin in October and end in September; the data are broken up by ice season rather than by year or by buoy. Some buoys or stations have data available for only one or two months of the three months presented on each map; the tables must again be consulted to identify the month(s) present.

The monthly trajectories are presented in Figure B1. The map scale is 188 km/cm. The map is an azimuthal equidistant projection tangent at the pole.

In Table B1 we present the location of each buoy or station in decimal degrees of latitude and longitude on the first day of each month. Internal and external identification numbers or names are also given. A list of data sources is given at the end of the report.

A total of 366 monthly displacements are presented here. These data cover a span of 25 years (from 1958 through 1982), with 17 of those years having some data available. Satellite-transmitted buoy data were first available in 1972.

The data are basically self-explanatory, and only a few comments and observations need to be made. Much of the early data, prior to 1967, comes from ice island T-3 and may not be representative of pack ice motion. Since a deep-draft ice island experiences a different set of driving forces than a flat ice sheet, it can at times move relative to the pack, especially during the summer when it is less likely to be frozen into the pack.

-B3-

A majority of the data were taken during the **AIDJEX** main experiment. This is unfortunate in a way, since it appears that the 1975-76 ice season was an anomalous one and possibly represents an extreme event. Not enough years of data exist yet to be sure of this. Nevertheless, one must not assume that, since a majority of the buoy data shows one pattern of ice motion, this is the typical motion. If one gives the motion data collected during 1975-76 equal weight with that from other years, we see that (1) typical motions are much larger than the mean using all buoy data would indicate, and (2) the **useful** data set is very small.

It should also be noted that a few of the buoys appeared to be caught in the fast ice near the Alaskan coast. Little or no motion near the coast does not imply much about the motion further away from the coast. It is generally assumed that a velocity discontinuity exists between the fast ice and the pack ice. Only during the winter of 1975-76, however, is this discontinuity evident from the data.

-B4-

References

- AIDJEX Staff (1972) "Station Positions, Azimuths, Weather - 1972 AIDJEX Pilot Study, Preliminary Data," AIDJEX Bulletin No. 14, University of Washington, Seattle, July.
- Colony, R., Personal communication. Ice Island T-3 position data are from historical ice drift data set obtained from the National Climatic Center, Asheville, N.C.
- Thorndike, A. S. (1977) "Measurements of Sea Ice Motion January 1977 to September 1977," Unpublished data report to OCSEAP, Polar Science Center, University of Washington, Seattle.
- Thorndike, A. S., and J. Y. Cheung (1977a) "AIDJEX Measurements of Sea Ice Motion 11 April 1975 to 14 May 1976," AIDJEX Bulletin No. 35, University of Washington, Seattle, January, 149 pp.
- Thorndike, A. S., and J. Y. Cheung (1977b) "Position Data Supplement No. 1, 14 May 1976 to 30 Nov 1976," Unpublished data report, Polar Science Center, University of Washington, Seattle.
- Thorndike, A. S., and J. Y. Cheung (1977c) "Measurements of Sea Ice Motion Determined from OCS Data Buoys, October 1975 to December 1976," Environmental Assessment of the Alaskan Continental Shelf, Annual Reports of Principal Investigators for the year ending March 1977, Vol. XVI Hazards, Outer Continental Shelf Environmental Assessment Program, Boulder, Colorado, pp. 179-251.
- Thorndike, A. S., and R. Colony (1980) "Arctic Ocean Buoy Program Data Report, 19 January 1979 to 31 December 1979," Polar Science Center, University of Washington, Seattle, 131 pp.
- Thorndike, A. S., and R. Colony (1981) "Arctic Ocean Buoy Program Data Report, 1 January 1980 to 31 December 1980," Polar Science Center, University of Washington, Seattle, 127 pp.
- Thorndike, A. S., R. Colony, and E. A. Munoz (1982) "Arctic Ocean Buoy Program Data Report, 1 January 1981 to 31 December 1981," Polar Science Center, University of Washington, Seattle, 137 pp.

-B5-

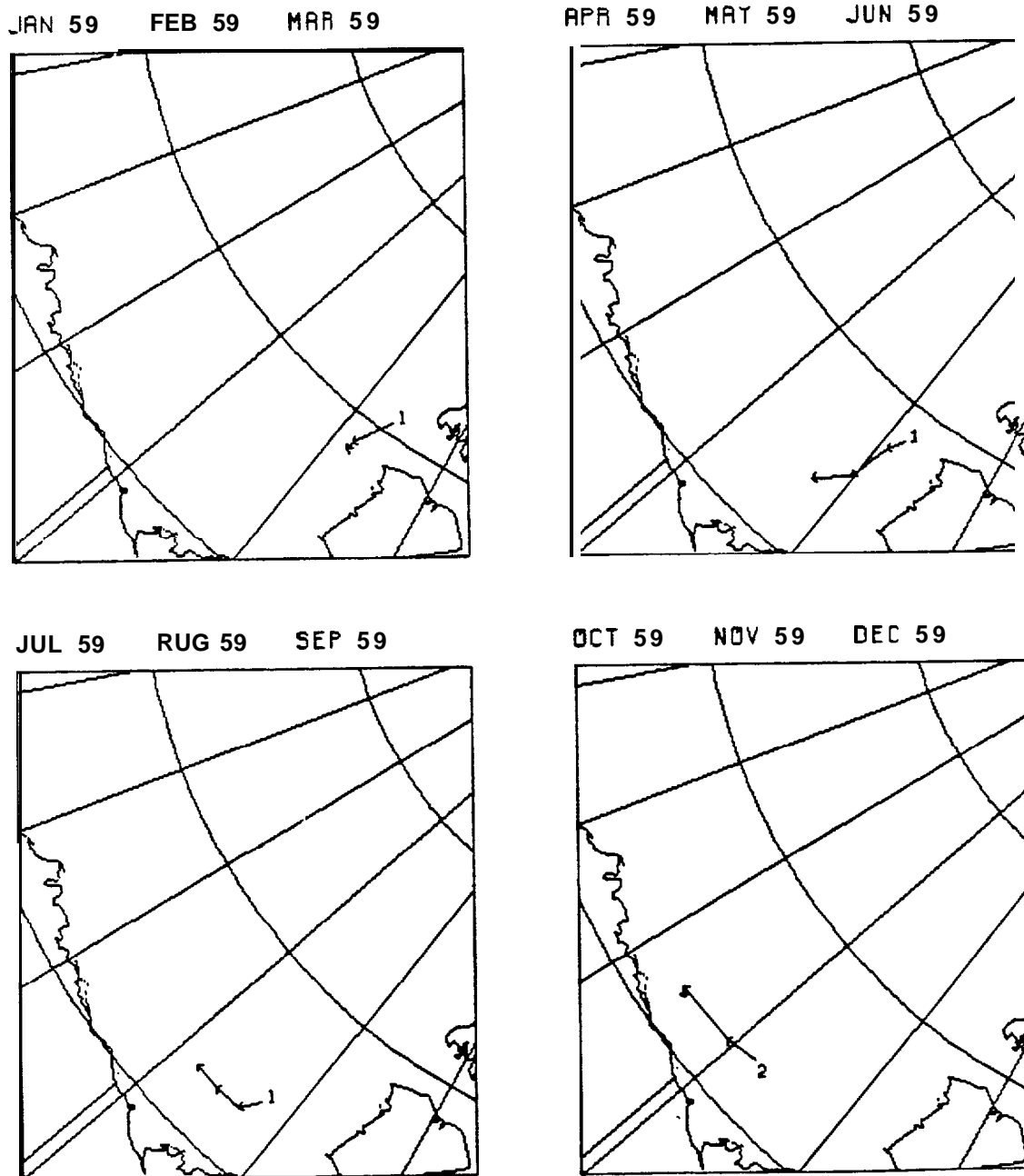


Figure B1. Observed Monthly Buoy Trajectories in the Beaufort Sea from 1959 Through 1981. Each Plot Represents a 3 Month Period.

-B6-

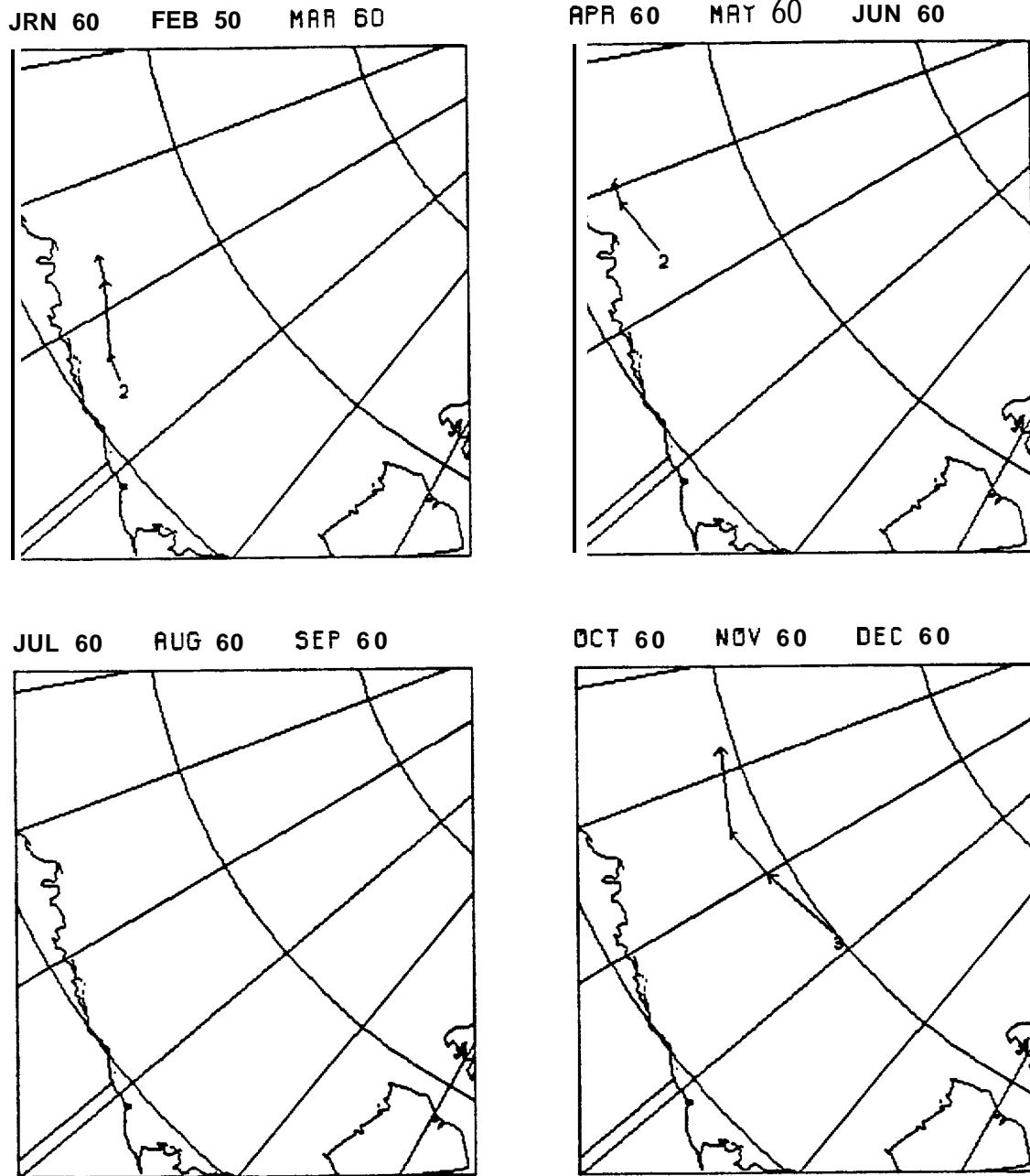


Figure B1. Observed Monthly Buoy Trajectories in the Beaufort Sea from 1959 Through 1981. Each Plot Represents a 3 Month Period (Continued).

-B7-

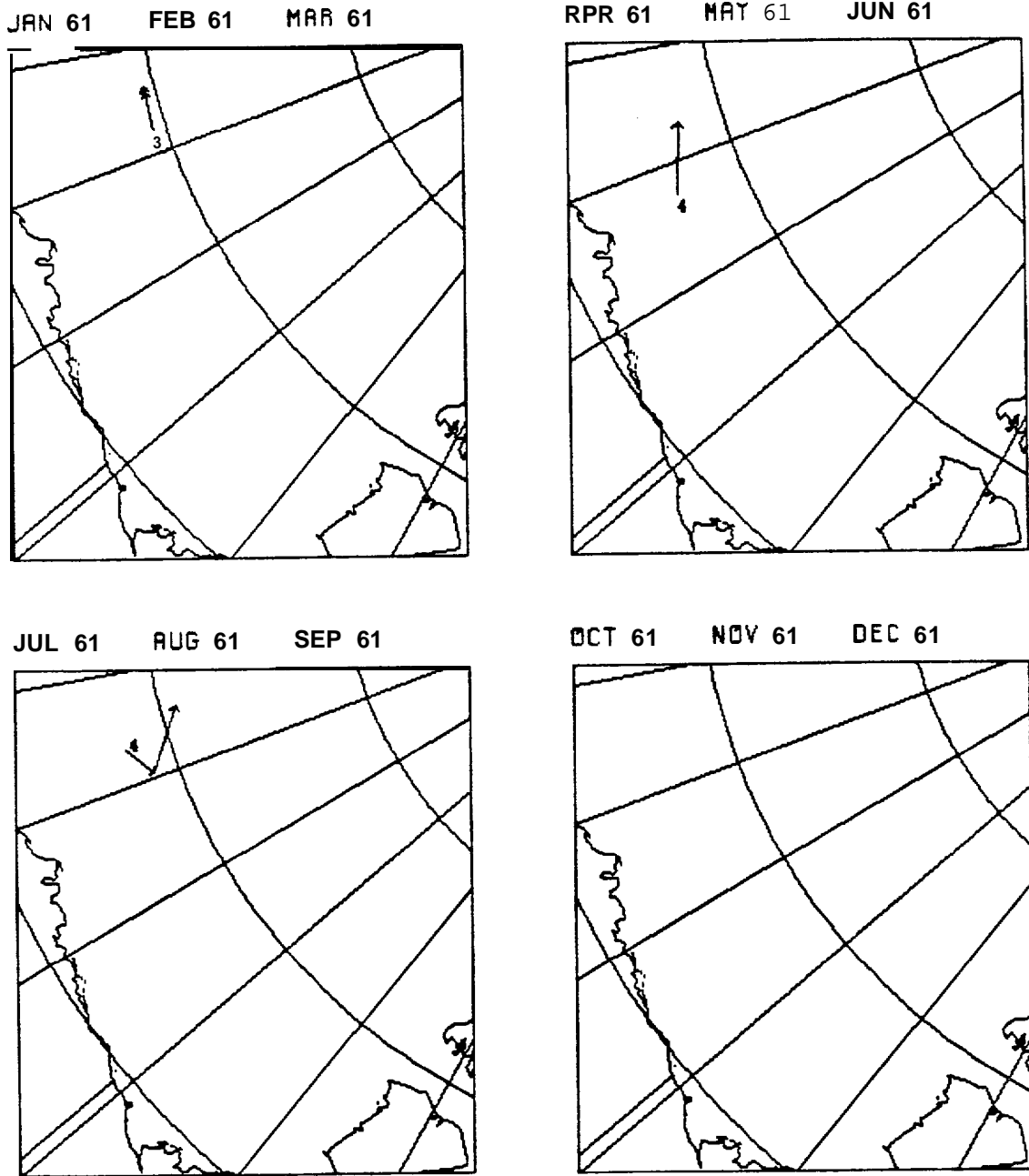


Figure B1. Observed Monthly Buoy Trajectories in the Beaufort Sea from 1959 Through 1981. Each Plot Represents a 3 Month Period (Continued).

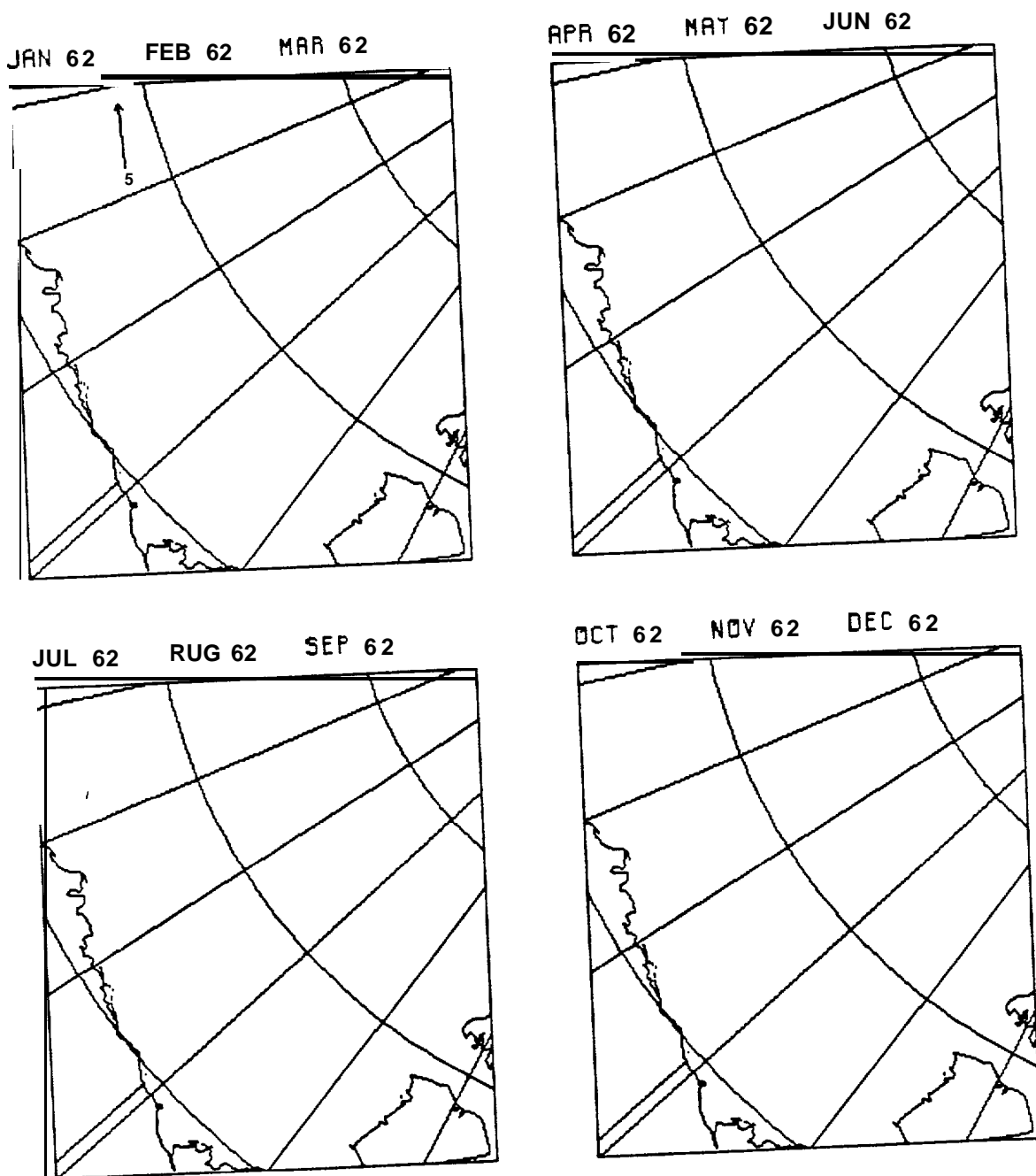


Figure B1. Observed Monthly Buoy Trajectories in the Beaufort Sea from 1959 Through 1981. Each Plot Represents a 3 Month Period (Continued).

-B9-

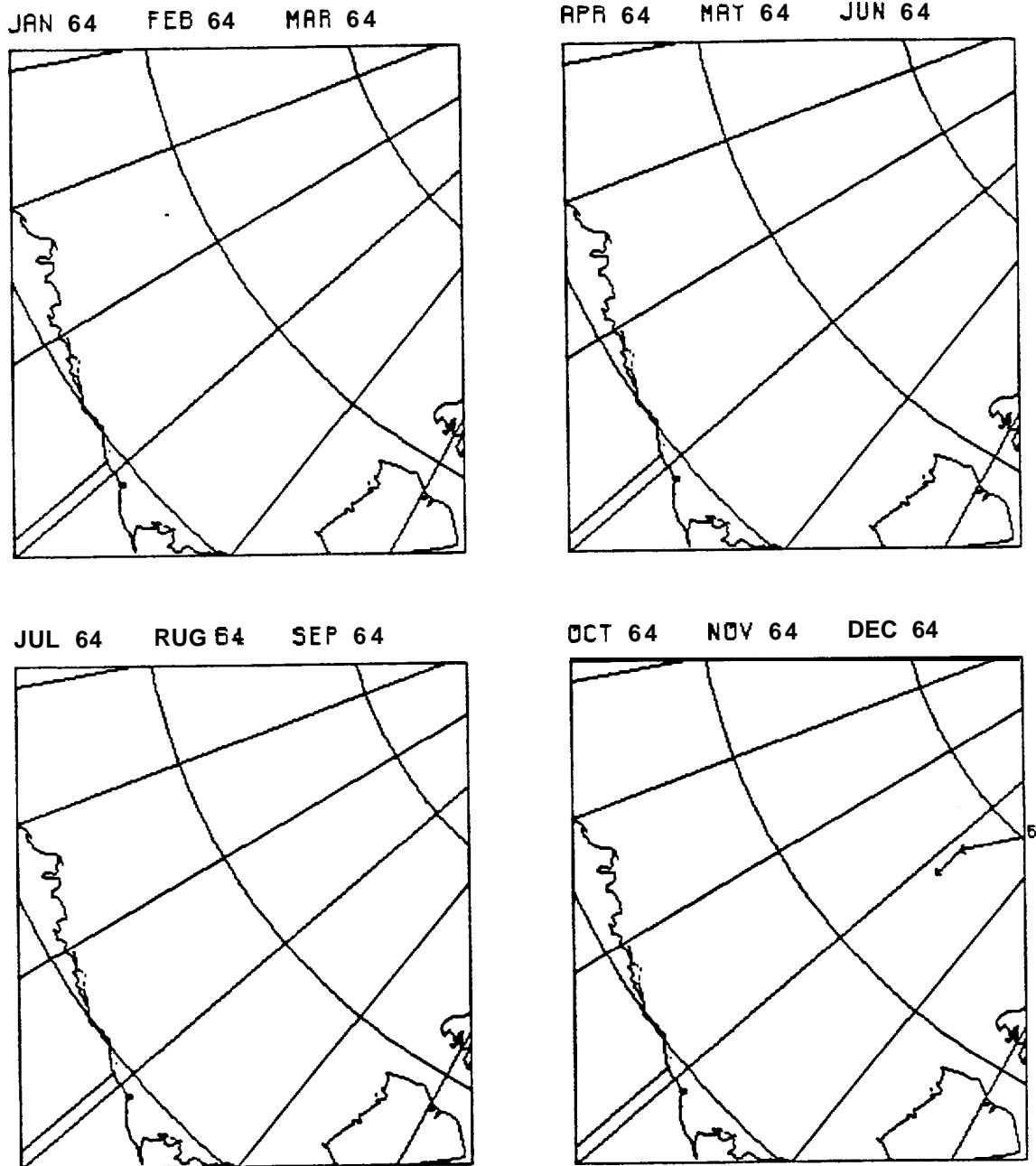


Figure B1. Observed Monthly Buoy Trajectories in the Beaufort Sea from 1959 Through 1981. Each Plot Represents a 3 Month Period (Continued).

-B10-

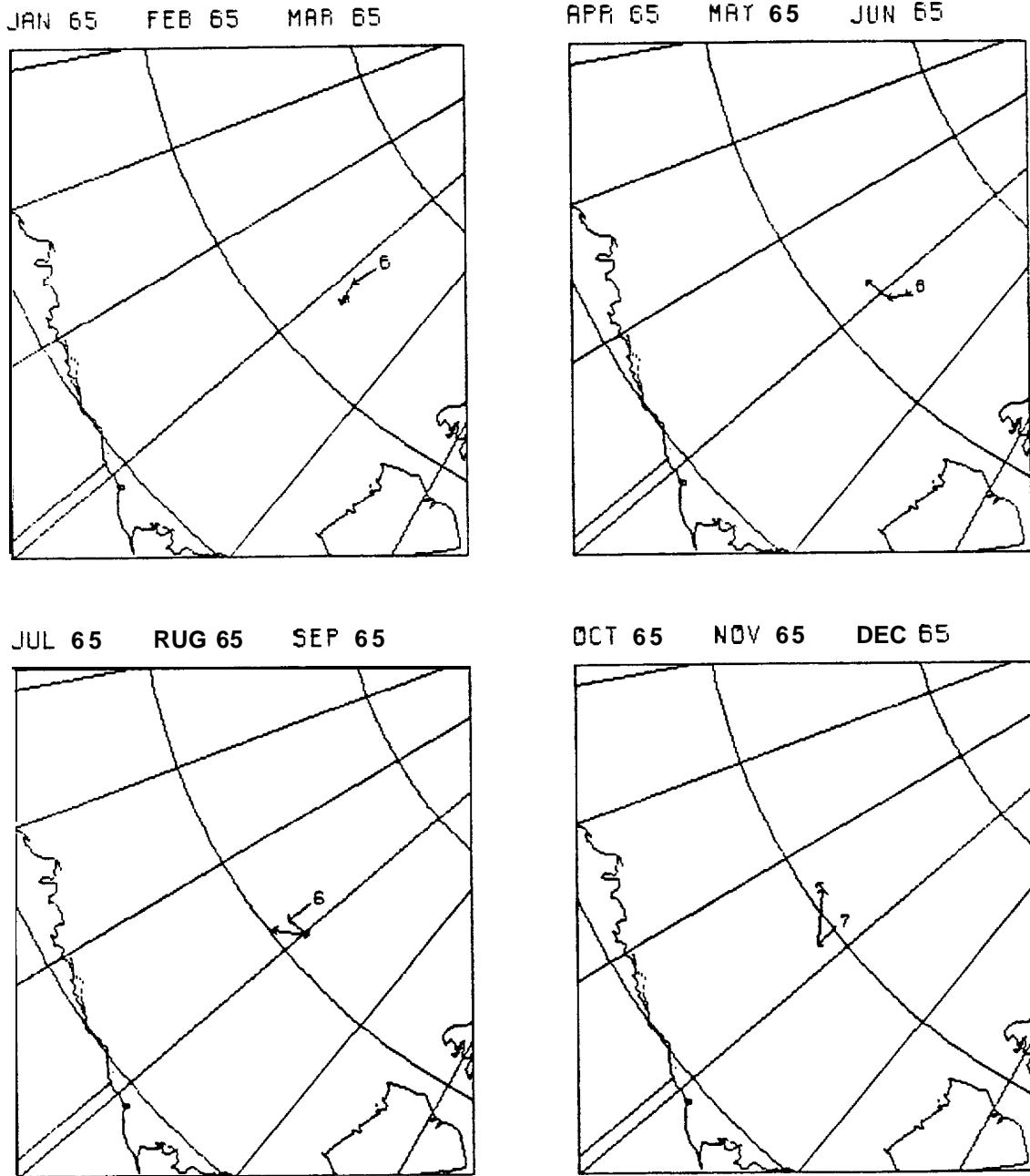


Figure B1. Observed Monthly Buoy Trajectories in the Beaufort Sea from 1959 Through 1981. Each Plot Represents a 3Month Period (Continued).

-B11-

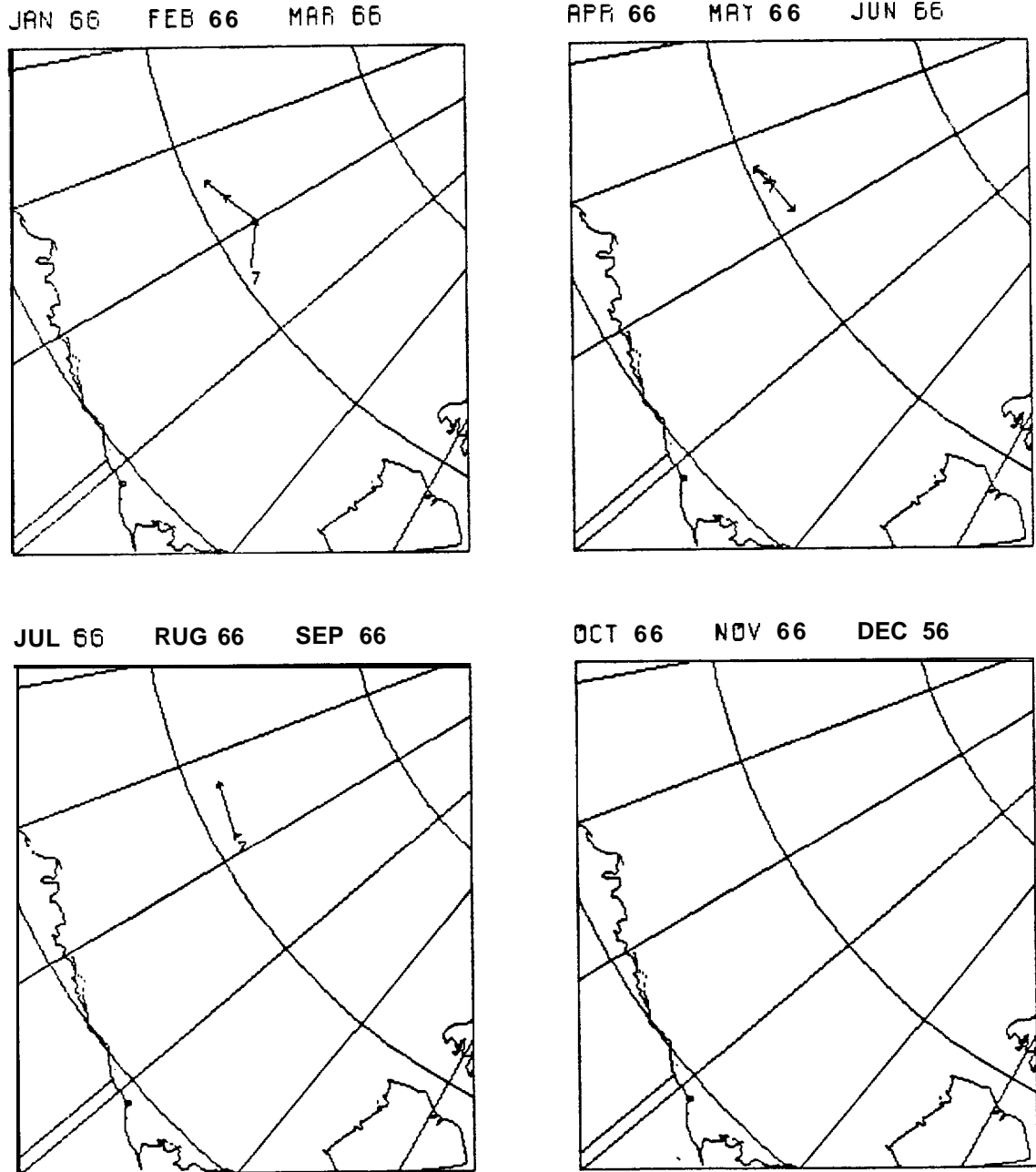


Figure B1. Observed Monthly Buoy Trajectories in the Beaufort Sea from 1959 Through 1981. Each Plot Represents a 3 Month period (Continued).

-B12-

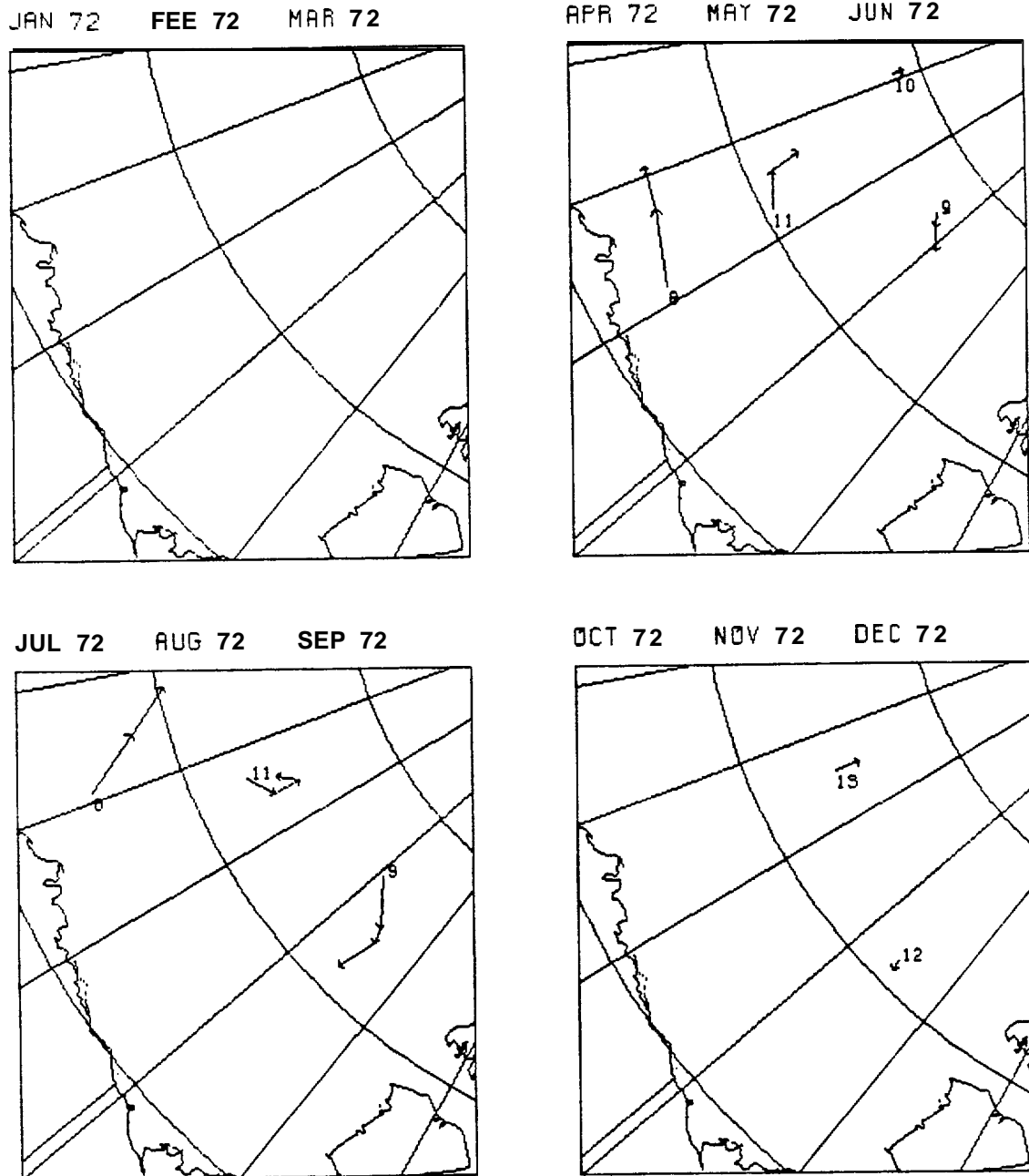


Figure B1. Observed Monthly Buoy Trajectories in the Beaufort Sea from 1959 Through 1981. Each Plot Represents a 3 Month Period (Continued).

-B 13-

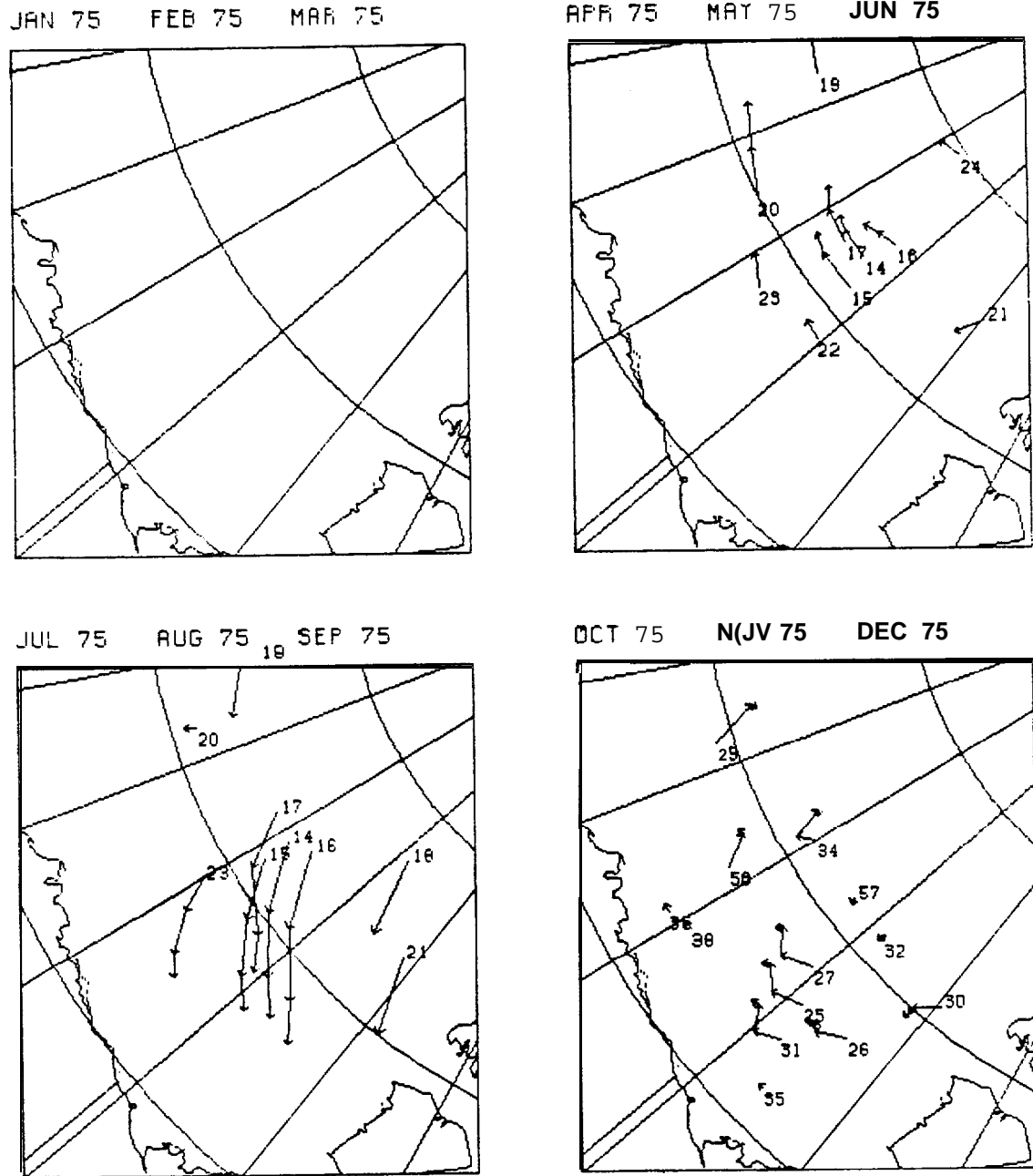


Figure B1. Observed Monthly Buoy Trajectories in the Beaufort Sea from 1959 Through 1981. Each Plot Represents a 3MonthPeriod (Continued).

-B14-

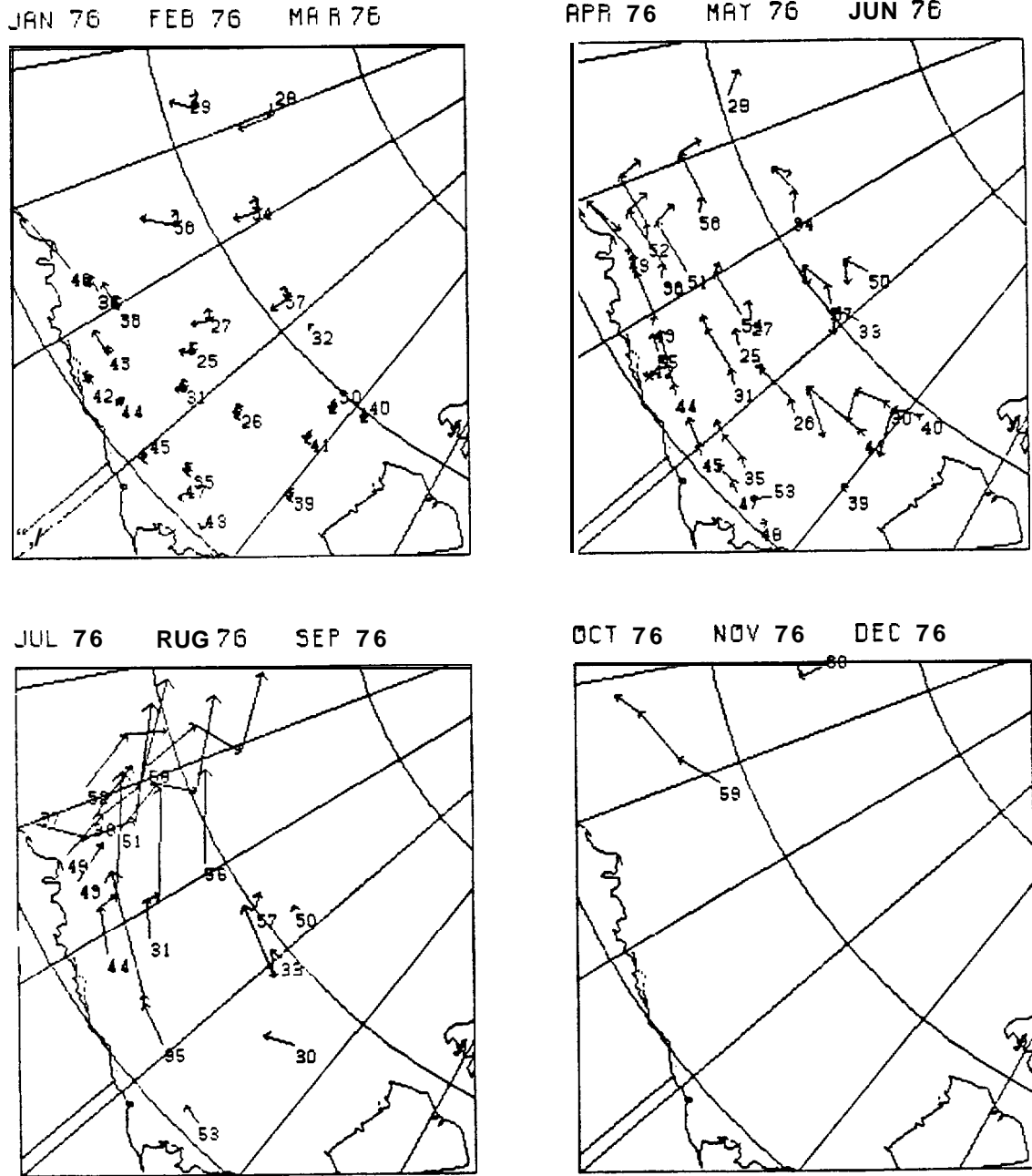


Figure B1. Observed Monthly Buoy Trajectories in the Beaufort Sea from 1959 Through 1981, Each Plot Represents a 3 Month Period (Continued).

-B15-

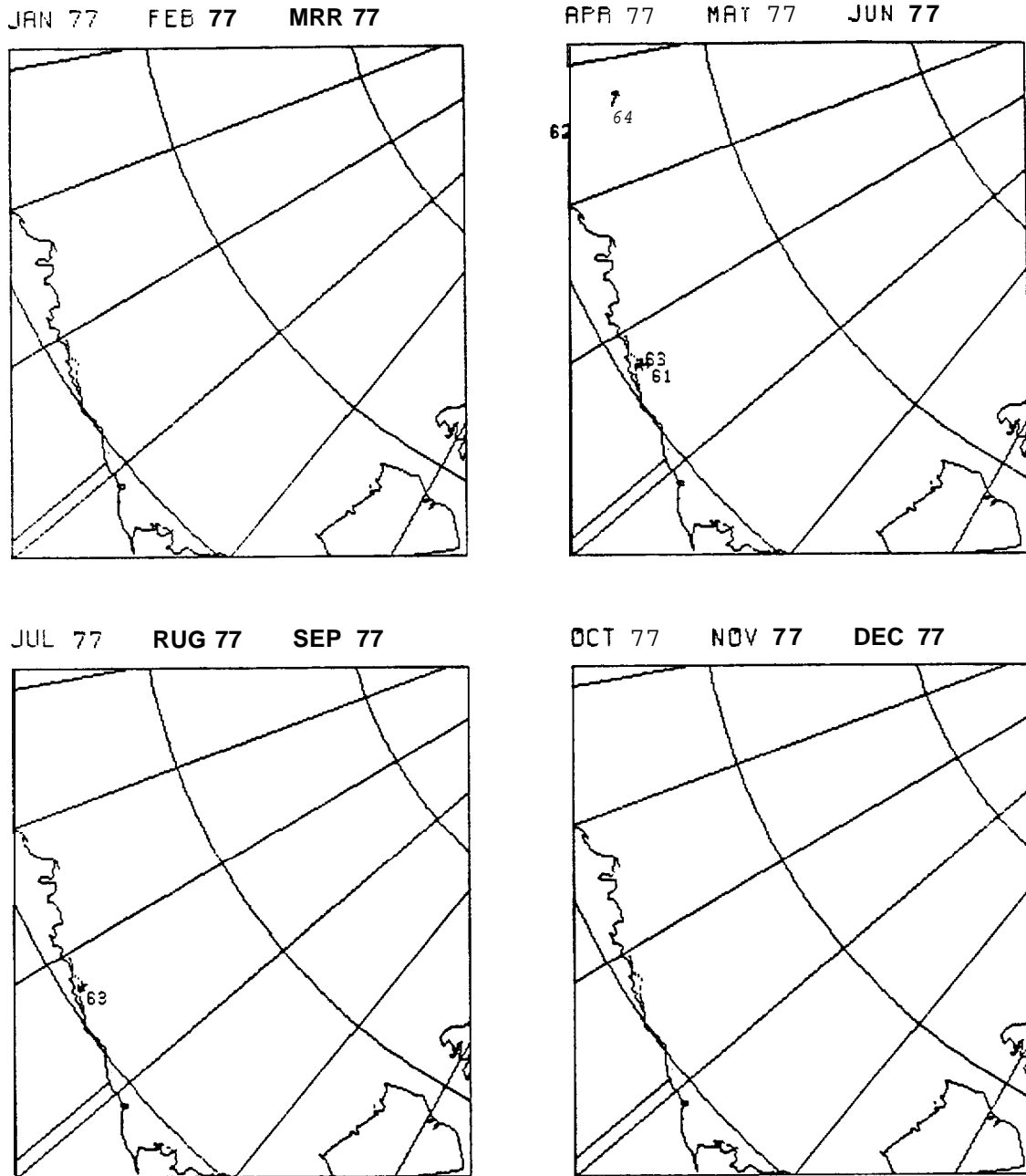


Figure B1. Observed Monthly Buoy Trajectories in the Beaufort Sea from 1959 Through 1981. Each Plot Represents a 3 Month Period (Continued).

-B16-

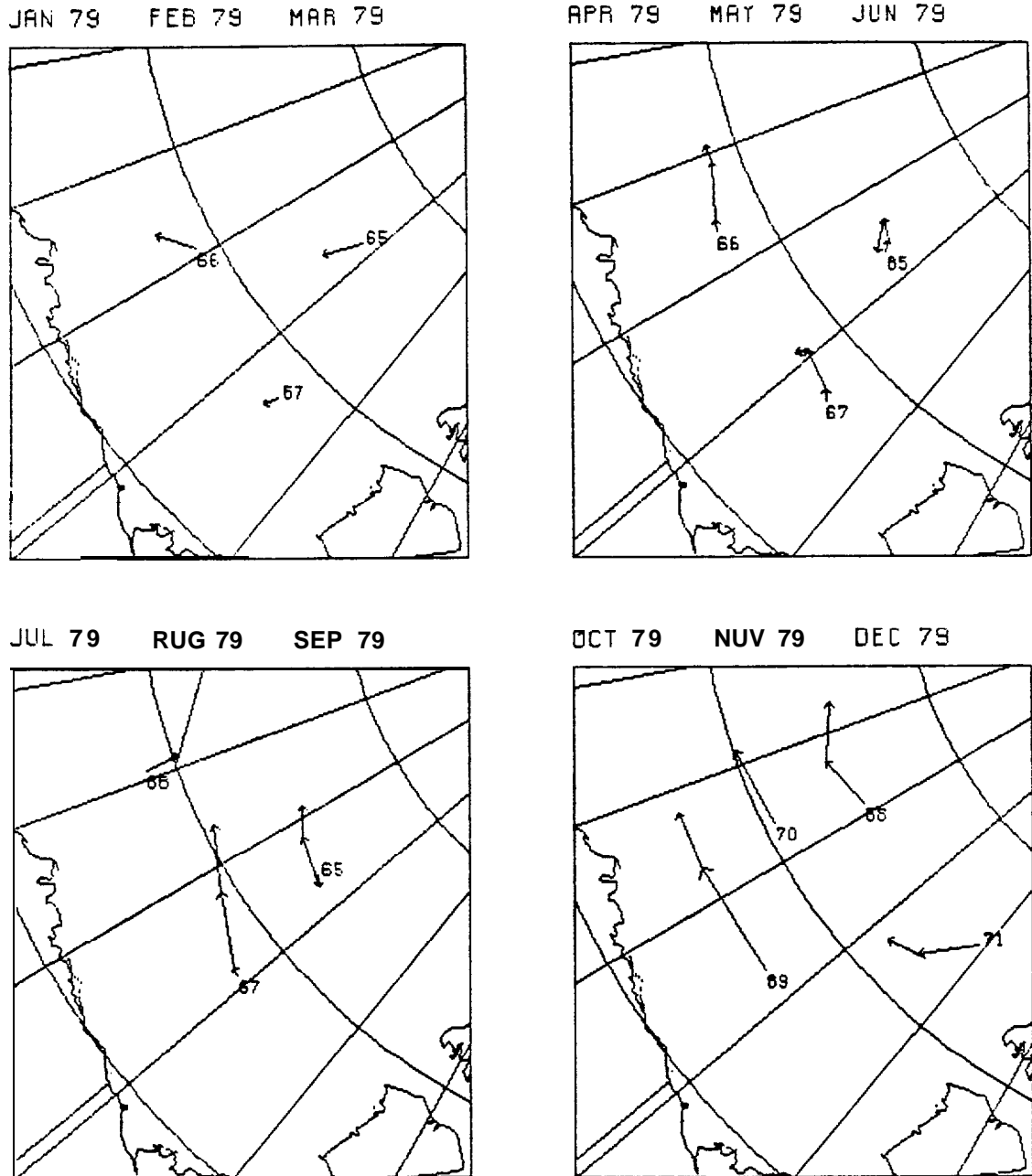


Figure B1. Observed Monthly Buoy Trajectories in the Beaufort Sea from 1959 Through 1981. Each Plot Represents a 3 Month Period (Continued).

-B17-

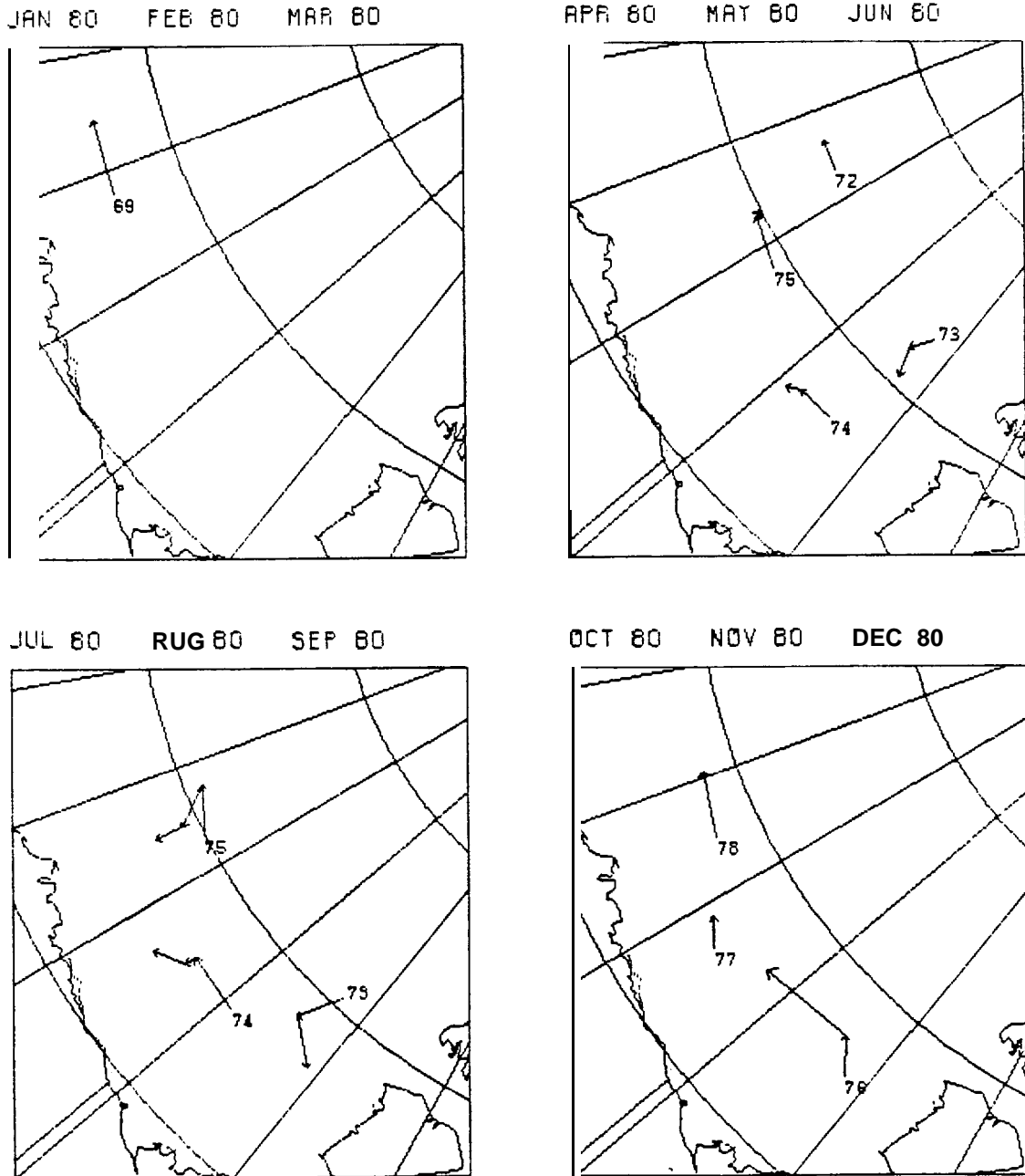


Figure B1. Observed Monthly Buoy Trajectories in the Beaufort Sea from 1959 Through 1981. Each Plot Represents a 3 Month period (Continued).

-B18-

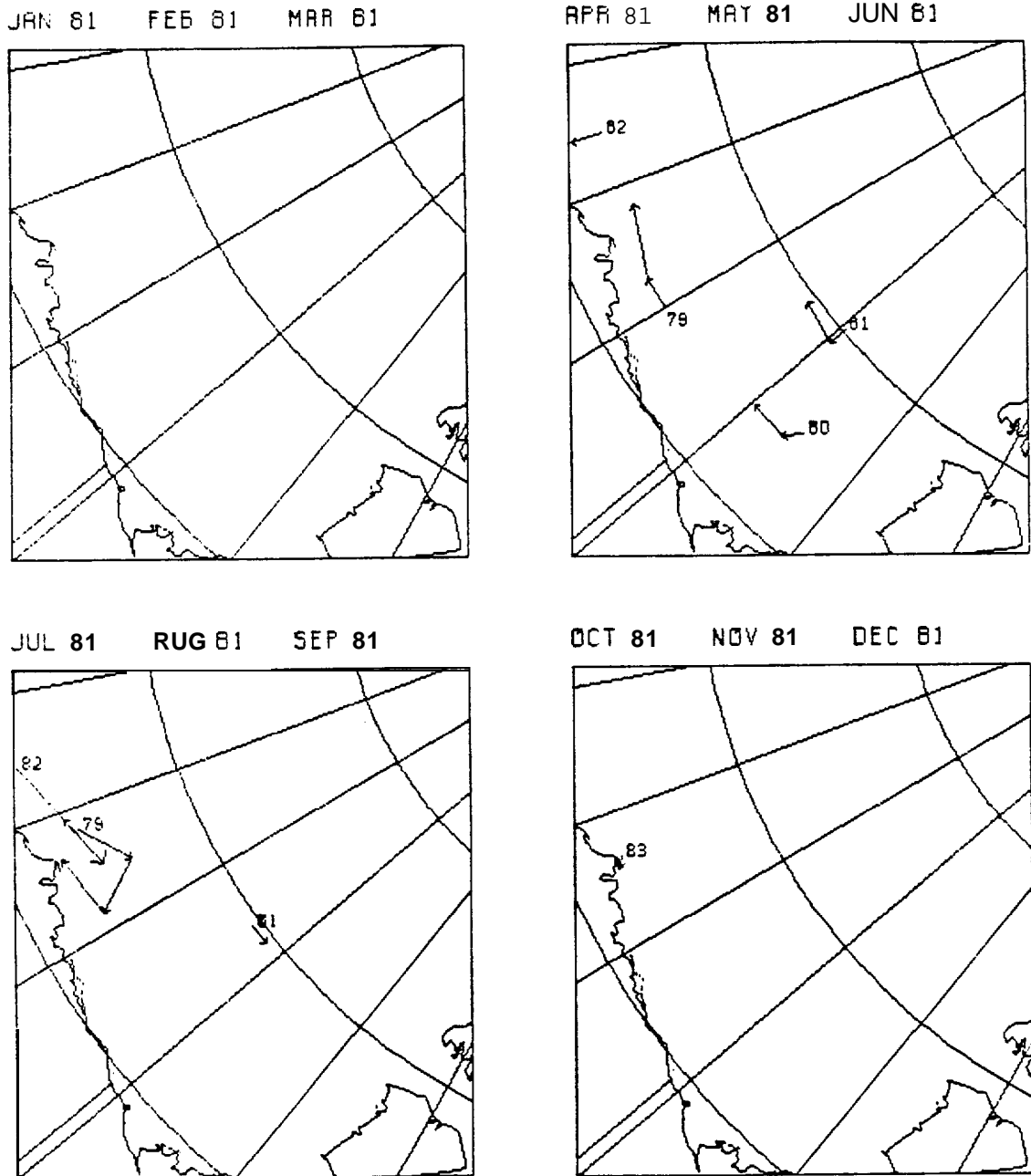


Figure B1. Observed Monthly Buoy Trajectories in the Beaufort Sea from 1959 Through 1981, Each Plot Represents a 3 Month Period (Concluded).

-B19-

395S-1959 ICE SEASON 1 10				1964-1965 ICE SEASON 1 12			
#1	ICE ISLAND T-3		10	#6	ICE ISLAND T-3		12
	JAN 59	75.302	126.375		NOV 64	80.063	133.918
	FEB 59	74.297	128.300		DEC 64	78.704	138.420
	MAR 59	74.089	128.333		JAN 65	77.840	138.252
	APR 59	74.087	128.396		FEB 65	77.176	138.679
	MAY 59	73.680	129.328		MAR 65	76.599	130.035
	JUN 59	72.602	130.174		APR 65	76.870	137.982
	JUL 59	71.940	132.482		MAY 65	76.708	137.941
	AUG 59	71.430	133.471		JUN 65	76.335	139.188
	SEP 59	71.420	135.836		JUL 65	76.196	141.809
	OCT 59	71.465	137.945		AUG 65	75.508	141.867
					SEP 65	75.680	139.388
					OCT 65	75.096	142.056
1959-1960 ICE SEASON 1 10				1965-1966 ICE SEASON 1 12			
#2	ICE ISLAND T-3		10	#7	ICE ISLAND T-3		12
	OCT 59	71.465	137.945		OCT 65	75.096	142.056
	NOV 59	71.270	140.610		NOV 65	74.451	141.724
	DEC 59	71.168	145.713		DEC 65	75.375	145.610
	JAN 60	71.052	145.051		JAN 66	75.369	146.478
	FEB 60	71.219	146.959		FEB 66	76.064	150.060
	MAR 60	72.049	152.047		MAR 66	75.667	153.684
	APR 60	72.181	154.046		APR 66	75.396	155.800
	MAY 60	71.80S	150.656		MAY 66	75.199	157.055
	JUN 60	71.822	160.220		JUN 66	75.406	155.096
	JUL 60	71.789	160.230		JUL 66	75.594	151.552
					AUG 66	75.571	151.858
					SEP 66	75.773	157.168
1960-1961 ICE SEASON 2 10				1971-1972 ICE SEASON 4 19			
#3	ARLIS 1		6	#8	AIDJEX PILOT NO.2		5
	OCT 60	74.965	142.127		MAY 72	72.064	151.301
	NOV 60	74.470	149.759		JUN 72	72.636	157.187
	DEC 60	74.136	154.059		JUL 72	72.758	160.747
	JAN 61	74.663	162.174		AUG 72	74.128	164.497
	FEB 61	74.741	165.731		SEP 72	75.176	167.950
	MAR 61	74.735	166.246	#9	AIDJEX PILOT NO.3		6
#4	ARLIS II		4		MAY 72	78.603	142.650
	JUN 61	73.276	157.435		JUN 72	78.365	141.559
	JUL 61	73.894	163.139		JUL 72	70.004	139.319
	AUG 61	74.403	160.340		AUG 72	77.062	135.299
	SEP 61	75.397	165.069		SEP 72	76.691	134.655
					OCT 72	75.687	135.696
1961-1962 ICE SEASON 1 2				#10 AIDJEX PILOT NO.4 2			
#5	ICE ISLAND T-3		2		MAY 72	79.301	160.851
	MAR 62	73.928	162.652		JUN 72	79.588	160.742
	APR 62	74.242	168.241				

Table B1. Observed Monthly Buoy Location and Motion in the Beaufort Sea from January 1959 Through December 1981.

-B20-

1971-1972 ICE SEASON			(Cent)	#19 AIDJEX STATION 7	4	
#11 AIDJEX PILOT NO. 6			6	JUN 75	77.5096	163.6679
MAY 72	75.226	152.740		JUL 75	77.5839	168.5818
JUN 72	75.627	155.993		AUG 75	77.0007	168.2S09
JUL 72	76.42'?	156.716		SEP 75	76.5630	163.1204,
AUG 72	76.920	153.944		#20 AIDJEX STATION S		4
SEP 72	77.601	154.001		MAY 75	74.9782	154.2100
OCT 72	77.117	155.676		JUN 75	7s. 3770	158.9122
				JUL 75	75.6493	163.1167
				AUG 75	75.3531	143.5152
1972-1973 ICE SEASON			2	4		

#12 AIDJEX PILOT NO. 3			2	#21 AIDJEX STATION 9		3
OCT 72	75.687	135.696		JUN 75	77.5419	129. S530
NOV 72	75.424	135.358		JUL 75	76.8421	131.3362
#13 AIDJEX PILOT NO. 6			2	AUG 75	75.0190	128.5141
OCT 72	77.117	155.676		#22 AIDJEX STATION 10		2
NOV 72	77.744	155.424		JUN 75	74.3114	140.3895
				JUL 75	74.3872	142.2449
1974-1975 ICE SEASON			11	46		

#14 AIDJEX STATION 0			6	#23 AIDJEX STATION 11		5
MAY 75	76.4698	143.7276		JUN 75	73.9268	147.2620
JUN 75	76.4252	147.0536		JUL 75	74.2063	149.8883
JUL 75	76.5534	148.6963		AUG 75	73.5134	148.4273
AUG 75	75.1930	144.0633		SEP 75	72.684	145.965
SEP 75	74.1563	139.4025		OCT 75	72.322	144.356
OCT 75	73.5138	136.6657		#24 AIDJEX STATION 12		2
#15 AIDJEX STATION 1			6	JUN 75	79.8474	146.8590
MAY 75	75.73'33	142.0811		JUL 75	79.6081	149.9589
JUN 75	75.6844	146.3603				
JUL 75	75.8421	148.4573		1975-1976 ICE SEASON 34 221		
AUG 75	74.6543	144.7962		-----		
SEP 75	73.6711	141.0793		#25 AIDJEX STATION 1		8
OCT 75	73.1731	138.7017		OCT 75	73.1731	138.7017
#16 AIDJEX STATION 2			6	NOV 75	72.7924	141.1706
MAY 75	77.2552	142.7120		DEC 75	73.2040	143.1017
JUN 75	77.1068	144.9446		JAN 76	73.0663	143.4680
JUL 75	76.9153	146.4370		FEB 76	73.0853	144.2076
AUG 75	75.3122	141.5880		MAR 76	72.9797	143.3092
SEP 75	74.1590	136.5076		APR 76	72.7220	144.1569
OCT 75	73.3718	134.0504		MAY 76	72.8778	145.4528
#17 AIDJEX STATION 3			6	#26 AIDJEX STATION 2		10
MAY 75	76.2909	146.0974		OCT 75	73.3718	134.0584
JUN 75	76.3022	149.8458		NOV 75	72.9570	136.3609
JUL 75	76.6779	152.0180		DEC 75	73.1146	136.9043
AUG 75	75.4068	148.4580		JAN 76	72.9397	137.1979
SEP 75	74.6227	142.8819		FEB 76	72.9547	137.7686
OCT 75	73.9821	140.5618		MAR 76	72.8191	137.0065
#18 AIDJEX STATION 5			2	APR 76	72.7174	137.1549
JUL 75	78.6467	138.6580		MAY 76	72.8825	138.0578
AUG 75	76.8112	135.5264		JUN 76	72.7870	141.55s0
				JUL 76	72.8680	141.7040

Table B1. Observed Monthly Buoy Location and Motion in the Beaufort Sea from January 1959 Through December 1981 (Continued).

-B2 1-

1975-1976 ICE SEASON			(Cont)	#33 AIDJEX STATION	12	6
-----				HAY 76	75.400	139.134
#27 AIDJEX STATION	3	B		JUN 76	75.143	141.535
OCT 75	73.9821	140.5616		JUL 76	74.713	139.720
NOV 75	73.5384	143.0396		AUG 76	74.664	140.835
DEC 75	73.9046	144.9896		SEP 76	74.296	138.781
JAN 76	73.0463	145.2221		OCT 76	74.814	145.609
FEB 76	73.8968	145.7865		#34 AIDJEX STATION	13	10
MAR 76	73.7887	144.7157		OCT 75	75.833	149.959
APR 76	73.36B3	145.3850		NOV 75	75.485	151.233
MAY 76	73.5482	146.7348		DEC 75	76.260	152.608
#28 AIDJEX STATION	7	3		JAN 76	76.171	152.134
FEB 76	77.6176	160.8068		FEB 76	76.373	152.045
MAR 76	77.4809	159.3993		MAR 76	76.220	150.869
APR 76	76.6684	159.5779		APR 76	75.606	151.388
#29 AIDJEX STATION	8	7		MAY 76	75.917	153.293
NOV 75	74.579	162.427		JUN 76	75.648	156.214
DEC 75	75.684	164.708		JUL 76	76.031	154.847
JAN 76	75.757	164.410		#35 AIDJEX STATION	14	11
FEB 76	7s. 981	164.254		DEC 75	71.057	136.077
MAR 76	75.7963	162.9106		JAN 76	71.064	136.451
APR 76	75.2410	164.3495		FEB 76	71.049	137.136
MAY 76	75.660	166.397		MAR 76	70.944	136.571
#30 AIDJEX STATION	5	11		APR 76	70.884	136.668
OCT 75	75.491	129.554		MAY 76	71.035	137.450
NOV 75	75.024	131.557		JUN 76	71.053	139.530
DEC 75	74.873	131.477		JUL 76	71.144	140.674
JAN 76	74.711	131.638		AUG 76	71.371	143.843
FEB 76	74.619	131.828		SEP 76	71.520	144.484
MAR 76	74.523	131.347		OCT 76	72.424	154.129
APR 76	74.434	131.370		#36 AIDJEX STATION	15	4
MAY 76	74.460	132.143		DEC 75	71.033	151.110
JUN 76	74.180	134.684		JAN 76	71.009	151.699
JUL 76	73.484	133.330		FEB 76	71.803	153.019
AUG 76	73.164	135.775		MAR 76	71.678	152.349
#31 AIDJEX STATION	10	13		#37 AIDJEX STATION	15	4
(3CT 75	72.194	137.925		JUL 76	71.183	159.778
NOV 75	71.831	139.702		AUG 76	72.231	157.254
DEC 75	72.368	140.956		SEP 76	73.505	157.035
JAN 76	72.297	141.631		OCT 76	74.799	166.406
FEB 76	72.319	142.175		#38 AIDJEX STATION	16	9
MAR 76	72.213	141.417		DEC 75	72.086	149.034
APR 76	72.046	141.947		JAN 76	72.047	149.715
MAY 76	72.226	142.947		FEB 76	72.169	150.670
JUN 76	72.307	146.736		MAR 76	72.014	149.789
JUL 76	72.417	147.835		APR 76	72.011	152.082
AUG 76	72.864	150.709		MAY 76	72.186	152.906
SEP 76	73.190	150.440		JUN 76	71.945	157.815
OCT 76	74.342	158.850		JUL 76	72.536	15s. 541
#32 AIDJEX STATION	12	4		AUG 76	73.892	161.565
NOV 75	75.732	138.157		#39 AIDJEX STATION	17	5
DEC 75	75.803	138.471		JAN 76	72.346	129.629
JAN 76	75.610	138.385		FEB 76	72.330	129.990
FEB 76	75.592	138.679		MAR 76	72.216	129.441

Table B1. Observed Monthly Buoy Location and Motion in the Beaufort Sea from January 1959 Through December 1981 (Continued).

-B22-

1975-1976 ICE SEASON (Cent)			#45 AIDJEX STATION 23 (Cent)		
#39 AIDJEX STATION 17		(Cent)	MAY 76	70.474	140.251
APR 76	72.171	129.612	JUN 76	70.642	142.092
MAY 76	72.203	130.220	#46 AIDJEX STATION 24		2
#40 AIDJEX STATION 18		7	JAN 76	71.466	154.265
JAN 76	74.960	128.895	FEB 76	70.151	164.333
FEB 76	74.906	128.983	#47 AIDJEX STATION 26		4
MAR 76	74.830	128.629	MAR 76	70.387	135.619
APR 76	74.751	120.677	APR 76	70.340	135.744
MAY 76	74.750	128.966	MAY 76	70.455	136.556
JUN 76	74.476	131.112	JUN 76	70.455	138.089
JUL 76	73.364	129.388	#48 AIDJEX STATION 27		3
#41 AIDJEX STATION 19		7	MAR 76	70.208	133.070
JAN 76	73.712	131.613	APR 76	70.173	133.015
FEB 76	73.680	131.843	MAY 76	70.302	132.745
MAR 76	73.558	131.401	#49 AIDJEX STATION 28		7
APR 76	73.466	131.466	APR 76	71.522	154.845
MAY 76	73.548	132.113	MAY 76	71.641	155.132
JUN 76	73.373	137.786	JUN 76	71.121	159.626
JUL 76	72.802	133.941	JUL 76	71.586	156.745
#42 AIDJEX STATION 20		7	AUG 76	72.766	158.515
JAN 76	70.470	145.962	SEP 76	73.916	159.645
FEB 76	70.548	146.643	OCT 76	75.303	168.336
MAR 76	70.445	146.984	#50 AIDJEX STATION 29		4
APR 76	70.440	146.197	MAY 76	76.370	142.411
MAY 76	70.438	146.194	JUN 76	76.062	144.672
JUN 76	70.444	146.250	JUL 76	75.775	142.540
JUL 76	70.439	146.206	AUG 76	75.805	142.773
#43 AIDJEX STATION 21		8	#51 AIDJEX STATION 33		6
JAN 76	71.269	147.291	MAY 76	72.633	151.570
FEB 76	71.333	147.751	JUN 76	72.492	156.147
MAR 76	71.206	147.110	JUL 76	73.041	156.794
APR 76	71.252	149.274	AUG 76	74.323	159.220
MAY 76	71.397	149.711	SEP 76	75.134	157.202
JUN 76	71.506	153.266	OCT 76	76.357	165.676
JUL 76	71.597	154.549	#52 AIDJEX STATION 36		6
AUG 76	72.503	156.414	APR 76	72.127	155.244
#44 AIDJEX STATION 22		10	MAY 76	72.279	156.330
JAN 76	70.827	143.842	JUN 76	72.079	160.611
FEB 76	70.820	144.074	JUL 76	72.687	161.167
MAR 76	70.769	143.555	AUG 76	73.997	164.363
APR 76	70.736	144.038	SEP 76	74.968	163.547
MAY 76	70.857	144.738	#53 AIDJEX STATION 37		3
JUN 76	71.058	146.811	JUN 76	70.822	133.723
JUL 76	71.314	148.562	JUL 76'	70.439	134.694
AUG 76	71.765	151.973	AUG 76	70.514	136.199
SEP 76	72.245	152.124	#54 AIDJEX STATION 38		3
OCT 76	73.604	161.337	MAY 76	73.232	146.185
#45 AIDJEX STATION 23			JUN 76	73.218	150.271
JAN 76	70.513	139.81:	JUL 76	73.421	150.717
FEB 76	70.409	139.898	#55 AIDJEX STATION 39		2
MAR 76	70.354	139.451	JUN 76	70.969	147.418
APR 76	70.325	139.535	JUL 76	71.122	148.673

Table B1. Observed Monthly Buoy Location and Motion in the Beaufort Sea from January 1959 Through December 1981 (Continued).

-B23-

1975-1976 ICE SEASON (Cent)			#64 AIDJEX STATION R1617 2		
-----			APR 77	72.433	166.303
#56 AIDJEX STATION 41		2	MAY 77	72. b20	167.300
SEP 76	74.547	150.973	1978-1979 ICE SEASON 3 24		
OCT 76	75.565	158.916	-----		
#57 AIDJEX STATION 44		9	#65 AOBP 1906		8
DEC 75	75.816	143.061	MAR 79	77.950	141.483
JAN 76	75.695	142.801	APR 79	77.006	143.276
FEB 76	75.763	143.019	MAY 79	77.228	143.956
MAR 76	75.645	142.035	JUN 79	77.432	146.256
APR 76	75.152	142.183	JUL 79	76.832	143.738
MAY 76	75.373	143.814	AUG 79	76.704	142.600
JUN 76	75.129	146.466	SEP 79	77.052	140.024
JUL 76	74. 996	144.819	OCT 79	77.468	151.176
AUG 76	75.290	145.056	#66 AOBP 1913		8
#58 AIDJEX STATION 66		12	MAR 79	74.463	150.681
NOV 75	73.637	151. 831	APR 79	73.726	153.398
DEC 75	74.351	1 53.937	MAY 79	73.810	154.413
JAN 76	74.301	154.347	JUN 79	74.312	159.120
FEB 76	74.454	154.607	JUL 79	74.295	160.754
MAR 76	74.313	1 53.429	AUG 79	75. 146	161.094
APR 76	73.554	155.398	SEP 79	76.381	169. 485
MAY 76	73.788	156.428	OCT 79	77.132	174.518
JUN 76	73. b73	140.552	#67 AOBP 1914		8
JUL 76	74.261	161.140	MAR 79	73.893	135.767
AUG 76	75.684	163.346	APR 79	73.516	136. 187
SEP 76	76.530	159.231	MAY 79	73.722	136.883
OCT 76	77.649	1 66. 840	JUN 79	73.999	140.573
1976-1977 ICE SEASON 6 20			JUL 79	73.767	140.921
-----			AUG 79	73.811	141.731
#59 AIDJEX STATION 10		4	SEP 79	74.627	147.847
OCT 76	74.342	158.850	OCT 79	75.293	153. 679
NOV 76	73.612	162.119	1979-1980 ICE SEASON 8 31		
DEC 76	73.010	166.813	-----		
JAN 77	72.514	16e. 540	#68 AOBP 1906		3
#60 AIDJEX STATION 66		4	OCT 79	77.468	151.176
OCT 76	77.649	166.040	NOV 79	77.069	157.145
NOV 76	77.053	166.307	DEC 79	77.627	163.168
DEC 76	77.096	168.545	#69 AOBP 1908		4
JAN 77	76.705	169.097	NOV 79	73.184	142.935
#61 AIDJEX STATION Rb32		2	DEC 79.	73.192	153.055
APR 77	70.716	146.937	JAN 80	73.205	157.998
MAY 77	70.723	146.924	FEB 80	73.342	164.420
#62 AIDJEX STATION R1052		2	#70 AOBP 1914		2
MAY 77	70.835	166.271	OCT 79	75.293	153.679
JUN 77	71.266	168.813	NOV 79	75.051	161.360
#63 AIDJEX STATION R1601		6	#71 AOBP 1918		3
APR 77	70.525	147.271	OCT 79	77.423	130.562
MAY 77	-70.527	147.252	NOV 79	76.237	134.694
JUN 77	70.520	147.299	DEC 79	75.975	137.990
JUL 77	70.520	147.290			
AUG 77	70.493	147.496			
SEP 77	70.331	147.327			

Table B1. Observed Monthly Buoy Location and Motion inthe BeaufortSea from January 1959 Through December 1981 (Continued).

